PHENOMENOLGY AT THE TERASCALE

A Dissertation

Presented to the Faculty of the Graduate School

of Cornell University

in Partial Fulfillment of the Requirements for the Degree of

Doctor of Philosophy

by

Andrew Paul Spray

August 2009

© 2009 Andrew Paul Spray
ALL RIGHTS RESERVED

PHENOMENOLGY AT THE TERASCALE

Andrew Paul Spray, Ph.D.

Cornell University 2009

In the next few years, particle collider experiments at CERN and dark matter searches throughout the world will directly and indirectly probe the physics of the Terascale. In preparation for these experiments, this thesis examines the possible signals of new physics, and what that new physics might be.

We first consider signals of dark matter that depend very little on its underlying nature. We now have precise measurements of the cosmological dark matter abundance; this allows us to predict the flux of high energy gamma rays from dark matter self-annihilation in a generic theory. We also draw attention to a feature in the spectrum that has previously been overlooked: the sharp decrease in the flux at the WIMP mass for photons emitted as final state radiation. This feature, if observed, would provide unambiguous evidence of a non-astrophysical source.

We next study a specific theory of new physics, the Littlest Higgs with T Parity. Assuming that this model offers the correct description of dark matter, we predict the expected flux of gamma rays and neutrinos, as well as the direct detection signal. Since each theory has a different pattern of signals, we can use the future experimental data to identify the model that best describes reality. This particular model is well hidden from these detection channels.

We then conclude by studying a new possible model for physics at the Terascale, based on combining string theory with the Randall-Sundrum theory of extra dimensions. We develop the theoretical framework for such a model, generalising known results in flat space into an effective field theory in curved space. We then

calculate the production and decay of one of the lightest new particles at the Large Hadron Collider in CERN; we find that detection is plausible at that experiment.

BIOGRAPHICAL SKETCH

Andrew Spray was born on September 11th, 1980 in the city of Plymouth in England to Paul and Valerie Spray. His primary education took place at Hyde Park Junior school in Plymouth; his secondary education at the Royal Hospital School, a boarding school near the village of Holbrook. After completing his A-Levels, he hoped to pursue an academic career in the physical sciences, but was unsure which field. He therefore applied to read Natural Sciences at Queens' College, Cambridge, which he began in 1998. In his final years there, he specialized in physics; and following the award of his Master of Natural Science in 2002, he crossed the Atlantic to do graduate study at Cornell University. His research has been in the field of high energy phenomenology, with particular interests in dark matter. In the Fall of 2009, he will start a Post-Doctoral position working for David Morrissey at the TRIUMF research center in Vancouver.

To Jennifer, Paul, Val and Nicholas.

ACKNOWLEDGEMENTS

I would above all like to thank my advisor, Maxim Perelstein, who has guided my development as a researcher for the last five years. I found his explanations, discussions and patience invaluable. I would also like to thank the other members of my Special Committee, Csaba Csaki and Rich Galik, for their support; as well as Lawrence Gibbons for stepping in to proxy at the proverbial last minute.

The work produced here was a joint effort. In addition to Maxim, I would like to thank my other collaborators Andreas Birkedal, Konstantin Matchev and Andrew Noble. I am also grateful for the contributions of Jay Hubisz, Patrick Meade, Dan Hooper, Marco Cirelli, Lisa Randall, Csaba Csaki, Sohang Ghandi, Liam McAllister and Matthew Reese. My research was supported by the National Science Foundation under grants PHY-0355005, PHY-0757868 and CAREER award PHY-0844667.

I would like to thank the Gannett Health Services center for its counseling services. I would also like to thank the Cornell International Students and Scholars Office for financial support during the 2007 Fall semester.

I would like to thank my parents, for letting me be myself and putting up with me never calling them back. Finally, I would like to thank Jennifer for getting me started and giving me self belief; without you I literally could not have done it.

TABLE OF CONTENTS

LIST OF TABLES

LIST OF FIGURES

CHAPTER 1

INTRODUCTION

1.1 The Standard Model

We live in interesting times. A plethora of experiments, either recent, current or forthcoming will change, and possibly revolutionize, our understanding of particle physics. Foremost among these experiments is the Large Hadron Collider (LHC), currently due to start running (again) in late 2009. The LHC will create TeV conditions in the laboratory for the first time, finally directly probing the Terascale energies recognized as important by Fermi 75 years ago [1]. Recent experiments, including WMAP [2] and Hubble [3], have heralded the era of precision cosmology, measuring the universal abundance of ordinary matter, dark matter and dark energy [4]. Finally, detectors such as Fermi/GLAST, PAMELA and CDMS offer the hope of the first non-gravitational measurement of dark matter.

At any given moment in time, any number of experiments are operational. To understand what makes the present so exciting, one must first understand the great success of the last thirty years of particle physics. The existing paradigm, demurely referred to as the "Standard Model", is a fusion of the electroweak theory of Glashow, Salaam and Weinberg [5]; the quark model of Gell-Mann [6]; and the asymptotically free strong interaction of Gross, Wilczek and Politzer [7]. It is thus an explanation of all non-gravitational physics. It unifies the electromagnetic and weak forces into a single electroweak interaction, spontaneously broken by the enigmatic Higgs boson. Protons, neutrons and other strongly interacting particles are understood as composite objects, with the fundamental entities being fractionally charged quarks and the force-carrying gluons. Finally, the joining of the two sectors is encoded by the Cabibbo-Kobayashi-Maskawa (CKM) matrix. [8]

Since the Standard Model's creation, it has agreed with almost every experimental result and observation. Among its successes, it successfully predicted the discoveries of the W boson, Z boson and top quark; correctly predicted the relative abundances of light elements produced in the early Universe; and agrees with electroweak precision measurements with percent accuracy or better [9]. In the last 30 years, 9 Nobel prizes in Physics (including the most recent) have been awarded to those who contributed to the theory's theoretical development and experimental support.

In spite of these successes, the Standard Model has several weaknesses that leave us looking for more answers. We have already mentioned the fact that it does not describe gravity; but in practice, this is not a pressing challenge. It tells us that the Standard Model can only be an effective theory, valid for energy scales below the Planck scale (where quantum gravity becomes strongly coupled). But since the Planck scale is approximately 10^{15} times greater even than the highest energies to be probed at the LHC, this is a small restriction. Other limitations of the Standard Model are its inability to explain the recently observed acceleration of the Universe's expansion [10], neutrino masses/oscillations [11] and the matter-antimatter asymmetry. Frustratingly, none of these difficulties gives us a clear sense of at what energy scale they might be resolved. In contrast, there are two very good reasons – one experimental, one theoretical – to think that the Standard Model *must* be modified, enhanced or replaced at the Terascale.

1.1.1 The Hierarchy Problem

The first reason to believe in new physics at TeV energies is a theoretical argument known as the "hierarchy problem". This argument invokes the fact that any quantum field theory must be an effective theory, valid below some energy scale

Λ; at the most, Λ is the Planck scale. All parameters in such a theory have two contributions: a "bare" term, that is determined by the unknown physics at energies above Λ; and quantum corrections, that depend both on Λ and the scale at which you measure them. We expect that these two terms, being caused by different physics, are unrelated in value. The field theory corrections, which we can predict, then represent a probable lower bound on the experimental value of the parameter. Alternatively, we can invert this statement: given the observed value of a particular physical quantity, we can find an upper bound on Λ.

For the majority of parameters in the Standard Model, this line of reasoning is of little use. Most of the corrections depend only logarithmically on Λ, leading to very weak bounds on the scale of new physics. What makes this relevant is the fact that the exception is a parameter that underpins the entire theory: the mass of the Higgs boson. The quantum corrections to this quantity are typically negative and proportional to Λ^2. If m_0^2 is the bare term,

$$m_h^2 \sim m_0^2 - \frac{1}{(4\pi)^2}\Lambda^2. \tag{1.1}$$

Inverting this, we find that a rough upper bound on Λ is $\Lambda \sim 4\pi m_h \sim 10 m_h$. The Higgs field, by breaking the electroweak interaction, provides masses for the W and Z bosons, the leptons and the quarks.[1] The Higgs must have a mass of at most a few hundred GeV to be consistent with precision measurements. This leads to the prediction that *new physics will be observed at energy scales of about 1 TeV!* Further, because the Higgs boson interacts weakly, this new physics *must* couple to the weak interaction; while precision measurements have disfavored the possibility that it also couples through a stronger force.

As an aside, note that if we try to force Λ to lie at the Planck scale, then Λ and m_0 must agree to one part in 10^{15}. This is the usual statement of the hierarchy

[1]Hadrons and mesons acquire mass from the strong interaction binding energy, so would remain massive even if there was no Higgs.

problem: that it is "unnatural" that these two unrelated numbers should just happen to agree to such precision, without any symmetry principle to enforce it. Interestingly, Weinberg [12] and others [13] have recently argued that it *is* justifiable to take Λ near the Planck scale, based on some of the results of string theory. While an interesting concept, we will not pursue it here.

1.1.2 Dark Matter

The second hint of a coming revolution is completely different in nature to the hierarchy problem. Not only is it an experimental argument, it comes from cosmology, not particle physics! The experimental history of dark matter goes back to Zwicky's application of the virial theorem to the Coma cluster in 1933 [14]. In the present era of precision cosmology, we not only have a precise measurement of the universal density of dark matter [2]; we also have strong evidence that it is not baryonic matter [2, 15] nor a modification of Newtonian gravity [16]. In short, dark matter *is* matter; but it *cannot* be any of the Standard Model particles.

What is particularly tantalizing is the amount of dark matter. The observed relic density is exactly what would be expected from a weakly-interacting massive particle (WIMP) with a mass in the range 100 GeV–10 TeV. While other possibilities exist, this congruence of scales – named the "WIMP miracle" – is highly suggestive. Why invoke additional physics when two separate problems can be solved simultaneously? Note also that this argument, like the hierarchy argument, anticipates new *weakly-interacting* physics.

In fact, the connection between the hierarchy problem and dark matter goes beyond a coincidence of scales. Many theories have been proposed to resolve the hierarchy problem, and it is common for these models to include discrete symmetries. The most famous example would be supersymmetry, where R parity

– a $\mathbb{Z}_2$ symmetry – is often invoked to prevent proton decay. The immediate consequence is that the lightest particle that is odd under R parity must be stable; and so if not too heavy, still present in the Universe today. If such a particle is charged, it is probably ruled out; if it is neutral, it will behave like dark matter.

In summary, when we try to solve the hierarchy problem, we often address the dark matter problem by accident, and vice versa. And, when we try to solve either, we most easily do so by invoking Terascale physics. This justifies our expectations of finding something new in the next few years.

1.2 Beyond the Standard Model

As we anticipate data from our experimental colleagues, we phenomenologists have the duty and pleasure of preparation. This preparation can be divided into two broad subtopics. First, we can work to simplify the analysis of the data that is to come; and second, we can attempt to fill out the space of theories that might be found. Obviously the latter will, to some extent, inform the former. However, we also want to approach the analysis as free of prejudice as possible, which drives us to separate them.

Indeed, in any predictions or interpretations of data, there is an essential trade-off. One must choose between conclusions that have broad applicability – "model independent" results – and conclusions that have an unambiguous strength – "model dependent" results. The two terms used might suggest a dichotomy, but really there is a continuum: the more assumptions that are made about the underlying physics, the smaller the region in theoretical space that it is possible to make statements about; but the stronger those statements are.

Within this thesis, we will address the preparatory issue from all of these vantage points. In chapter 2, we consider one possible means of detecting dark matter,

and study it in a manner that is largely independent of the underlying physics. The mechanism we discuss is robust and the main assumption we make is that dark matter is a WIMP with the measured cosmological abundance. In chapter 3, we adopt a different approach, looking at a number of different dark matter searches within the framework of a single model, the Littlest Higgs Theory with T Parity (LHT). Finally, in chapter 4 we will add to the range of possible theories, by considering string theory in the Randall-Sundrum (RS) model of extra dimensions. We use the remainder of this introduction to consider background material to each of these chapters.

1.3 Gamma Rays from Dark Matter

There are three basic methods available to find dark matter. First, one can attempt to produce it in the laboratory at a particle accelerator such as the LHC. This method has the advantage that we can control the environment and thus more easily measure the properties of what we produce. However, without other measurements we cannot know that we have found truly is dark matter. Thus, a second approach is to look for interactions between dark matter passing through the Earth and ordinary matter that we control. The drawback to this idea is that the relevant scattering cross sections are essentially undetermined without the framework of a particular model. The final means is to look for the products of dark matter annihilation in high energy cosmic rays. This "indirect" style of search will be our focus.

The advantage of indirect searches is that the same process that produces the annihilation products we search for, are also responsible for determining the dark matter density. As the Universe expanded, there came a point where the dark matter particles were too far sparse to efficiently annihilate and thermal

equilibrium was lost. The comoving density has then remained nearly constant since that time. The point where this transition occurred is set by the annihilation cross section. The present precise measurements of the relic density then give us a fairly robust value for the total annihilation cross section.

One possible channel for indirect searches is based on high energy photons. This avenue has the advantage that the galaxy is essentially transparent to gamma rays; so all the dark matter in the Milky Way contributes to the signal, and the features of the spectrum are unaltered. There are traditionally two sources of photons that are considered:

- "Monochromatic" photons produced by direct annihilation into $\gamma\gamma$, $h\gamma$ or $Z\gamma$ final states;
- "Fragmentation" photons produced during hadronization and from hadronic decays, e.g. $\pi^0 \to \gamma\gamma$.

The first of these is loop suppressed while the latter produces a softer, featureless spectrum. However, there is one additional source of photons that has been relatively overlooked:

- "FSR" photons produced by final state radiation off a charged Standard Model particle.

Compared to fragmentation photons, the FSR spectrum is harder and in many cases has a distinct feature – a "step" – at the dark matter mass. This feature would play an important role in identifying the observed flux as originating from dark matter; it is difficult to conceive of an astrophysical process that could produce such a spectral feature.

While monochromatic photons also have a clear feature at the dark matter mass, the FSR signal is significantly larger for three reasons. First, monochromatic photons are typically suppressed by the fine structure constant α^2, whereas

FSR photons (with only a single electroweak coupling) are only suppressed by α. Second, FSR photons benefit from collinear logarithmic enhancement that exists even for very hard photons. Finally, the only Standard Model final states that will not lead to FSR photons are neutrinos – even the neutral Z and h final states will produce FSR photons from their decay products – so more possible final states are available.

In chapter 2, we study the production of gamma rays in a generic dark matter framework. We find that including these FSR photons significantly adds to the detection reach of gamma ray searches. We also find that extracting relevant information about dark matter from the spectrum is eased by the FSR photons.

1.4 The Littlest Higgs: A Model of Dark Matter

The hierarchy problem has been known since at least the 1970s [17]. Many theories of physics beyond the Standard Model have been developed that attempt to solve the problem and offer valid descriptions of physics all the way to the Planck scale. Both supersymmetry and technicolor are examples of such attempted Theories of Everything-but-Gravity. However, following the precision electroweak measurements of the 1990s and 2000s, a new problem arose in the form of precision electroweak measurements. These measurements indirectly probe particles with masses greater than about 100 GeV, states that we have been otherwise unable to produce or rule out. The stubborn refusal of nature to deviate from the Standard Model in these tests tells us something about the Terascale: no "generic" new physics is expected below approximately 10 TeV. This tension – between the scale of new physics suggested by the Higgs mass, and the scale of new physics suggested by the precision tests – is called the "little hierarchy". It ruled out or strongly constrained many of the early models for new physics.

The little hierarchy problem also helped draw attention to another line of reasoning. Given that we will be unable to probe energies above 10 TeV for the foreseeable future, all we need is a theory that can describe physics below that scale. In short, rather than try to solve the full hierarchy, one need only solve the little hierarchy problem. Perhaps the best known class of theories to take that approach is the Little Higgs family. These models return to Georgi's concept [18] of the Higgs as a Pseudo-Goldstone Boson of a TeV-scale symmetry breaking. Models within the class are differentiated by the nature of the symmetry breaking that they use.

One of the most popular and elegant Little Higgs model is the Littlest Higgs. Based on the breaking of a global $SU(5)$ to $SO(5)$, the Littlest Higgs was so named because of the small number of new particles – just one triplet scalar, one $SU(2)$ vector and one fermion. Unfortunately, it was shown that this simple model actually failed to solve the little hierarchy problem and was ruled out by electroweak precision measurements [19]. In response to this finding, Cheng and Low [20] added a discrete $\mathbb{Z}_2$ symmetry to the model, called T parity and directly analogous to R parity of supersymmetry. This allowed the new model, the Littlest Higgs with T Parity, to solve the little hierarchy, at the cost of doubling the fermionic content of the theory. It also incidentally provided a dark matter candidate, the lightest T-odd particle.

Whenever a new model is proposed, the immediate question is what that model would look like in present or planned experiments. This allows us to tell what signals are characteristic, so that if nature happens to match something we've already thought of we can find out easily. In chapter 3, we study the family of dark matter detection experiments, and find what we expect to discover if the LHT model is the one chosen by nature. We find that, unfortunately, this model

is good at hiding from our experiments (except in the one channel not reviewed here, see [21]).

1.5 Warped Reggeons: An Unconsidered Model

The final section of this work draws attention to a previously overlooked construction that could potentially be detectable at the LHC. This construction essentially arises from the fusion of two different existing ideas: string theory, and the Randall-Sundrum model of warped extra dimensions. The combination leads to Terascale states that have large spin and potentially strong couplings.

String theory is based on the proposition that the fundamental objects of reality are not 0-dimensional particles, but 1-dimensional strings. From this simple origin, a consistent theory of quantum gravity not only can be constructed, but is inevitable. This fact alone makes string theory very interesting. What is relevant here, however, is the connection between strings and objects that we are more accustomed to handling – particles of definite mass and spin.

Ordinary strings, such as those used in musical instruments, have a range of different vibrational modes. The lowest frequency mode is the fundamental, but there is also an infinite tower of harmonics with steadily increasing frequencies. Quantum strings are no different; but the relation between frequency and energy that was first proposed by Planck implies that the fundamental is the state of lowest mass, with progressively heavier harmonics – called "Reggeons". More precisely, the fundamentals are typically massless[2], while the Reggeons have masses set by the string scale M_S. Finally, we note that if the fundamental mode has spin s, then the nth harmonic has spin $s + n$. String theory thus represents an exception to the general rule that fields of spin greater than 2 are inconsistent, and fields of

[2]Up to low energy symmetry breaking effects, such as the Higgs mechanism.

spin greater than 1 must be gravitational.

The connection between string theory and gravity means that M_S is related to the fundamental scale of gravity. For this reason, we might think that Reggeons would have Planck-scale masses and be completely undetectable. However, string theory also predicts that there are more than four dimensions of spacetime. In 1999, Randall and Sundrum observed that if there is a curved extra dimension, large masses in the five-dimensional Lagrangian need not correspond to massive states in four dimensions [22]. Even though the fundamental scale of gravity (and hence also M_S) are very large in the Randall-Sundrum (RS) model, we might hope to find TeV-scale Reggeons. This possibility has been largely overlooked till now.

The specific element of string theory in RS that we are interested in are Regge partners of the gluon. The lightest such partner would have spin two. Outside of string theory, a spin two field must be a graviton, with very weak couplings to other particles; or a Kaluza-Klein (KK) graviton, with universal couplings. A *strongly-interacting* spin two state with *non-universal* interactions would immediately stand out. In chapter 4, we develop an effective theory that describes such a particle. We start by working in the warped five-dimensional RS spacetime, and then find the four-dimensional action that follows. This theoretical grounding will allow later works to discuss the experimental signals of this model.

CHAPTER 2

ROBUST GAMMA RAY SIGNATURE OF WIMP DARK MATTER

2.1 Introduction

The presence of dark matter in the universe has been firmly established by observations of galaxy rotation curves, large scale structure, and cosmic microwave background radiation. The microscopic nature of dark matter, however, remains unknown. According to the "WIMP hypothesis", dark matter consists of stable, weakly interacting massive particles (WIMPs) with masses roughly within the 10 GeV – 10 TeV range.[1] From the theoretical point of view, this hypothesis is perhaps the most attractive among the proposed candidate theories. There is as yet no direct evidence for its validity; however, it does predict several potentially observable new phenomena. In particular, pairs of WIMPs accumulated in the Milky Way and other galaxies should occasionally annihilate into lighter particles. These lighter particles (or their decay products) can then be found in cosmic rays, providing an "indirect" signature of galactic WIMPs.

The same process, pair annihilation of WIMPs into lighter particles, is also responsible for maintaining the thermal equilibrium between the WIMPs and the rest of the cosmic fluid in the early universe. As a result, the temperature at which the WIMPs decouple depends sensitively on the pair annihilation cross section. This implies that a measurement of the present dark matter density (currently known with an accuracy of about 5% [2, 23]) provides a determination of the annihilation cross section under the conditions prevailing at the time of decoupling. Since WIMPs are non-relativistic at decoupling, it is useful to expand the total

[1] In principle, it remains possible that dark matter consists of microscopic black holes made out of ordinary particles. However, we do not know of a compelling cosmological scenario in which this possibility is realized.

annihilation cross section as a power series in terms of the WIMP relative velocity v:

$$\sigma v = a + bv^2 + \ldots . \tag{2.1}$$

In a generic situation, one of the two terms in this equation dominates the cross section at decoupling ($v^2 \sim 3T/M \sim 0.1$): if s wave annihilation is unsuppressed, the cross section is dominated by the a term, whereas if the annihilation predominantly occurs in a p wave, the b term dominates. Therefore, a measurement of the present dark matter density determines the quantity $\sigma_{\rm an}$ defined in Ref. [24] as the coefficient of the dominant term (i.e. $\sigma_{\rm an} = a$ for s-annihilators and $\sigma_{\rm an} = b$ for p-annihilators). This result, shown in Fig. 2.1, is completely independent of the particle physics model responsible for the WIMPs; the only requirement is that the spectrum be generic, which ensures that co-annihilation processes and resonances are unimportant[2]. Moreover, $\sigma_{\rm an}$ is largely independent of the WIMP mass and spin: roughly, $\sigma^s_{\rm an} = 0.85$ pb for s-annihilators and $\sigma^p_{\rm an} = 7$ pb for p-annihilators.

In this chapter, we extend the model-independent approach of Ref. [24] to predict the fluxes of anomalous cosmic rays due to WIMP annihilation. Indirect WIMP searches predominantly concentrate on three signatures: anomalous high-energy gamma rays, antimatter (positrons, antiprotons, etc.), and neutrinos [26]. While the dark matter density measurement determines the *total* cross section of WIMP annihilation, the distribution between the various possible final states (e^+e^-, $q\bar{q}$, $\gamma\gamma$, W^+W^-, etc.) is not constrained. In order to keep the analysis as model-independent as possible, we focus on the signatures that are least sensitive to this distribution, i.e. those that appear for the maximal number of final states. High-energy neutrinos and positrons are only produced if the WIMPs annihilate directly into $\nu\bar{\nu}$ or e^+e^- pairs, respectively, or (in smaller numbers) if the pri-

[2]The analysis can also be extended to the case of superWIMP dark matter [25].

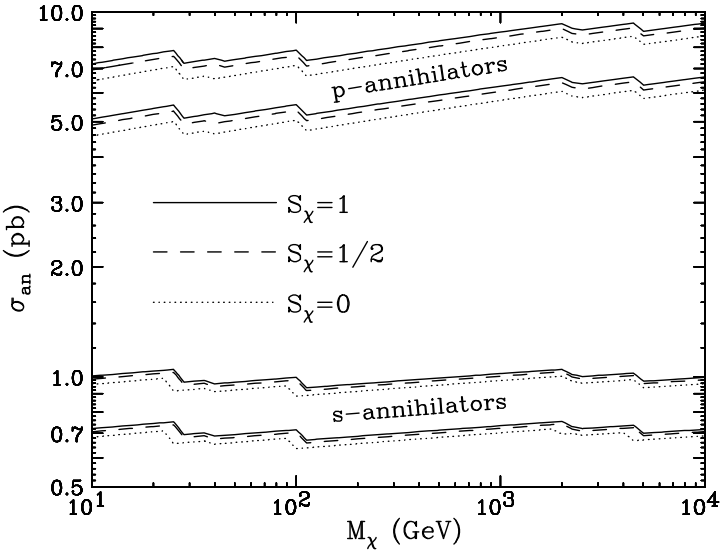

Figure 2.1: Values of the quantity $\sigma_{\rm an}$ allowed at 2σ level as a function of WIMP mass. The lower and upper bands correspond to models where the WIMP is an s- and p-annihilator, respectively. Reproduced from Ref. [24].

mary annihilation final state contains W or Z bosons. Gamma rays, on the other hand, are produced almost independently of the primary final state (with $\nu\bar{\nu}$ being the only exception among two-body final states), and we therefore focus on this signature.

There are several ways in which gamma rays can be produced in WIMP annihilation events. Two well known processes [27, 28, 29, 30, 31, 32, 33] are the direct annihilation to photon-photon or photon-Z pairs ($\chi\chi \to \gamma\gamma, \gamma Z$, where χ denotes the WIMP) and fragmentation following WIMP annihilation into final states containing quarks and/or gluons. While these processes can be easily described within our approach, we will concentrate on another source of photons, the final state radiation (FSR), which has until now received far less attention in the literature[3]. The FSR component of the gamma ray spectrum has several important advantages. First, FSR photons are produced whenever the primary products of

[3]A discussion of the FSR flux in the context of a specific model (universal extra dimensions) and a subset of primary final states (charged leptons) is contained in [34].

WIMP annihilation are charged: e.g. charged leptons, quarks or W bosons. Even if the WIMPs annihilate into ZZ, Zh, or hh pairs, the charged decay products of these particles will contribute to the FSR flux; only the $\nu\bar{\nu}$ channel does not contribute. In contrast, the monochromatic photons are only produced when the WIMPs annihilate into $\gamma\gamma$, γZ or γh pairs; since these processes can only occur at one-loop level [29, 30], only a small fraction of WIMP annihilation events results in these final states. The fragmentation photons are not produced for leptonic final states. In this sense, out of the three components of the photon flux, the FSR component is the most robust. Second, even though the energy spectrum of the FSR photons is broad, in many cases (whenever the WIMPs annihilate directly into charged fermion pairs) the spectrum contains a sharp edge feature at an energy close to the WIMP mass [34]. This feature can be extremely useful in differentiating the WIMP signal from the astrophysical background: while no detailed theoretical understanding of the background is available, it seems very unlikely that such a feature in the relevant energy range can be produced by conventional physics. This is in sharp contrast with the fragmentation photons, whose broad and featureless spectrum makes it difficult to rule out a more conventional astrophysical explanation if an excess over the expected background is observed.

This chapter is organized as follows. In section 2.2 we present the model-independent approximate formulas for the energy spectrum of the FSR photons produced in WIMP annihilation events. We test the accuracy of our analytical results against explicit numerical calculations in specific models. In section 2.3, we use these results to predict the gamma ray fluxes from WIMP dark matter annihilation in the Milky Way. After discussing the relevant backgrounds in section 2.4, we estimate the sensitivity reach of the typical space-based and ground-based gamma ray telescopes in section 2.5. We reserve section 2.6 for our conclusions.

2.2 Final State Radiation in WIMP Annihilation

If a WIMP pair can annihilate into a pair of charged particles, X and $\bar{X}$, annihilation into a three-body final state $X\bar{X}\gamma$ is always also possible. As long as the X particles in the final state are relativistic, the phase space integral diverges in the regime where the photons are approximately *collinear* with either X or $\bar{X}$. Provided that there are no other singular regions, the *total* cross-section will then be dominated by these photons, which are referred to as the "final state radiation" (FSR) photons. In this kinematic regime, the cross section factorizes into the short-distance part, $\sigma(\chi\chi \to X\bar{X})$, and a universal collinear factor:

$$\frac{\mathrm{d}\sigma}{\mathrm{d}x}(\chi\chi \to X\bar{X}\gamma) \approx \frac{\alpha Q_X^2}{\pi}\,\mathcal{F}_X(x)\,\log\left(\frac{s(1-x)}{m_X^2}\right)\sigma(\chi\chi \to X\bar{X}), \tag{2.2}$$

where α is the fine structure constant, Q_X and m_X are the electric charge and the mass of the X particle, s is the center-of-mass energy ($s \approx 4m_\chi^2$ for non-relativistic WIMPs), and $x = 2E_\gamma/\sqrt{s}$. The splitting function $\mathcal{F}$ is independent of the short-distance physics, depending only on the spin of the X particles. If X is a fermion, the splitting function is given by

$$\mathcal{F}_f(x) \;=\; \frac{1+(1-x)^2}{x}, \tag{2.3}$$

whereas if X is a scalar particle,

$$\mathcal{F}_s(x) \;=\; \frac{1-x}{x}. \tag{2.4}$$

If X is a W boson, unfortunately this formalism does not apply. This is because our underlying assumption fails; in the regime where the W boson is relativistic, there are additional infrared singularities in the phase space integral coming from regions where the W is "soft". Both the infrared and collinear divergences are cut off by the W mass, and so they are the same order of magnitude; however, the infrared divergences are model dependent, as we discuss in more detail in

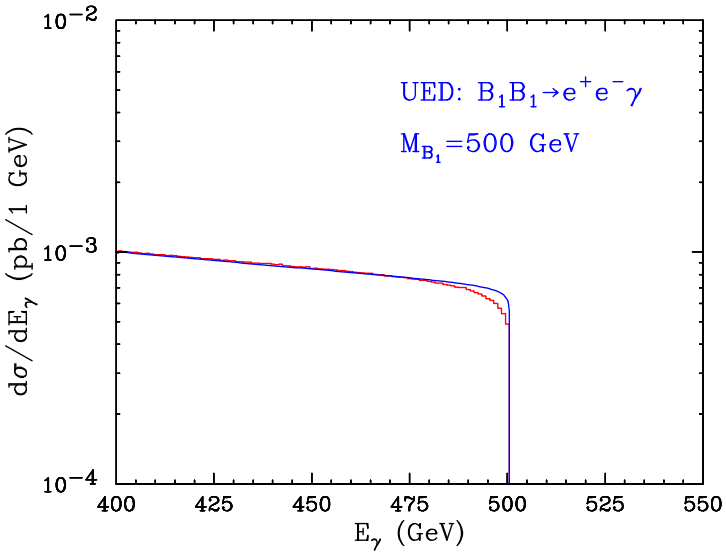

Figure 2.2: Comparison of the photon spectrum obtained by a direct calculation in the UED model with the radius of the extra dimension $R = (499.07\ \text{GeV})^{-1}$ (red histogram) and the spectrum predicted by Eq. (2.2) (blue line) for the case of $B_1B_1 \to e^+e^-\gamma$ annihilation at $\sqrt{s} = 1001$ GeV. The mass of the lightest Kaluza-Klein particle (the first excited mode B_1 of the hypercharge gauge boson) is 500 GeV.

section 3.4. The factorization of Eq. (2.2) does not occur and we can make no definite predictions about fluxes.

Does Eq. (2.2) provide a good approximation of the FSR photon spectrum from galactic WIMP annihilation in a realistic situation? To address this question, we compare the FSR photon spectrum obtained by a direct calculation in a specific model with the prediction of Eq. (2.2) with the appropriate parameters. For this comparison, we have used the minimal universal extra dimension (UED) model [35]. We computed the cross section of the process $B_1B_1 \to e^+e^-\gamma$ using the `CompHEP` package [36]. (B_1, the first Kaluza-Klein excitation of the hypercharge gauge boson, plays the role of the WIMP dark matter candidate in the UED model [37, 38].) We have fixed the radius of the extra dimension to be $R = (499.07\ \text{GeV})^{-1}$, corresponding to a B_1 mass of 500 GeV. While Eq. (2.2)

holds for any WIMP momentum, we have chosen the colliding WIMPs to be non-relativistic ($\sqrt{s}$ = 1001 GeV), to approximate the kinematics typical of galactic WIMP collisions. The result of the direct cross section calculation is shown by the red histogram in Fig. 2.2. The blue (continuous) line corresponds to the prediction of Eq. (2.2) with the same $\sqrt{s}$ = 1001 GeV, $X = e$, and the appropriate value of $\sigma(\chi\chi \to e^+e^-) \approx 5.67$ pb. The good agreement between the line and the histogram proves the validity of the collinear approximation for the total cross section. Remarkably, the spectrum has a sharp step-like edge feature at the endpoint, $E \to M_\chi$. The origin of the feature is obvious from Eqs. (2.2) and (2.3): ignoring the x dependence of the logarithm in Eq. (2.2), which only has a small effect on the spectrum, it is easy to see that the differential cross section approaches a non-zero constant value at $x \to 1$, whereas it obviously has to vanish for $x > 1$. Since it is difficult to imagine an astrophysical process providing a similarly sharp endpoint feature at the relevant energy scales, observing the step would provide a strong evidence for WIMPs [34].

If the primary product of WIMP annihilation is a lepton pair (e^+e^-, $\mu^+\mu^-$), the FSR mechanism discussed above is the dominant source of secondary photons. On the other hand, if the WIMPs annihilate into quark-antiquark or $\tau^+\tau^-$ pairs, an additional contribution to the secondary photon flux arises from hadronization and fragmentation. This contribution is dominated by the decays of neutral pions. While the fragmentation photons are more numerous than the FSR photons, they tend to be softer. The spectrum close to the endpoint is still dominated by the FSR component, and can be predicted using Eq. (2.2), with an appropriate choice of the "effective" value of m_X in the logarithm. This is illustrated in Figure 3, which shows the secondary photon fluxes from a primary u quark of 250 GeV energy. The upper (blue) histogram shows the total γ spectrum, including both fragmentation

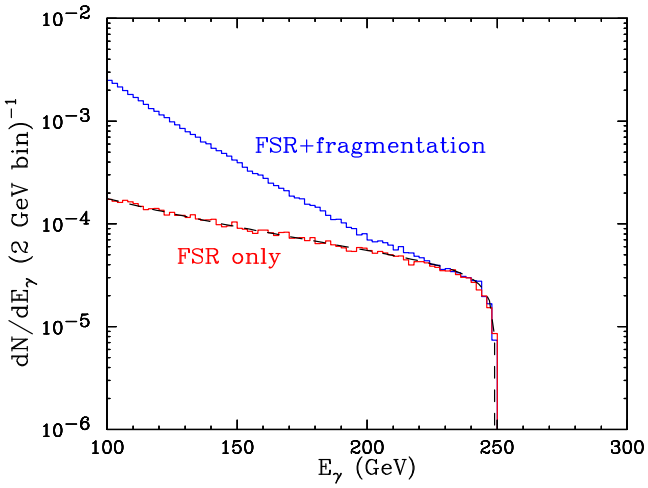

Figure 2.3: Photon spectrum produced by final state radiation and fragmentation of a primary u quark with an energy of 250 GeV. The histograms represent PYTHIA predictions for the total photon flux (blue) and the final state radiation flux alone (red). The black dashed line represents the prediction of Eq. (2.2).

and FSR components, calculated using the PYTHIA package [39]; the lower (red) histogram shows the PYTHIA prediction for the FSR flux alone. The total flux above about 225 GeV ($x = 0.9$) is dominated by the FSR component, and exhibits the expected edge feature. The FSR spectrum predicted by PYTHIA is consistent with the prediction of Eq. (2.2); however, to obtain a good fit, the quantity m_u in the logarithm should be replaced with the "effective mass" $m_u^{\rm eff}$, which takes into account soft gluon radiation and other effects of strong interactions. The black dashed line in Fig. 2.3 represents the prediction of Eq. (2.2) using the best-fit value of $m_u^{\rm eff} = 20$ GeV. An excellent fit to the PYTHIA output is obtained. We conclude that the sharp endpoint with a shape given by Eqs. (2.2), (2.3) exists whenever the primary WIMP annihilation products are charged fermions: it does not matter whether they are leptons or quarks.

Based on the above discussion, we will replace the bare mass with the "effective" mass whenever we apply Eq. (2.2) to light quarks; this substitution will be implicit

for the rest of the chapter. For simplicity, we will assume $m_u^{\rm eff} = m_d^{\rm eff} = m_s^{\rm eff} = 0.2$ GeV, since the scale for the effective mass is set by the QCD confinement scale. In reality, the situation is more complicated, since the effective mass may depend on the energy and flavor of the primary quark. Note also that the values needed to fit the `PYTHIA` predictions are substantially higher than $\Lambda_{\rm QCD}$, but the interpretation of this result is not clear due to large uncertainties inherent in the showering algorithm and the fit. However, since the dependence on the mass is logarithmic, changing $m^{\rm eff}$ has only a moderate effect on the photon flux predictions. We have confirmed that replacing our simple assumption with an energy-dependent value of $m^{\rm eff}$ based on a fit to `PYTHIA` predictions does not substantially affect any of the estimates of photon fluxes and telescope sensitivities made below.

Unfortunately, a model-independent prediction of the sharp endpoint is not valid if the primary annihilation products of the WIMP are bosons. We have already noted the model-dependent nature of the flux from $W^+W^-\gamma$ final states. Annihilation to scalars, such as the charged Higgs bosons in the minimal supersymmetric standard model (MSSM), does have the model-independent factorization, but according to Eq. (2.4), $\lim_{x\to 1} \mathcal{F}_s(x) = 0$. Because of this, the flux near the endpoint is dominated by the model-dependent non-collinear contributions, and no firm model-independent prediction of the shape of the endpoint spectrum is possible.

FSR photons will also be produced when the WIMPs annihilate into neutral, unstable particles, whose decay products are charged: in the Standard Model, these could be ZZ, Zh, or hh pairs. For example, consider the process $\chi\chi \to ZZ$ with the subsequent Z decay into charged fermions ($\ell^+\ell^-$ or $q\bar{q}$), which in turn emit an FSR photon. The photon spectrum in the Z rest frame is given by Eq. (2.2), with the substitutions $s \to m_Z^2$ and $\sigma(\chi\chi \to X\bar{X}) \to 2\sigma(\chi\chi \to ZZ)\,\mathrm{Br}(Z \to X\bar{X})$.

Performing the boost to return to the laboratory frame yields

$$\frac{\mathrm{d}\sigma}{\mathrm{d}x} = \frac{\alpha}{\pi}\,\sigma(\chi\chi \to ZZ)\,\Psi_Z(x), \tag{2.5}$$

where

$$\Psi_Z = 2\theta(m_\chi - m_Z)\,\frac{1}{x}\left[1 + \frac{1-x}{v} - \frac{2x^2}{v(v+1)} + \frac{2x}{v}\log\frac{2xv}{1+v}\right] \times \sum_X Q_X^2\,\mathrm{Br}(Z \to X\bar{X})\,\log\left(\frac{m_Z^2}{m_X^2}\right). \tag{2.6}$$

In this equation, $x = E_\gamma/m_\chi$, $v = \sqrt{1 - m_Z^2/m_\chi^2}$ is the velocity of the Z boson, and the sum runs over all the charged fermion pairs that Z can decay into. We have ignored the corrections that are not enhanced by $\log(m_Z^2/m_X^2)$. If $m_\chi \gg m_Z$, the Z bosons are relativistic and the spectrum is given by

$$\Psi_Z = 2\,\frac{2 - x + 2x\log x - x^2}{x}\,\sum_X Q_X^2\,\mathrm{Br}(Z \to X\bar{X})\,\log\left(\frac{m_Z^2}{m_X^2}\right). \tag{2.7}$$

For the Zh and hh final states, we obtain expressions analogous to (2.5). The corresponding functions Ψ_{Zh} and Ψ_h can be easily obtained from Eq. (2.6) by replacing the parameters of the Z boson with those of the Higgs where appropriate. In particular, in the limit $m_\chi \gg m_h$ we obtain

$$\Psi_{hZ}(x) = \frac{2 - x + 2x\log x - x^2}{x}\,\sum_X Q_X^2\left[\mathrm{Br}(Z \to X\bar{X})\,\log\left(\frac{m_Z^2}{m_X^2}\right) + \mathrm{Br}(h \to X\bar{X})\,\log\left(\frac{m_h^2}{m_X^2}\right)\right], \tag{2.8a}$$

$$\Psi_h(x) = 2\,\frac{2 - x + 2x\log x - x^2}{x}\,\sum_X Q_X^2\,\mathrm{Br}(h \to X\bar{X})\,\log\left(\frac{m_h^2}{m_X^2}\right). \tag{2.8b}$$

These expressions include only fermionic decays of the Higgs; we assumed that the Higgs is too light to decay into W or Z pairs. The analysis can be straightforwardly generalized to include these decays. Unfortunately, it is clear from the above equations that the spectrum of FSR photons produced in Z/h decays does not

possess a sharp endpoint; instead, it approaches 0 gradually in the $x \to 1$ limit. This means that the non-universal, model-dependent contributions may become dominant near the endpoint.

2.3 FSR Photon Flux Estimates

In general, the differential γ flux from WIMP annihilations observed by a telescope can generally be written as

$$\frac{\mathrm{d}^2\Phi}{\mathrm{d}E\mathrm{d}\Omega} = \left(\sum_i \left\langle \frac{\mathrm{d}\sigma_i}{\mathrm{d}E} v \right\rangle B_i\right) \frac{1}{4\pi m_\chi^2} \int_\Psi \rho^2(l) dl, \tag{2.9}$$

where the sum runs over all possible annihilation channels containing photons, and σ_i and B_i are the annihilation cross section and the number of photons per event in a given channel, respectively. The average is over the thermal ensemble of WIMPs in the galaxy. The integral is computed along a line of sight in the direction parametrized by $\Psi = (\theta, \phi)$, and $\rho(l)$ is the mass density of WIMP dark matter at a distance l from the observer. To obtain the FSR photon flux, we substitute the differential cross section for the final states containing such photons, given in Eqs. (2.2) and (2.5), into Eq. (2.9), and take into account that $B_i = 1$ for these final states. We also define $\mathcal{F}_W \equiv \mathcal{F}_s$; this is inspired by the Goldstone boson equivalence theorem, and (since $\mathcal{F}_s(x) \to 0$ as $x \to 1$) should be a conservative estimate of the flux at the endpoint. We obtain

$$\begin{aligned}\frac{\mathrm{d}^2\Phi_{\mathrm{FSR}}}{\mathrm{d}E\mathrm{d}\Omega} = \Big[\sum_X \theta(m_\chi - m_X) Q_X^2 \langle\sigma_X v\rangle \mathcal{F}_X(x) \log\left(\frac{4m_\chi^2(1-x)}{m_X^2}\right) \\ + \langle\sigma_Z v\rangle \Psi_Z(x) + \langle\sigma_{hZ} v\rangle \Psi_{hZ}(x) + \langle\sigma_h v\rangle \Psi_h(x)\Big] \times \frac{\alpha}{\pi} \frac{1}{4\pi m_\chi^3} \int_\Psi \rho^2 dl,\end{aligned} \tag{2.10}$$

where $x = E/m_\chi$. The sum runs over all possible two-body final states with charged particles X and $\bar{X}$, and $\sigma_X = \sigma(\chi\chi \to X\bar{X})$. To simplify notation, we have also defined $\sigma_Z = \sigma(\chi\chi \to ZZ)$, $\sigma_h = \sigma(\chi\chi \to hh)$, and $\sigma_{hZ} = \sigma(\chi\chi \to Zh)$.

In the spirit of Ref. [24], we define the total WIMP annihilation cross section, $\sigma_0 = \sigma(\chi\chi \to \text{anything})$, and the "annihilation fractions" for the two-particle final states, $\kappa_X = \langle \sigma_X v \rangle \,/\, \langle \sigma_0 v \rangle$. (Note that $\sum_X \kappa_X = 1$, up to a small correction due to the contribution of the processes with three or more particles in the final state.) With these definitions, the FSR flux can be written as

$$\frac{\mathrm{d}^2\Phi_{\mathrm{FSR}}}{\mathrm{d}E\mathrm{d}\Omega} \;=\; \frac{\alpha}{\pi}\frac{1}{4\pi m_\chi^3}\,\langle\sigma_0 v\rangle\,\mathcal{G}(x)\int_\Psi \rho^2 dl, \tag{2.11}$$

where

$$\mathcal{G}(x) = \sum_X \theta(m_\chi - m_X) Q_X^2 \kappa_X \mathcal{F}_X(x) \log\left(\frac{4m_\chi^2(1-x)}{m_X^2}\right) + \kappa_Z \Psi_Z(x) \,+\, \kappa_{hZ}\Psi_{hZ}(x) \,+\, \kappa_h \Psi_h(x). \tag{2.12}$$

Notice that almost all WIMP annihilation channels, with the exception of $\nu\bar{\nu}$ and gg final states, contribute to the FSR photon flux; only the details of the flux depend on the distribution of the cross section among the channels.

The photon flux prediction is subject to large uncertainties in the distribution of dark matter in the galaxy. These uncertainties are conventionally parametrized by a dimensionless function

$$\bar{J}(\Psi, \Delta\Omega) \equiv \frac{1}{8.5\ \mathrm{kpc}}\left(\frac{1}{0.3\ \mathrm{GeV/cm}^3}\right)^2 \frac{1}{\Delta\Omega}\int_{\Delta\Omega} d\Omega \int_\Psi \rho^2 dl, \tag{2.13}$$

where $\Delta\Omega$ denotes the field of view of a given experiment. The values of $\bar{J}$ depend on the galactic halo model. The optimal line of sight for WIMP searches is towards the galactic center; in this case, the uncertainty is particularly severe due to the possibility of a sharp density enhancement at the center. At $\Delta\Omega = 10^{-3}$ sr, for example, typical values of $\bar{J}$ range from 10^3 for the NFW profile [40] to about 10^5 for the profile of Moore et.al. [41], and can be further enhanced by a factor of up to 10^2 due to the effects of adiabatic compression [42].

Using Eq. (2.11) and the above definition of $\bar{J}$ yields the FSR flux integrated over the field of view:

$$\frac{\mathrm{d}\Phi_{\mathrm{FSR}}}{\mathrm{d}E} = \Phi_0 \left(\frac{\langle\sigma_0 v\rangle}{1\ \mathrm{pb}}\right) \left(\frac{100\ \mathrm{GeV}}{m_\chi}\right)^3 \mathcal{G}(x)\bar{J}(\Psi, \Delta\Omega)\Delta\Omega, \tag{2.14}$$

where $\Phi_0 = 1.4 \times 10^{-14}\ \mathrm{cm}^{-2}\ \mathrm{sec}^{-1}\ \mathrm{GeV}^{-1}$.

While Eq. (2.14) provides a complete description of the FSR photon spectrum, the shape and the normalization of the flux for the most energetic photons (close to $x = 1$) is of particular interest due to the possibility of the observable edge feature. In this region, the flux is dominated by the photons radiated by fermion products of WIMP annihilation. Neglecting the x dependence in the logarithm, whose only effect is to slightly smooth out the edge in the region $1 - x \ll 1$, the flux is approximately given by

$$\frac{\mathrm{d}\Phi_{\mathrm{FSR}}}{\mathrm{d}E} = \Phi_0\, g \left(\frac{100\ \mathrm{GeV}}{m_\chi}\right)^3 \mathcal{F}_f(x)\bar{J}(\Psi, \Delta\Omega)\Delta\Omega. \tag{2.15}$$

Here, the dimensionless parameter g contains all the information about the primary WIMP annihilation processes:

$$g = \left(\frac{\langle\sigma_0 v\rangle}{1\ \mathrm{pb}}\right) \sum_f Q_f^2 \kappa_f \log\left(\frac{4m_\chi^2}{m_f^2}\right), \tag{2.16}$$

where the sum runs over all kinematically accessible fermionic final states. Depending on the microscopic model giving rise to the WIMP, the parameter g can vary between 0 (if, for example, the WIMPs can only annihilate into neutral states) and about 35 in the most favorable case of very heavy WIMPs annihilating into electron-positron pairs in an s wave.

The normalization of the FSR photon flux is determined by the quantity $\langle\sigma_0 v\rangle$. As we argued in section 2.1, the measurement of the present cosmological abundance of dark matter determines the total WIMP annihilation cross section at decoupling ($v^2 \sim 0.1$). A typical relative velocity of galactic WIMPs is much

smaller, $v \sim 10^{-3}$. In models where the s-wave annihilation is unsuppressed, the quantity σv is velocity-independent at low v, allowing us to make a robust model-independent prediction:

$$\langle \sigma_0 v \rangle \;=\; \sigma_{\rm an}^{s} \;\approx\; 0.85 \text{ pb}. \tag{2.17}$$

If, on the other hand, the cross section at decoupling is dominated by the b term, no firm prediction for the quantity $\langle \sigma_0 v \rangle$ is possible: even a small a term, if present, may become dominant for galactic WIMPs due to the low value of v. If no a term is present, we estimate $\langle \sigma_0 v \rangle = \sigma_{\rm an}^{p} v^2 \sim 10^{-5}$ pb; a larger cross section is possible if an a term is present, with the upper bound provided by Eq. (2.17). Given the uncertainty present in the p-annihilator case, we will use the s-annihilator WIMP examples to illustrate our approach in the remainder of this chapter.

2.4 Background Fluxes

Estimating the sensitivity of WIMP searches also requires the knowledge of background fluxes. The searches for anomalous cosmic γ rays are conducted both by space-based telescopes and by ground-based atmospheric Cerenkov telescopes (ACTs). The space-based telescopes observe photons directly, and the only source of irreducible background in this case is the cosmic γ rays of non-WIMP origin. The ACTs observe the Cerenkov showers created when a cosmic ray strikes the upper atmosphere, and are subject to the additional backgrounds of Cerenkov showers from leptonic and hadronic cosmic rays. In our estimates of the experiments' sensitivities, we will use simple power-law extrapolations of the background fluxes measured at low energies. For the non-WIMP photon flux, we use [31]

$$\frac{{\rm d}^2\Phi_{\gamma,{\rm bg}}}{{\rm d}E{\rm d}\Omega} = 4\times 10^{-12}\, N_0(\Psi)\, \left(\frac{100 \text{ GeV}}{E}\right)^{2.7} \text{ cm}^{-2}\text{s}^{-1}\text{GeV}^{-1}\text{sr}^{-1}, \tag{2.18}$$

where the function N_0 describes the angular distribution of the photons (an approximation is given in Refs. [31, 43].) In our analysis, we will make the simplifying replacement $N_0(\Psi) \to \max N_0 \approx 89$. This generally overestimates the background; however, the effect is small, especially for the line of sight close to the direction to the galactic center. The non-photonic background flux for the ACTs is estimated as [31]

$$\frac{\mathrm{d}^2\Phi_{\mathrm{lep}}}{\mathrm{d}E\mathrm{d}\Omega} = 1.73 \times 10^{-8} \left(\frac{100\ \mathrm{GeV}}{E}\right)^{3.3}\ \mathrm{cm}^{-2}\mathrm{s}^{-1}\mathrm{GeV}^{-1}\mathrm{sr}^{-1}; \tag{2.19a}$$

$$\frac{\mathrm{d}^2\Phi_{\mathrm{had}}}{\mathrm{d}E\mathrm{d}\Omega} = 4.13 \times 10^{-8}\, \epsilon_{\mathrm{had}} \left(\frac{100\ \mathrm{GeV}}{E}\right)^{2.7}\ \mathrm{cm}^{-2}\mathrm{s}^{-1}\mathrm{GeV}^{-1}\mathrm{sr}^{-1}, \tag{2.19b}$$

where ϵ_{had} is the telescope-dependent probability that a hadronic Cerenkov shower will be misidentified as a photonic shower, normalized so that it is equal to one for the Whipple telescope (see Ref. [31]).

It is worth emphasizing that the fluxes (2.18) and (2.19) are merely extrapolations; in both cases the background cannot be accurately predicted from theory. While we will use these fluxes in our estimates, one should keep in mind that there are large uncertainties associated with them. This is why merely observing a flux enhancement is in general not sufficient to provide convincing evidence for WIMPs; a discovery of the step-like edge feature in the spectrum would greatly strengthen the case.

2.5 Sensitivity Reach of Future Telescopes

To illustrate the prospects for observational discovery of the FSR edge, we will use two toy scenarios. In the first scenario, the annihilation fractions for two-body final states are taken to scale as $Y^4 N_c$, where Y is the hypercharge of the final state particles, and $N_c = 3$ for quarks and 1 for other states[4]. An explicit example

[4]Note that Eq. (2.2) can be applied to polarized final states. Therefore, accounting for the different hypercharge of left-handed and right-handed fermions is straightforward.

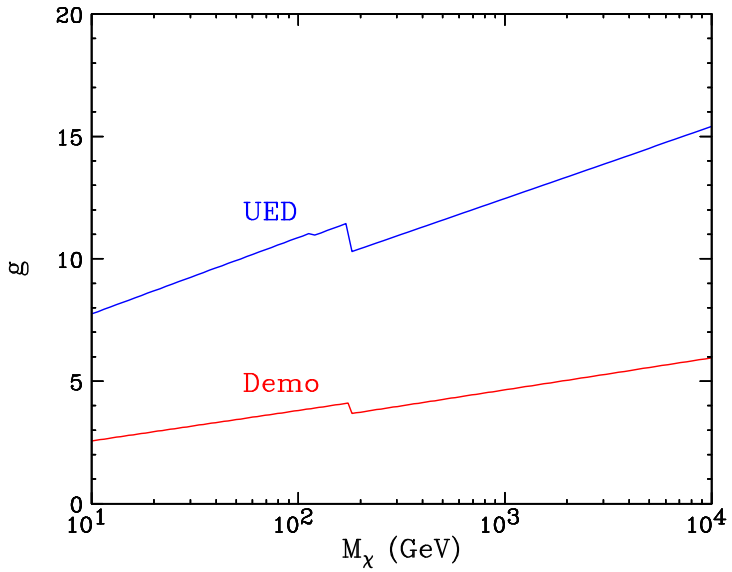

Figure 2.4: The quantity g, defined in Eq. (2.16), as a function of the WIMP mass m_χ, in the UED scenario (blue line) and the "democratic" scenario (red line). In the UED scenario, the annihilation fractions for two-body final states are taken to scale as $Y^4 N_c$, where Y is the hypercharge of the final state particles, and $N_c = 3$ for quarks and 1 for other states. In the second scenario, the annihilation fractions for all kinematically accessible two-fermion final states are equal (up to a factor of N_c).

in which this scenario is realized is provided by the model with universal extra dimensions [35], and we will therefore label it as UED. In the second scenario, the WIMPs do not annihilate into bosonic final states, while the annihilation fractions κ_i for all kinematically accessible fermion final states are equal (up to a factor of N_c). We will refer to this scenario as "democratic". In both scenarios, we assume that the WIMPs can only annihilate into Standard Model particles, and use a Higgs mass of 120 GeV. The values of the quantity g, defined in Eq. (2.16), as a function of the WIMP mass m_χ, in the two scenarios under consideration are shown in Figure 2.4. In both cases, we assume that WIMPs are s-annihilators, with the total annihilation cross section given by Eq. (2.17).

The magnitude of the FSR photon flux in each scenario is easily estimated

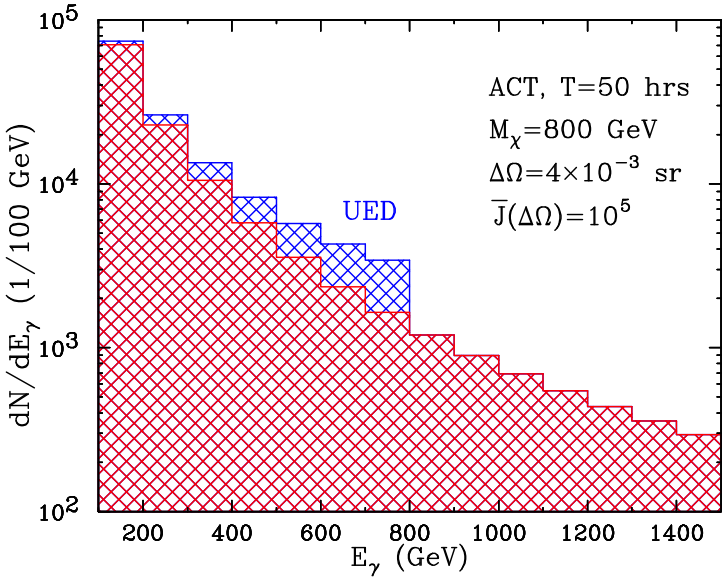

Figure 2.5: The number of signal (blue) and background (red) events at a representative atmospheric Cerenkov telescope with a collection area given in Eq. (2.20), an exposure time $T = 50$ hrs, and a field of view $\Delta\Omega = 4 \times 10^{-3}$ sr. The signal is computed assuming the UED scenario with an 800 GeV WIMP and a galactic model with $\bar{J}(\Delta\Omega) = 10^5$.

using Eq. (2.14). As an example, Fig. 2.5 shows the number of events per 100 GeV bin expected to be observed at an ACT with an exposure time $T = 50$ hrs, and a field of view $\Delta\Omega = 4 \times 10^{-3}$ sr. (These parameters are similar to those of the VERITAS [44] and HESS [45] telescope arrays.) The effective collection area of the ACTs depends on the photon energy; in our analysis, we use an analytic fit to the effective area of the VERITAS array shown in Fig. 4, Ref. [44]:

$$A(E) \;=\; 1.2 \exp\left[-0.513\left(\log\frac{E}{5\ \mathrm{TeV}}\right)^2\right] \times 10^9\ \mathrm{cm}^2. \qquad (2.20)$$

We assumed the UED scenario with an 800 GeV WIMP. We have further assumed $\bar{J}(\Delta\Omega) = 10^5$, which is the case in the NFW galactic profile [40] with an adiabatic compression enhancement factor of about a 100 [42], or in the profile of Moore et. al. [41] with no adiabatic compression. It is clear from the figure that the edge

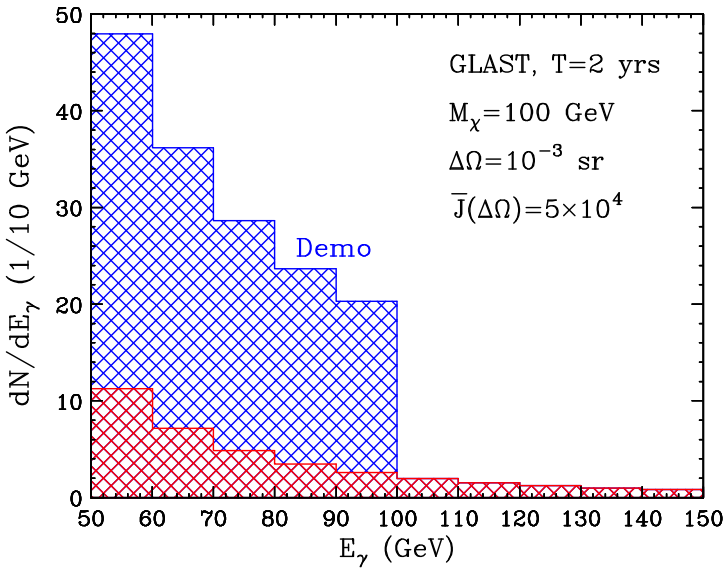

Figure 2.6: The number of signal (blue) and background (red) events at the Fermi/GLAST space telescope (collection area $A = 10000$ cm^2, exposure time $T = 2$ years, field of view $\Delta\Omega = 10^{-3}$). The signal is computed assuming the "democratic" scenario with a 100 GeV WIMP and a galactic model with $\bar{J}(\Delta\Omega) = 5 \times 10^4$.

feature due to the FSR photon emission following WIMP annihilation should be easily discernible in this data set.

An analogous plot illustrating the observability of the edge feature at the Fermi/GLAST[5] space telescope [46] is shown in Fig. 2.6. We have assumed a collection area $A = 10000$ cm^2, an exposure time $T = 2$ years, and a field of view[6] $\Delta\Omega = 10^{-3}$ sr. We have further assumed the "democratic" scenario with a 100 GeV WIMP, and a galactic model with $\bar{J}(\Delta\Omega) = 5 \times 10^4$. Again, the edge feature would be easily discernible for these parameters.

[5]The telescope was known by the acronym GLAST till shortly before launch, when it was rechristened Fermi.

[6]The field of view at Fermi can be varied between about 5×10^{-6} sr (the angular resolution of the telescope) and 2.3 sr (the full field of view). While larger values of $\Delta\Omega$ are advantageous from the point of view of statistics, focusing narrowly on the galactic center can lead to improved signal/background ratio if the dark matter density has a sharp peak at the center. However, reducing $\Delta\Omega$ substantially below 10^{-3} typically results in insufficient statistics with the assumed collection area and exposure time.

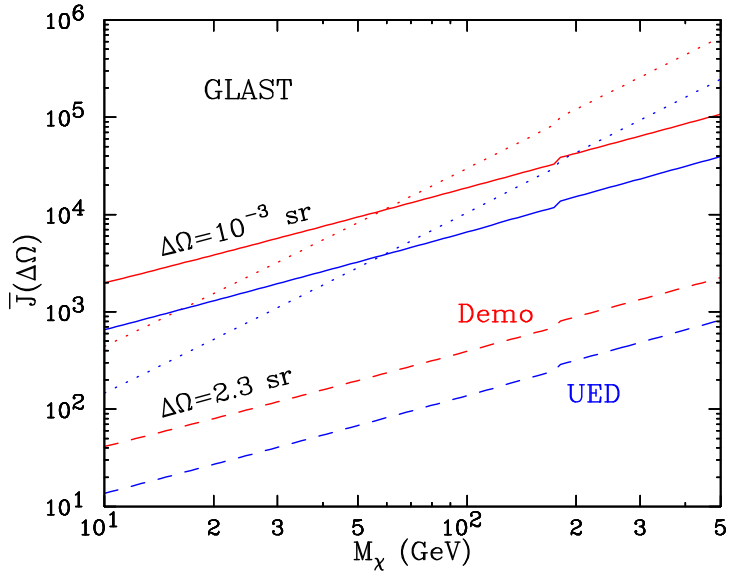

Figure 2.7: The minimal value of $\bar{J}$ required for the discovery of the edge feature due to WIMP annihilation at the Fermi/GLAST telescope (collection area $A = 10000$ cm^2, exposure time $T = 2$ years, energy resolution $\delta = 10\%$), for the field of view $\Delta\Omega = 2.3$ sr (dash lines) and $\Delta\Omega = 10^{-3}$ sr (solid lines show the minimum value of $\bar{J}$ for which a 3σ deviation from the background occurs, while dotted lines represent the minimum value of $\bar{J}$ for which the edge bin contains at least 10 signal events.)

In addition to the FSR photon flux plotted in Figs. 2.5 and 2.6, photons are also expected to be produced both by quark fragmentation and the loop-induced $\chi\chi \to \gamma\gamma, \gamma Z, \gamma h$ annihilation processes. As we showed in section 2.2, the fragmentation component is subdominant to the FSR flux near the endpoint, and therefore will not affect the edge feature. However, this component may dominate the flux at lower energies, in which case the edge feature would be accompanied by a sharp change in the slope of the spectrum. The monochromatic photon flux from $\chi\chi \to \gamma\gamma$ will contribute to the signal in the bin containing $E_\gamma = m_\chi$. This contribution is also generally subdominant since $\sigma(\chi\chi \to \gamma\gamma)/\sigma(\chi\chi \to X\bar{X}\gamma) \sim \alpha \sim 10^{-2}$. If present, the line contribution will make the edge feature even sharper than our predictions based on the FSR flux alone.

To observe the FSR edge feature in the photon spectrum, the experiments need to search for a large drop in the number of events between two neighboring energy bins. A statistically significant discovery requires that the drop be larger than what can be expected from a fit to the rest of the spectrum. While a detailed analysis of the reach of any particular telescope is beyond the scope of this work, a simple estimate of the reach can be obtained as follows. Consider the energy bin $[m_\chi(1-\delta), m_\chi(1+\delta)]$, where δ is the fractional energy resolution of a telescope[7]. The number of signal events in this bin is

$$N_{\rm sig} \approx 1.4 \times 10^{-12}\, g\, \delta \left(\frac{100\ {\rm GeV}}{m_\chi}\right)^2 \bar{J}(\Delta\Omega)\, A_{\rm cm^2} T_{\rm sec}\, \Delta\Omega\,, \tag{2.21}$$

where $A_{\rm cm^2}$ and $T_{\rm sec}$ are the area of the telescope in $\rm cm^2$ and the collection time in sec, respectively. Assuming that the fit to the high energy part of the spectrum ($E > m_\chi$) produces an estimate of the background consistent with Eqs. (2.18) and (2.19), the expected number of background events $N_{\rm bg}$ in the energy bin $[m_\chi(1-\delta), m_\chi(1+\delta)]$ can be computed. Requiring

$$N_{\rm sig} \geq 3\sqrt{N_{\rm bg}} \tag{2.22}$$

for a statistically significant discovery of the step, we find that a discovery at a space-based telescope is possible if

$$g\bar{J}(\Delta\Omega) \;\geq\; 6 \times 10^8\, (A_{\rm cm^2} T_{\rm sec} \delta \Delta\Omega)^{-1/2} \left(\frac{m_\chi}{100\ {\rm GeV}}\right)^{1.15}. \tag{2.23}$$

This condition, together with the "minimal signal" requirement,

$$N_{\rm sig} \geq 10, \tag{2.24}$$

[7]The assumption that the bin is centered at m_χ represents the worst-case scenario for the reach; the reach can be improved by up to a factor of $\sqrt{2}$ by optimizing the binning to maximize the significance. In addition, our estimates ignore the possible monochromatic photon flux from $\chi\chi \to \gamma\gamma$, which would appear in the same bin. The fragmentation photon flux, which is subdominant to the FSR component but could still enhance the signal, is also ignored. In this sense, our reach estimates are rather conservative.

can be used to determine the reach of the Fermi telescope. The reach is shown in Fig. 2.7, where we plot the minimal value of $\bar{J}$ required for the discovery, as a function of the WIMP mass m_χ, in the UED and "democratic" scenarios. The reach is shown for two values of $\Delta\Omega$: 2.3 sr, corresponding to utilizing the full field of view of the telescope, and 10^{-3} sr, corresponding to focusing narrowly on the galactic center. (We assume the collection area $A = 10000$ cm^2, the exposure time $T = 2$ years, and the energy resolution $\delta = 10\%$.) For $\Delta\Omega = 2.3$ sr, the minimal signal criterion (2.24) is always weaker than the 3σ requirement in Eq. (2.22), and we do not plot it. For $\Delta\Omega = 10^{-3}$ sr, on the other hand, the minimal signal criterion (2.24) dominates the reach determination for large masses; the dotted lines in Fig. 2.7 indicate the minimal value of $\bar{J}$ for which it is satisfied. Note that, while the reach in terms of $\bar{J}$ is clearly higher for the larger $\Delta\Omega$ due to higher statistics, the values of $\bar{J}$ in most galactic halo models are substantially enhanced at low values of $\Delta\Omega$.

The discovery reach for an ACT, assuming that the background is dominated by leptonic showers[8], is given by

$$g\bar{J}(\Delta\Omega) \geq 4 \times 10^9 (A_{\rm cm^2} T_{\rm sec} \delta \Delta\Omega)^{-1/2} \left(\frac{m_\chi}{100 \text{ GeV}}\right)^{0.85}. \qquad (2.25)$$

To estimate the discovery potential of the VERITAS and HESS ACT arrays, consider an ACT with the collection area given in Eq. (2.20), an exposure time $T = 50$ hrs, and the energy resolution $\delta = 15\%$. The discovery reach for such a telescope is shown in Fig. 2.8. Dashed contours correspond to an experiment utilizing the full field of view of the ACT, assumed to be 4×10^{-3} sr. Solid contours indicate the reach of an experiment focusing narrowly on the galactic center, with the angular resolution of 0.07° corresponding to $\Delta\Omega = 5 \times 10^{-6}$ sr. (Galactic halo model predictions for $\bar{J}$ for this value of $\Delta\Omega$ range from about 10^4 to a few$\times 10^8$.) In the latter

[8]The leptonic background is dominant over the entire range of WIMP masses of interest, provided that $\epsilon_{\rm had} \lesssim 0.1$.

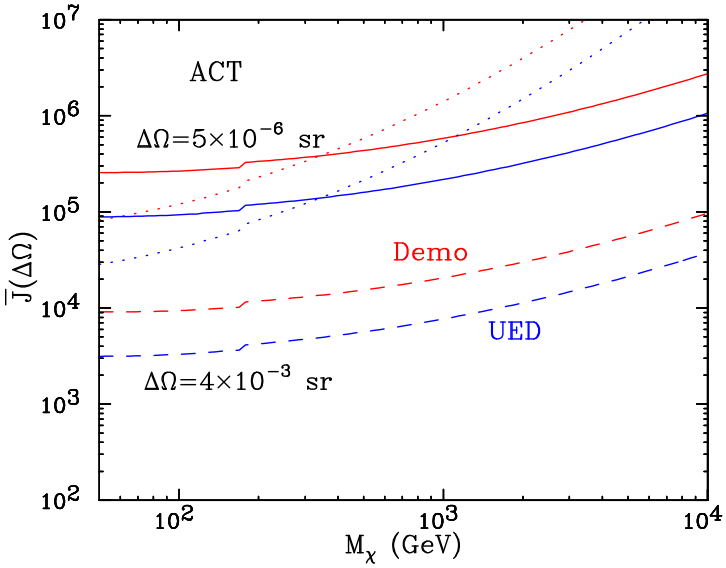

Figure 2.8: The minimal value of $\bar{J}$ required for the discovery of the edge feature due to WIMP annihilation at a representative atmospheric Cerenkov telescope (collection area given in Eq. (2.20), exposure time $T = 50$ hrs, energy resolution $\delta = 15\%$), for the field of view $\Delta\Omega = 4 \times 10^{-3}$ sr (dash lines) and $\Delta\Omega = 5 \times 10^{-6}$ sr (solid lines show the minimum value of $\bar{J}$ for which a 3σ deviation from the background occurs, while dotted lines represent the minimum value of $\bar{J}$ for which the edge bin contains at least 10 signal events.)

case, the minimal signal requirement (2.24) dominates the reach determination for large m_χ, and is shown in the figure using the dotted lines.

Given a model for galactic halo profile and a set of assumptions about the relevant annihilation fractions, Figs. 2.7 and 2.8 can be used to estimate the reach of the telescopes in terms of the highest value of the WIMP mass for which the edge feature can be observed. The estimate indicates that the prospects for observing the feature are quite good. For example, with a rather conservative assumption $\bar{J}(\Delta\Omega = 4 \times 10^{-3}\,\mathrm{sr}) = 10^4$, an ACT with the parameters used in our study would be able to discover the feature for m_χ up to about 2 TeV in the UED model, covering the entire range where the model is cosmologically consistent [38].

Comparing Figs. 2.7 and 2.8 indicates that the VERITAS and HESS arrays have a sensitivity comparable to Fermi. The experiments are complementary in terms of the range of WIMP masses that can be covered: the ACT will be sensitive to values of m_χ between about 50 GeV and 10 TeV, while Fermi can observe the FSR edge if m_χ is in the 10 – 250 GeV mass range. We conclude that both space based telescopes and ACTs could provide sufficient sensitivity in the near future to discover the edge feature in the γ flux if WIMPs are s-annihilators and the galactic halo profile and annihilation fractions are favorable.

Since the edge feature appears at $E_\gamma = m_\chi$, an observation of this feature would provide a direct measurement of the WIMP mass, with an accuracy determined by the energy resolution of the telescope, potentially better than 10% . This is especially interesting because this parameter would be difficult to measure in a collider experiment, since WIMPs are pair-produced and escape the detector without interacting. Thus, observation of the edge feature would provide information complementary to what will be obtained at the LHC. For example, in the case of supersymmetry, the LHC can often determine the mass differences between some of the superpartners and the lightest neutralino, but not always the overall mass scale [47]. This ambiguity could be resolved if the edge feature in the gamma ray spectrum is observed.

2.6 Summary of Robust Signature of WIMP Dark Matter

In this chapter, we have obtained a prediction for the flux of photons produced as final state radiation in galactic WIMP annihilation processes. The prediction relies on the determination of the total WIMP annihilation cross section, which is provided by the measurement of the current cosmological dark matter abundance. As emphasized in [24], this determination does not require any assumptions about

the fundamental physics giving rise to the WIMP, apart from the mild condition of a generic mass spectrum. While the distribution of the cross section among various possible final states is not constrained by cosmological arguments, the FSR photons are produced for almost every possible final state (with the exception of $\nu\bar{\nu}$ and gg), making this signature quite model-independent. Moreover, if the final state of WIMP annihilation is a pair of charged fermions (leptons or quarks), the FSR flux has a well-defined step-like edge feature, dropping abruptly at the energy equal to the WIMP mass. Observing such a feature would provide strong evidence for the WIMP-related nature of the flux distortion, and yield a measurement of the WIMP mass.

If WIMPs are s-annihilators, the predicted FSR fluxes can be quite sizable, and the edge feature can be easily discernible above the expected background. Using a rough statistical criterion, we have shown that both ground-based ACTs such as HESS and VERITAS and space-based gamma ray telescopes such as Fermi have a good chance of observing the edge feature. It is likely that our simplified analysis underestimates the ability of the experiments to observe a step-like feature in the photon spectrum; a more sophisticated statistical analysis is clearly needed to obtain a more realistic estimate of the reach.

In the p-annihilator WIMP case, the fluxes are expected to be lower, and it is difficult to make model-independent predictions due to the possible presence of an a term in the annihilation cross section which would not affect the WIMP relic abundance, but could dominate galactic WIMP annihilation. Nevertheless, it would be interesting to analyze if observable FSR photon fluxes can be produced in models with p-annihilator WIMPs, such as the bino-like neutralino in supersymmetric models.

In summary, the flux of FSR photons emitted in the process of WIMP annihila-

tion in the center of Milky Way could be observable. An observation of the step-like edge feature characteristic of this flux could provide the first robust signature of WIMP dark matter. We encourage the collaborations involved in the analysis of the data coming from ground-based and space-based gamma ray telescopes to perform systematic searches for this important signature in a model-independent fashion as presented here.

CHAPTER 3

LITTLE HIGGS DARK MATTER

3.1 Introduction

In the previous chapter, we began by observing the firmly established result that about 25% of the energy density in the universe exists in the form of nonrelativistic, non-baryonic, non-luminous matter, so called "dark matter" [4]. The microscopic composition of dark matter remains a mystery, but it is clear that it cannot consist of any elementary particles that have been directly observed in the laboratory so far. One attractive scenario is that it consists of stable weakly-interacting massive particles (WIMPs), with masses around the weak scale, ∼100-1000 GeV. If the WIMPs were in thermal equilibrium with other species in the early universe, their relic abundance naturally matches the observed dark matter density. Accepting the WIMP hypothesis, we made predictions about experimental signals of dark matter that were robust, in the sense of not depending on the underlying particle physics.[1]

However, many theories which extend the standard model (SM) of electroweak interactions contain new particles with the properties of WIMPs. Perhaps the best known example is the lightest neutralino of supersymmetric (SUSY) models; another common candidate is the lightest Kaluza-Klain excitation in models with universal extra dimensions. There are two main advantages to working within a specific particle physics model in contrast to our previous model-independence. First, the more constrained our framework is, the stronger the predictions we can make. Second, different models will present different signals; this will allow us to resolve which model best fits reality when we have experimental results. This

[1]The work presented in this paper was previously published in Physical Review D, ©2009 by the American Physical Society [48, 49].

latter reason, in particular, propels us to find the experimental signals of as many models as possible, so as to ease the eventual data analysis.

Recently, a new class of theories extending the SM at the TeV scale, "Little Higgs" (LH) models, has been proposed [50] (for reviews, see [51, 52]). The LH models contain a light (possibly composite) Higgs boson, as well as additional gauge bosons, fermions, and scalar particles at the TeV scale. The Higgs is a pseudo-Nambu-Goldstone boson, corresponding to a global symmetry spontaneously broken at a scale $f \sim 1$ TeV. The global symmetry is also broken explicitly by the gauge and Yukawa couplings of the Higgs. As a result of this breaking, the Higgs acquires a potential; however, the leading (one-loop, quadratically divergent) contribution to this potential vanishes due to the special "collective" nature of the explicit global symmetry breaking, and the lightness of the Higgs can be achieved without fine-tuning. The dynamics of the Higgs and other degrees of freedom relevant at the TeV scale are described by a non-linear sigma model (nlsm), valid up to the cutoff scale $\Lambda \sim 4\pi f \sim 10$ TeV. In particular, the Higgs mass term is dominated by a one-loop, logarithmically enhanced contribution from the top sector, which can be computed within the nlsm and shown to have the correct sign to trigger electroweak symmetry breaking, providing a simple and attractive explanation of this phenomenon. Above the cutoff scale, the model needs to be embedded in a more fundamental theory; however, for many phenomenological applications, including the analysis of this chapter, the details of that theory are not relevant and the nlsm description suffices.

The Littlest Higgs model [50] is simple and economical, and it has been the focus of most phenomenological analyses to date [53]. Unfortunately, the model suffers from severe constraints from precision electroweak fits, due to the large corrections to low-energy observables from the tree-level exchanges of the non-

SM TeV-scale gauge bosons and the small but non-vanishing weak-triplet Higgs vacuum expectation value (vev) [19]. To alleviate this difficulty, the symmetry of the theory can be enhanced to include a Z_2 discrete symmetry, named "T parity" [20]. In the Littlest Higgs model with T parity (LHT) [54], the non-SM gauge bosons and the triplet Higgs are T-odd, forbidding all tree-level corrections to precision electroweak observables[2]. Loop corrections to precision electroweak observables in the LHT model were considered in [55], and the model was shown to give acceptable electroweak fits in large regions of parameter space compatible with naturalness.

An interesting side effect of T parity is that the lightest T-odd particle (LTP) is guaranteed to be stable. Analyzing the spectrum of the model, Hubisz and Meade [56] have argued that the LTP is likely to be the electrically neutral, weakly interacting "heavy photon" (or, more precisely, the T-odd partner of the hypercharge gauge boson) B_H. This particle is an attractive dark matter candidate, and initial calculations [56] showed that its relic abundance is within the observed range for reasonable choices of model parameters.[3] In this chapter, we begin by reviewing the details of the LHT model in section 3.2. Then in section 3.3 we will present a somewhat more detailed relic density calculation, including the possibility of coannihilations between the B_H and other T-odd particles. In the remainder of the paper, we outline most of the available dark matter signals: gamma rays in section 3.4, direct detection in section 3.5 and neutrinos in section 3.6.[4]

[2]In the version of the model considered here, there is one non-SM T-even state, the "heavy top" T_+. However it only contributes at tree level to observables involving the weak interactions of the top quark, which are at present unconstrained.

[3]While the LHT dark matter candidate is a spin-1 heavy photon, this is not an unambiguous prediction of Little Higgs models. For example, the "Simplest Little Higgs" models [57] supplemented by T-parity may contain a stable heavy neutrino which can play the role of dark matter [58], while closely related "theory space" models can give rise to a scalar WIMP dark matter candidate [59].

[4]The main other signal, high energy positrons, has previously been discussed in [21].

3.2 The Model

Our analysis will be performed within the framework of the Littlest Higgs model with T parity, which has recently been studied in Refs. [55, 56]. Let us briefly sketch the salient features of the model relevant here; for more details, see [55, 56] or the review article [52].

The model is based on an $SU(5)/SO(5)$ global symmetry breaking pattern; the Higgs doublet of the SM is identified with a subset of the Goldstone boson fields associated with this breaking. The symmetry breaking occurs at a scale $f \sim 1$ TeV. At energies below the cutoff $\Lambda \sim 4\pi f$, the dynamics of this sector is described by a non-linear sigma model. A subgroup $\mathcal{G} = [SU(2) \times U(1)]^2$ of the $SU(5)$ is gauged; this is broken at the scale f down to the diagonal subgroup, $SU(2)_L \times U(1)_Y$, identified with the SM electroweak gauge group. The extended gauge structure results in four additional gauge bosons at the TeV scale, $W_H^\pm$, W_H^3 and B_H.[5]

T parity is an automorphism which exchanges the two $[SU(2) \times U(1)]_i$ gauge fields; under this transformation, the TeV-scale gauge fields are odd, whereas the SM gauge bosons are even. The odd gauge bosons have masses

$$M(W_H^a) \approx gf, \quad M \equiv M(B_H) \approx \frac{g'f}{\sqrt{5}} \approx 0.16f, \tag{3.1}$$

where g and g' are the SM $SU(2)_L$ and $U(1)_Y$ gauge couplings, and the normalization of f is the same as in Ref. [55]. (Electroweak symmetry breaking at the scale $v \ll f$ induces corrections to these formulas of order v^2/f^2.) The "heavy photon" B_H is the lightest new gauge boson, and in fact is quite light compared to f. This is due to the combination of the smallness of g' and the favorable group theory factor, $1/\sqrt{5}$. Since the masses of the other T-odd particles are generically

[5]The W_H^3 and B_H fields mix to form the two neutral mass eigenstates; however, the mixing angle is of order v/f and can typically be neglected.

of order f, we will assume that the B_H is the lightest T-odd particle (LTP), and it will play the role of dark matter candidate.

The only direct coupling of the heavy photon to the SM sector is via the Higgs, resulting in weak-strength cross sections for B_H scattering into SM states. The heavy photon then provides yet another explicit example of a WIMP dark matter candidate, and it is not surprising that we will find reasonable regions of parameter space where it can account for all of the observed dark matter. For later convenience, we denote the mass of this particle by M. The range of the allowed values for this parameter is determined by the precision electroweak constraints, which put a lower bound on f, typically of about 600 GeV [55]. While there is no firm upper bound on f, we will assume $f \lesssim 2$ TeV to avoid reintroducing fine tuning in the Higgs sector. Using Eq. (3.1), this corresponds to the WIMP masses in the range

$$100 \text{ GeV} \lesssim M \lesssim 300 \text{ GeV}. \tag{3.2}$$

In the scalar sector, the uneaten $SU(5)/SO(5)$ Nambu-Goldstone bosons decompose into a T-even $SU(2)$ doublet H, identified with the SM Higgs, and a T-odd $SU(2)$ triplet Φ, which acquires a mass $m_\phi = \sqrt{2} m_h f/v$ at one loop. After imposing T-Parity, Φ (being odd) has no vacuum expectation value. In the fermion sector, each SM doublet (Q_i^a and L_i, where $a = 1 \ldots 3$ is a color index and $i = 1 \ldots 3$ is a generation index), acquires a T-odd vector-like partner, $\tilde{Q}_i^a$ and $\tilde{L}_i$. The masses of these particles are also free parameters,[6] with the natural scale set by f. To avoid proliferation of parameters, we will assume a universal T-odd fermion mass $\tilde{M}$ for both lepton and quark partners; we will require $\tilde{M} > M$ to avoid charged or colored LTPs, and assume $\tilde{M} \gtrsim 300$ GeV, since otherwise the colored T-odd particles would have been detected in the squark searches at

[6] If the flavor structure of the T-odd quark mass matrix is generic, with order-one flavor mixing angles, the masses of the T-odd quarks need to be degenerate at the few per cent level [60].

Table 3.1: Interaction vertices involving the heavy photon B_H that appear in the calculations of this chapter. Here $\alpha = \cos^{-1}(M_{T_-}/M_{T_+})$, and $\tilde{Y} = 1/10$.

$B_H^\mu B_H^\nu h$	$-\frac{i}{2} g'^2 v g^{\mu\nu}$
$B_H^\mu B_H^\nu hh$	$-\frac{i}{2} g'^2 g^{\mu\nu}$
$B_H^\mu \tilde{Q}_i^a Q_j^b$	$i\tilde{Y}\, g' \gamma^\mu P_L \delta_{ij} \delta^{ab}$
$B_H^\mu \tilde{L}_i L_i$	$i\tilde{Y}\, g' \gamma^\mu P_L \delta_{ij}$
$B_H^\mu T_- t$	$i\left(\frac{2}{5}\right)\, g' \gamma^\mu \sin\alpha \left(\sin\alpha \frac{v}{f} P_L + P_R\right)$

the Tevatron. In addition, non-observation of four-fermion operator corrections to SM processes such as $e^+e^- \to q\bar{q}$ places an *upper* bound on the T-odd fermion masses [55]:

$$\tilde{M}_{\rm TeV} < 4.8\, f_{\rm TeV}^2\,, \tag{3.3}$$

where $\tilde{M}$ and f are expressed in units of TeV. To cancel the one-loop quadratic divergence in the Higgs mass due to top loops, two additional new fermions are required in the top sector, the T-even T_+ and the T-odd T_-.[7] Their masses are related by

$$M_{T_+} \;=\; M_{T_-} \left(1 - \frac{m_t^2 f^2}{v^2 M_{T_-}^2}\right)^{-1/2}\,, \tag{3.4}$$

so that there is just one additional independent parameter in this sector. We will choose it to be M_{T_-}, and assume $M_{T_-} > M$ to avoid a charged LTP. With our assumptions, the spectrum and the (renormalizable) couplings of the LHT model are completely described in terms of the three parameters, f, $\tilde{M}$, and M_{T_-}, in addition to the familiar parameters of the SM. The couplings of the heavy photon B_H which will be used in the calculations of this chapter are summarized in Table 3.1.

[7] In Ref. [61], a variation of the model has been constructed where a single T-odd top partner is sufficient to cancel the divergences. Since the top sector will only play a minor role in the analysis of this chapter, we expect our results to hold, at least qualitatively, in that model.

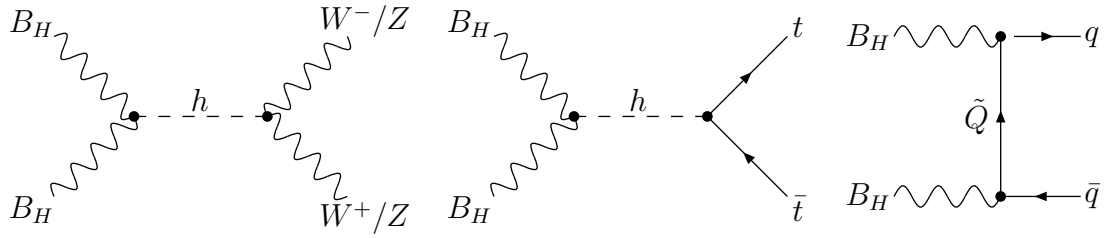

Figure 3.1: The leading $2 \leftrightarrow 2$ processes which maintain the heavy photon in equilibrium with the rest of the cosmic fluid at high temperatures.

3.3 Relic Density Calculation

In the early universe, the heavy photons are in equilibrium with the rest of the cosmic fluid. In the simplest case of generic (non-degenerate) T-odd particle mass spectrum, the equilibrium is maintained via the heavy photon pair-annihilation and pair-creation reactions; the leading $2 \leftrightarrow 2$ processes that contribute are shown in Fig. 3.1. The present relic abundance of heavy photons is determined by the behavior of pair-annihilation rates in the non-relativistic limit, namely, by the sum of the quantities

$$a(X) = \lim_{u \to 0} \sigma(B_H B_H \to X) u, \tag{3.5}$$

over all possible final states X. Here, u is the relative velocity of the annihilating particles. Note that, unlike the bino-like neutralinos typically predicted by the constrained minimal supersymmetric standard model (cMSSM), the s-wave annihilation of the heavy photons is unsuppressed: in the language of Ref. [24], the heavy photons are "s-annihilators", analogous to the Kaluza-Klein photons of the "universal extra dimensions" (UED) model [32, 37]. It is straightforward to compute $a(X)$ using the Feynman rules in Table 3.1. We obtain

$$a(W^+W^-) = \frac{2\pi\alpha^2}{3\cos^4\theta_W} \frac{M^2}{(4M^2 - m_h^2)^2 + m_h^2\Gamma_h^2} \left(1 - \mu_w + \frac{3}{4}\mu_w^2\right) \sqrt{1-\mu_w}; \tag{3.6a}$$

$$a(ZZ) = \frac{\pi\alpha^2}{3\cos^4\theta_W} \frac{M^2}{(4M^2 - m_h^2)^2 + m_h^2\Gamma_h^2} \left(1 - \mu_z + \frac{3}{4}\mu_z^2\right) \sqrt{1-\mu_z}\,, \tag{3.6b}$$

where $\mu_i = m_i^2/M^2$, θ_W is the SM weak mixing angle, and m_h and Γ_h are the mass and the width of the SM Higgs boson. If $M > m_t$, the LTPs can also annihilate into pairs of top quarks; ignoring the contribution from the t- and u-channel T_- exchanges, we obtain[8]

$$a(t\bar{t}) \;=\; \frac{\pi\alpha^2}{4\cos^4\theta_W}\,\frac{M^2}{(4M^2-m_h^2)^2+m_h^2\Gamma_h^2}\,\mu_t(1-\mu_t)^{3/2}\,. \tag{3.7}$$

If $M > m_h$, annihilation into a pair of Higgs bosons is possible, with the cross section

$$a(hh) = \frac{\pi\alpha^2 M^2}{2\cos^4\theta_W}\,\left[\frac{\mu_h(1+\mu_h/8)}{(4M^2-m_h^2)^2+m_h^2\Gamma_h^2} \;+\; \frac{1}{24M^4}\right]\,\sqrt{1-\mu_h}. \tag{3.8}$$

Finally, LTPs can also annihilate into light SM fermions via t-channel exchanges of the T-odd fermions; this channel was not included in the analysis of Ref. [56]. For a fermion f ($f = \ell^\pm, \nu, u, d$) we obtain

$$a(f\bar{f}) \;=\; \frac{16\pi\alpha^2\tilde{Y}^4 N_c^f}{9\cos^4\theta_W}\,\frac{M^2}{(M^2+\tilde{M}^2)^2}\,, \tag{3.9}$$

where $N_c^f = 1$ for leptons and 3 for quarks, and $\tilde{Y} = 1/10$ is the $B_H f\tilde{f}$ coupling in units of g'. Because of the small value of $\tilde{Y}$, the annihilation into light fermions is strongly suppressed, even for relatively small values of $\tilde{M}$. The WMAP collaboration data [2, 23] provides a precise determination of the present dark matter abundance: at two-sigma level,

$$\Omega_{\rm dm}h^2 = 0.104 \pm 0.009. \tag{3.10}$$

For s annihilators, this determines the quantity $a \equiv \sum_X a(X)$: $a = 0.8 \pm 0.1$ pb. (The precise central value of a depends on the WIMP mass; however, this dependence is very mild, see Fig. 1 of Ref. [24].) Using this constraint and the above formulas, it is straightforward to map out the regions of the model parameter

[8]The T_- exchanges are negligible throughout most of the parameter space, but will nevertheless be fully included in the numerical calculation of the relic abundance described below.

space where the heavy photons can account for all of the observed dark matter. The results are consistent with the updated analysis of Hubisz and Meade, see Fig. 3 of Ref. [56]. For given m_h, there are two values of M which result in the correct relic density. There is one solution on either side of the Higgs resonance. For WIMP masses in the interesting range, Eq. (3.2), these can be approximated by simple analytic expressions:

$$m_h \approx 24 + 2.38M, \quad \text{or} \quad m_h \approx -83 + 1.89M, \tag{3.11}$$

where M and m_h are in units of GeV. We will refer to these solutions as "low" and "high", respectively. The analytic expressions (3.11) reproduce the values of M and m_h consistent with the WMAP central value of $\Omega_{\rm dm}h^2$ with an error of at most a few GeV throughout the interesting parameter range. This accuracy will be sufficient for the analysis of detection prospects in sections 3.4 through 3.6.

Throughout the parameter space consistent with the WMAP value of the present dark matter density, the dominant heavy photon annihilation channels are W^+W^- and ZZ; the $t\bar{t}$ channel contributes at most about 5% of the total annihilation cross section, while the hh final state is always kinematically forbidden. Moreover, the ratio of the W^+W^- and ZZ contributions is approximately 2:1, as is evident from Eqs. (3.6), so that $a(W^+W^-) \approx 0.53$ pb, $a(ZZ) \approx 0.27$ pb throughout the parameter space. Since B_H is an s-annihilator, the same cross sections govern the rate of heavy photon annihilation in the galactic halo, which in turn determines the fluxes relevant for indirect detection, see Section 3.4.

If some of the T-odd particles are approximately degenerate in mass with the heavy photon, the simple analysis above is no longer applicable, since coannihilation reactions between B_H and other states significantly affect the relic abundance. In the LHT model, the masses of the T-odd weak gauge bosons W_H and the triplet scalar ϕ are predicted unambiguously once the scale f and the Higgs mass m_h are

fixed; these particles are always much heavier than the B_H and their effect is negligible. On the other hand, the common mass scale of the T-odd leptons and quarks $\tilde{M}$ is a free parameter, and for $M \sim \tilde{M}$ the coannihilations between these states and the B_H can be important. We have performed a more detailed analysis of the B_H relic density, taking this possibility into account.

In the presence of coannihilations, the abundance calculation requires solving a system of coupled Boltzmann equations. We approached this problem numerically. The interactions of the LHT model were incorporated in the CalcHEP package [62], which was used to compute the scattering matrix elements for the appropriate processes. The rest of the calculation was performed using the `DM++` package,[9] recently developed by Birkedal. The package first uses the matrix elements to compute the thermal averages $\langle \sigma u \rangle$, which determine the reaction rates entering the Boltzmann equation. Then, the freeze-out temperature of the dark matter is determined iteratively, using the Turner-Scherrer approximation [65]. Finally, the integral of $\langle \sigma u \rangle$ from freeze-out to present day (usually called $J(x_F)$ in the literature) is evaluated, providing the relic abundance.

The results of this analysis are illustrated by Figure 3.2, which shows the contours of constant heavy photon relic density in the $f - \tilde{M}$ (or, equivalently, $M - \tilde{M}$) plane. The typical situation for a heavy Higgs is shown in the left panel ($m_h = 300$ GeV). There are two regions in which the heavy photon can account for the observed dark matter:

- The two vertical *pair-annihilation bands*, where the coannihilation processes are unimportant. The heavy photon abundance in these regions is indepen-

[9] The `DM++` package is currently being prepared for public release. It can be applied to compute the relic abundance of the WIMP for any particle physics model that can be incorporated in CalcHEP. The `DM++` is inspired by the `micrOMEGAs` code [63], which was originally designed to compute the relic abundance of neutralinos in the MSSM. The recently developed new version of this code, `micrOMEGAs2.0` [64], is also applicable to any CalcHEP model defined by the user. This package is also being prepared for public release.

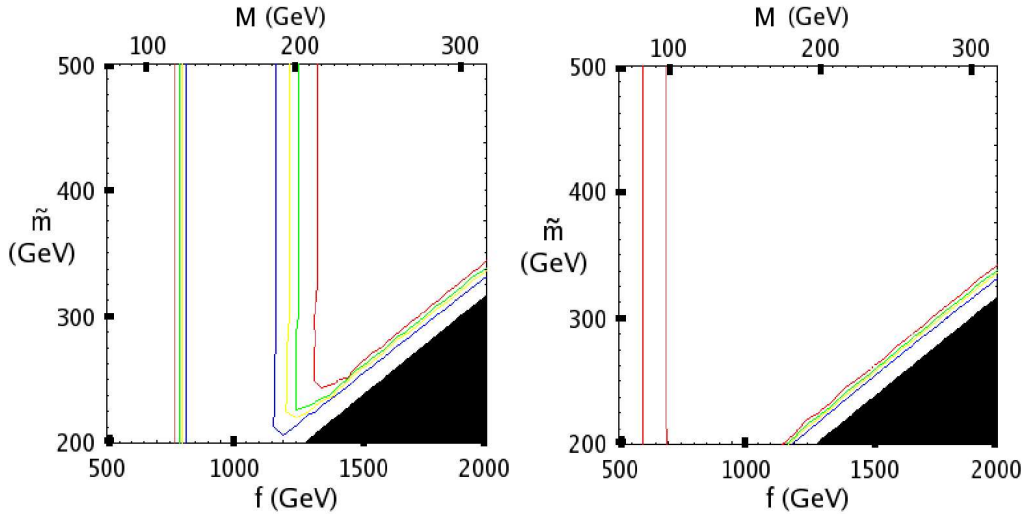

Figure 3.2: The contours of constant present abundance of the heavy photon LTP, $\Omega_{\rm LTP}h^2$, in the $M - \tilde{M}$ plane. The Higgs mass is taken to be 300 GeV (left panel) and 120 GeV (right panel). The red and green contours correspond to the upper and lower bounds from WMAP, Eq. (3.10), assuming that the LTP makes up all of dark matter. The yellow and blue lines correspond to the LTP contributing 50% and 70%, respectively, of the measured dark matter density. The shaded region corresponds to a charged and/or colored LTP.

dent of $\tilde{M}$. The bands appear on either side of the s-channel Higgs resonance dominating the pair-annihilation processes, corresponding to the "high" and "low" solutions of Eq. (3.11). (The bands are analogous to the "Higgs funnel" region in the cMSSM.)

- The *coannihilation tail*, where the heavy photon abundance is predominantly set by coannihilation processes. Since the T-odd fermions are assumed to be degenerate, all of them participate in the coannihilation reactions. The location and shape of this feature are similar to the tau coannihilation tail in the cMSSM.

As the Higgs mass is decreased, the pair-annihilation bands appear for lower WIMP masses, and for light Higgs (115–150 GeV) the "low" band disappears, since

the required values of f are already ruled out by data. The "high" band persists until the Higgs mass is close to the current experimental bound. To illustrate this, consider the right panel of Fig. 3.2, where $m_h = 120$ GeV. The band between the two red lines ($90 \lesssim M \lesssim 100$ GeV) is allowed. Note that the behavior of the relic density as a function of M within this band is non-trivial: The relic density first drops with increasing M due to the fact that the threshold for the reaction $B_H B_H \to ZZ$ is passed. It then bottoms out at a value consistent with the measured $\Omega_{\rm dm} h^2$, and begins increasing as increasing M further takes the center-of-mass energy away from the Higgs resonance, suppressing annihilation. Clearly, this situation is quite non-generic, and for somewhat higher m_h the Z threshold becomes irrelevant and relic density is a uniformly increasing function of M in the "high" band. The coannihilation tail is present for low as well as high values of m_h. The tail can be described by a simple analytic formula

$$\tilde{M} \approx M + 20 \text{ GeV}, \tag{3.12}$$

which is approximately independent of the Higgs mass.

It should be noted that the remaining free parameter of our model, the mass of the second T-odd top quark M_{T_-}, was fixed to be equal to f, so that $M_{T_-} \gg M$ and this particle did not have an effect on the B_H relic abundance. We expect that a second coannihilation tail appears when $M_{T_-} \sim M$; the structure should be very similar to the one found above, with slight numerical differences due to smaller multiplicity of the coannihilating states.

3.4 Indirect Detection via Anomalous Gamma Rays

As discussed in Section 3.3, WIMP annihilation processes have to occur with approximately weak-scale cross sections to ensure that the relic abundance of WIMPs

is consistent with observations. Since the heavy photons of the LHT model are s-annihilators, their annihilation rates are approximately velocity-independent in the nonrelativistic regime. This implies that the WIMPs collected, for example, in galactic halos, have a substantial probability to pair-annihilate, resulting in anomalous high-energy cosmic rays which could be distinguished from astrophysical backgrounds. In particular, high-energy gamma rays (photons) and positrons are considered to be the most promising experimental signatures. The gamma ray signal is particularly interesting because the gamma rays in the relevant energy range travel over galactic scales with no scattering, so that if the signal is observed, information about the WIMP (e.g. its mass) could be extracted from the spectrum. In this section, we will compute the gamma ray fluxes predicted by the LHT model, and evaluate their observability. (Positron fluxes from the heavy photon dark matter annihilation in the LHT model were recently considered in Ref. [21].)

There are three principal mechanisms by which hard photons can be produced in WIMP annihilation:

- Monochromatic photons produced via direct annihilation into a two body final state ($\gamma\gamma, h\gamma$ or $Z\gamma$);
- Photons produced via radiation from a final state charged particle;
- Photons radiated during the hadronization and fragmentation of strongly interacting particles produced either directly in WIMP annihilation (e.g. $B_H B_H \to q\bar{q}$) or in hadronic decays of the primary annihilation products (e.g. $B_H B_H \to ZZ$ followed by $Z \to q\bar{q}$).

Let us consider each of these mechanisms in turn in the LHT model.

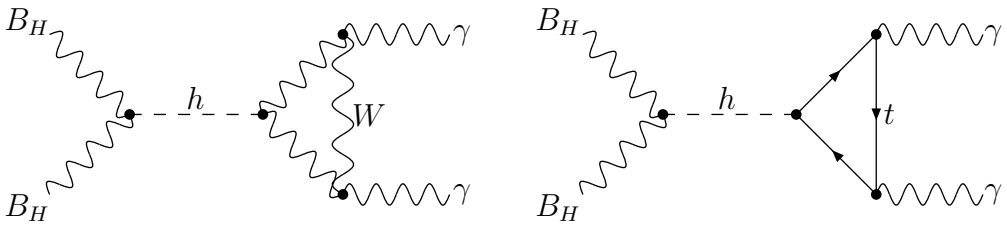

Figure 3.3: The diagrams which dominate the monochromatic photon pair-production in the B_H annihilation in the galactic halo.

3.4.1 Photon Flux from $B_H B_H \to \gamma\gamma$ Annihilation

WIMPs being electrically neutral, production of monochromatic photons can only occur at loop level. We first consider the two-photon final state. The $B_H B_H \to \gamma\gamma$ process is dominated by the one-loop diagrams inducing the effective $h\gamma\gamma$ vertex, see Fig. 3.3.[10] The corresponding cross section can be easily evaluated using the well-known formulas for the Higgs boson partial widths:

$$\sigma_{\gamma\gamma} u \equiv \sigma\left(B_H B_H \to \gamma\gamma\right) u = \frac{g'^4 v^2}{72 M^4} \frac{s^2 - 4sM^2 + 12M^4}{(s - m_h^2)^2 + m_h^2 \Gamma_h^2} \frac{\hat{\Gamma}\left(h \to V_1 V_2\right)}{\sqrt{s}}, \qquad (3.13)$$

where u is the relative velocity of the annihilating WIMPs, and $s \approx 4M^2$ in the non-relativistic regime relevant for the galactic WIMP annihilation. The hat on Γ indicates that the substitution $m_h \to \sqrt{s}$ should be performed in the standard expressions for on-shell Higgs decays [66, 67], and the loops of new particles present in the LHT model should be included. We obtain

$$\hat{\Gamma}(h \to \gamma\gamma) \;=\; \frac{\alpha^2 g^2}{1024\pi^3} \frac{s^{3/2}}{m_W^2} \left| \mathcal{A}_1 + \mathcal{A}_{1/2} + \mathcal{A}_0 \right|^2, \qquad (3.14)$$

[10] A complete calculation would also include the contribution of the box diagrams with T-odd and T-even quarks running in the loop, analogous to the quark/squark boxes entering in the case of MSSM neutralino annihilation [30]. In the LHT case, this contribution is expected to be subdominant since the matrix element contains a factor of $\tilde{Y}^2 = 0.01$.

where $\mathcal{A}_s$ denotes the contribution from loops of particles of spin s. These contributions are given by

$$\mathcal{A}_1 = \sum_i c_i Q_i^2 \frac{\tau_W}{\tau_i} F_1(\tau_i); \tag{3.15a}$$

$$\mathcal{A}_{1/2} = \sum_i \frac{\sqrt{2} Q_i^2 y_i}{g} \frac{\tau_W^{1/2}}{\tau_i^{1/2}} F_{1/2}(\tau_i); \tag{3.15b}$$

$$\mathcal{A}_0 = \sum_i \frac{2 Q_i^2 \lambda_i}{g^2} \frac{\tau_W}{\tau_i} F_0(\tau_i), \tag{3.15c}$$

where the sums run over all the charged particles of a given spin, and implicitly include summations over colors and other quantum numbers where necessary. The particles in the sums have masses m_i and electric charges (in units of the electron charge) Q_i; their trilinear couplings to the Higgs boson are given by $\lambda_i v$, $y_i/\sqrt{2}$, and $c_i g M_W \eta^{\mu\nu}$, for particles of spin 0, 1/2, and 1, respectively. (With these normalization choices, $c_i = 1$ for the SM $W^\pm$, and y_i's are the usual Yukawas for the SM fermions.) We have also defined $\tau_i = 4m_i^2/s$. The functions $F_s(\tau)$ are given by

$$F_1(\tau) = 2 + 3\tau + 3\tau\,(2-\tau)\,f(\tau); \tag{3.16a}$$

$$F_{1/2}(\tau) = -2\tau\,(1 + (1-\tau)\,f(\tau))\,; \tag{3.16b}$$

$$F_0(\tau) = \tau\,(1 - \tau f(\tau))\,, \tag{3.16c}$$

where

$$f(\tau) = \begin{cases} \left[\sin^{-1}\left(\sqrt{\frac{1}{\tau}}\right)\right]^2 & \text{if } \tau > 1; \\ -\frac{1}{4}\left[\log\left(\frac{1+\sqrt{1-\tau}}{1-\sqrt{1-\tau}}\right) - i\pi\right]^2 & \text{if } \tau < 1. \end{cases} \tag{3.17}$$

Using these expressions, we find that the contributions of the T-odd states are subdominant compared to the SM loops. The contributions of the T-odd fermion loops and the T-even heavy top loop are suppressed because their coupling to the Higgs is of order v^2/f^2. The contributions of charged T-odd heavy gauge bosons and scalars are suppressed due to their large masses, of order f. The deviation

of the effective $h\gamma\gamma$ coupling from its Standard Model value due to these states is of order a few per cent.[11] Given the much larger astrophysical uncertainties inherent in the anomalous photon flux predictions, we will ignore these effects in our analysis.

The monochromatic flux due to the $\gamma\gamma$ final state, observed by a telescope with a line of sight parametrized by $\Psi = (\theta, \varphi)$ and a field of view $\Delta\Omega$ can be written as [31]

$$\Phi \;=\; \left(1.1 \times 10^{-9}\mathrm{s}^{-1}\mathrm{cm}^{-2}\right) \left(\frac{\sigma_{\gamma\gamma} u}{1\ \mathrm{pb}}\right) \left(\frac{100\ \mathrm{GeV}}{M}\right)^2 \bar{J}(\Psi, \Delta\Omega)\Delta\Omega, \tag{3.18}$$

where $\bar{J}$ contains the dependence of the flux on the halo dark matter density distribution, and was defined in Eq. (2.13). Many models of the galactic halo predict a sharp peak in the dark matter density in the neighborhood of the galactic center, making the line of sight towards the center the preferred one for WIMP searches.[12] However, the features of the predicted peak are highly model-dependent, resulting in a large uncertainty in the predicted $\bar{J}$. For example, at $\Delta\Omega = 10^{-3}$ sr, characteristic of ground-based Atmospheric Cerenkov Telescopes (ACTs), typical values of $\bar{J}$ range from 10^3 for the NFW profile [40] to about 10^5 for the profile of Moore et.al. [41], and can be further enhanced by a factor of up to 10^2 due to the effects of adiabatic compression [42].

The monochromatic photon fluxes (assuming $\bar{J}\Delta\Omega = 1$) predicted by the LHT model in the parameter regions where the heavy photon accounts for all of the observed dark matter, are shown in Fig. 3.4. The left panel corresponds to the pair-annihilation bands, and the right panel to the coannihilation region. Searches

[11] The deviations of the $h \to \gamma\gamma$ and $gg \to h$ vertices from the SM in the LHT model were recently analyzed in detail in Ref. [68].

[12] Note, however, that a powerful point-like source of ultra high energy gamma rays has been recently detected in the galactic center region [69]. The energy spectrum of this source, smooth and extending out to at least a few TeV, makes its interpretation in terms of WIMP annihilation unlikely. Detection of the potential gamma flux from WIMP annihilation in the same spatial region is clearly made more difficult by the presence of the source.

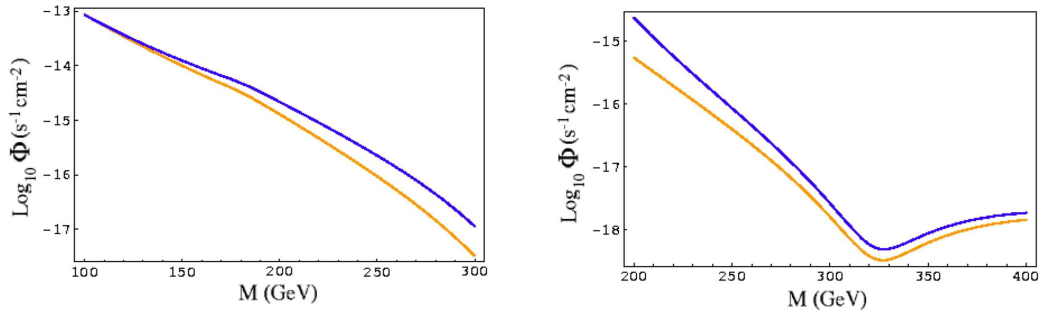

Figure 3.4: The flux of the monochromatic photons from the reaction $B_H B_H \to \gamma\gamma$ in the pair-annihilation bands (left panel) and the coannihilation region (right panel). On the left panel, the blue/upper and the orange/lower lines correspond to the high and low solutions in Eq. (3.11), respectively. On the right panel, the blue/upper line corresponds to $m_h = 300$ GeV, the orange/lower line to $m_h = 120$ GeV. The plots assume $\bar{J}(\Psi, \Delta\Omega)\Delta\Omega = 1$; all fluxes scale linearly with this parameter.

for gamma rays from WIMP annihilation have to be able to distinguish them from the astrophysical background. In the case of the monochromatic photons, the signal is concentrated in a single bin (the energy uncertainty of the telescopes is about 10%, much larger than the intrinsic line width), and the background can be effectively measured in the neighboring bins and subtracted. In the relevant energy range, the flux sensitivity for ground-based Atmospheric Cherenkov Telescopes (ACTs) such as VERITAS [44] and HESS [45] is estimated to be around $(1-5)\times 10^{-12}$ cm^{-2} sec^{-1}, whereas the sensitivity of the upcoming space-based telescope Fermi/GLAST is limited by statistics at 10^{-10} cm^{-2} sec^{-1}, assuming that 10 events are required to claim discovery [70]. It is clear that the monochromatic flux predicted by the LHT model is beyond the reach of Fermi, but could be observed at the ACTs if the dark matter distribution in the halo exhibits a substantial spike or strong clumping, $\bar{J} \gtrsim 10^5$ at $\Delta\Omega \approx 10^{-3}$.

3.4.2 Photon Flux from $B_H B_H \to Z\gamma$ Annihilation

The second possible source of monochromatic photons is from the $Z\gamma$ final state. Naïvely, we might expect that this channel would be suppressed relative to the $\gamma\gamma$ final state, since only half as many photons are produced per annihilation. This turns out not to be the case; due to an accidental cancellation, the cross section for this process is substantially higher than that previously computed.

The $B_H B_H$ annihilation in the LHT model is dominated by processes with an s-channel Higgs boson exchange. The contributing diagrams are those of Fig. 3.3, with one of the photons replaced by a Z; we can again use the relation between the cross section and the partial Higgs decay widths, Eq. (3.13).[13] Using the well-known results for the partial Higgs decay width in the $Z\gamma$ channel [66, 67], we obtain[14]

$$\hat{\Gamma}\left(h \to Z\gamma\right) = \frac{\alpha\, g^2}{2048\pi^4}\frac{s^{3/2}}{m_W^2} \mid \mathcal{A}_F + \mathcal{A}_G \mid^2 \left(1 - \frac{m_Z^2}{s}\right)^3 . \tag{3.19}$$

Here, $\mathcal{A}_F$ and $\mathcal{A}_G$ are the contributions to the matrix element from fermions and gauge bosons, respectively:

$$\mathcal{A}_F = -4\sum_f \frac{\sqrt{2} y_f \tau_W^{1/2}}{g \tau_f^{1/2}} N_{c_f} Q_f V_f \left[I_1\left(\tau_f, \lambda_f\right) - I_2\left(\tau_f, \lambda_f\right)\right] ; \tag{3.20a}$$

$$\mathcal{A}_G = -\sum_g \frac{c_g \tau_W}{\tau_g} V_g Q_g \Bigg\{ 4(3 - t_W^2) I_2(\tau_g, \lambda_g) + \left[\left(1 + \frac{2}{\tau_g}\right) t_W^2 - \left(5 + \frac{2}{\tau_g}\right)\right] I_1(\tau_g, \lambda_g) \Bigg\} , \tag{3.20b}$$

where $t_W = 0.548$ is the tangent of the Weinberg angle, and

$$\tau_i \equiv \frac{4m_i^2}{s} , \qquad \lambda_i \equiv \frac{4m_i^2}{m_Z^2} . \tag{3.21}$$

The sums run over all particles of the relevant type (including both the SM and the additional particles of the LHT model), with the electric charge, the multiplicity

[13] With the obvious modification, $\gamma\gamma \to Z\gamma$.

[14] We neglect the contribution to the Higgs width from the loops of the T-odd scalar Φ.

and the coupling to the Z boson of each particle given by Q_i, N_{c_i}, and V_i, respectively. For fermions, V_i denotes the vector part of the $i\bar{i}Z$ coupling; there is no contribution from the axial part. In particular, for the extra vector-like fermions of the LHT model, we obtain

$$V_i = \frac{g}{c_W}\left(T_3(i) - s_W^2 Q(i)\right) , \tag{3.22}$$

where $T_3(\tilde{U}, \tilde{N}) = 1/2,\ T_3(\tilde{D}, \tilde{E}) = -1/2$, and $T_3(T_+, T_-) = 0$. The functions $I_{1,2}$ are given by

$$I_1(a,b) = \frac{a\,b}{2(a-b)} + \frac{a^2 b^2}{2(a-b)^2}\left[f(a) - f(b)\right] + \frac{a^2 b}{(a-b)^2}\left[g(a) - g(b)\right] ; \tag{3.23a}$$

$$I_2(a,b) = -\frac{a\,b}{2(a-b)}\left[f(a) - f(b)\right] , \tag{3.23b}$$

where $f(x)$ is defined in Eq. (3.17), and g is given by

$$g(x) = \begin{cases} \sqrt{x-1}\sin^{-1}\left(\sqrt{\frac{1}{x}}\right) & \text{if } x > 1; \\ \frac{1}{2}\sqrt{1-x}\left[\log\left(\frac{1+\sqrt{1-x}}{1-\sqrt{1-x}}\right) - i\pi\right] & \text{if } x < 1. \end{cases} \tag{3.24}$$

For a telescope with line of sight parameterized by $\Psi = (\theta, \phi)$ and an angular acceptance $\Delta\Omega$, the anomalous photon flux due to $B_H B_H \to Z\gamma$ is given by [31]

$$\Phi = \left(5.5 \times 10^{-10}\ \text{s}^{-1}\ \text{cm}^{-2}\right)\left(\frac{\sigma_{Z\gamma} u}{1\,\text{pb}}\right)\left(\frac{100\,\text{GeV}}{M}\right)^2 \bar{J}\left(\Psi, \Delta\Omega\right)\Delta\Omega. \tag{3.25}$$

Note that this is half of Eq. (3.18), as would be expected. The photon energy is

$$E_\gamma = M\left(1 - \frac{M_Z^2}{4M^2}\right) . \tag{3.26}$$

This is slightly displaced from the energy of the photons from the $\gamma\gamma$ final state. The thermal broadening of the line is much smaller than the energy resolution of any existing telescope, and can be neglected.

The flux expected in the "high" pair-annihilation region of the LHT model is plotted in Fig. 3.5. For comparison, the flux due to $B_H B_H \to 2\gamma$, computed in

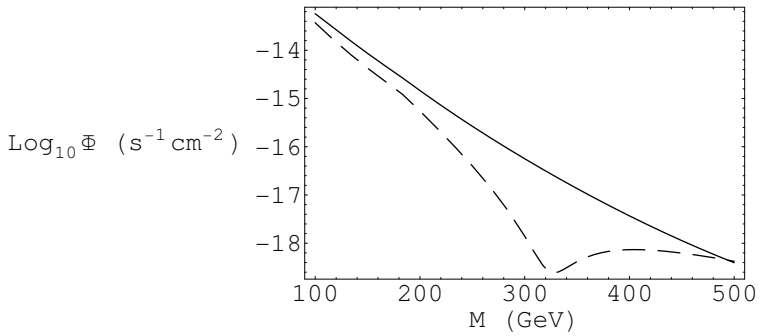

Figure 3.5: Photon fluxes from WIMP annihilation into $Z\gamma$ (solid line) and $\gamma\gamma$ (dashed line), in the "high" pair-annihilation region of the LHT model. The fluxes in the "low" pair-annihilation and coannihilation regions are similar. The fluxes are normalized to $\bar{J}\Delta\Omega = 1$, and scale linearly with this parameter.

the previous section, is also shown. Throughout the parameter space, the $Z\gamma$ final state provides a stronger monochromatic photon flux, with the ratio of the $Z\gamma$ to $\gamma\gamma$ flux varying between about 1.5 and 100. (The largest values of this ratio are obtained for $M \sim 300$ GeV, where the $\gamma\gamma$ cross section is suppressed due to an accidental cancelation.) Similar results are obtained in the "low" pair-annihilation and the coannihilation regions of the parameter space.

Experimental searches for the anomalous high-energy gamma rays using Atmospheric Cerenkov telescopes (ACTs), such as HESS [45] and VERITAS [44], are currently under way, as is the space-based Fermi/GLAST telescope [70]. The $Z\gamma$ line predicted in the LHT model would be observable at GLAST and the ACTs only if the fluxes are enhanced by a strong spike in the dark matter concentration around the galactic center: depending on the B_H mass, values of $\bar{J}\Delta\Omega$ in the $10^2 \ldots 10^4$ range are required. Many (though not all) models of the galactic halo contain such spikes: for example, the profile of Moore et al. [41] predicts $\bar{J} \approx 10^5$ for $\Delta\Omega = 10^{-3}$ sr.

3.4.3 Photon Flux from $B_H B_H \to h\gamma$ Annihilation

The final annihilation process giving rise to monochromatic photons, $B_H B_H \to h\gamma$, is strongly suppressed. It cannot occur via an s-channel Higgs exchange, because the process $h^* \to h\gamma$ is forbidden by the Ward identity of Quantum Electrodynamics. The proof is as follows: Let the photon and on-shell Higgs have momenta k and p, respectively. The matrix element has the form

$$\mathcal{M}\left(h^* \to h\gamma\right) \equiv \varepsilon_\mu^*\left(k\right) \hat{\mathcal{M}}^\mu \,, \tag{3.27}$$

where $\hat{\mathcal{M}}^\mu$ can be decomposed as

$$\hat{\mathcal{M}}^\mu = A\left(k,p\right)\, k^\mu + B\left(k,p\right)\, p^\mu \,. \tag{3.28}$$

The Ward identity requires that $k_\mu \hat{\mathcal{M}}^\mu = 0$. For the first term this is true since $k^2 = 0$. For the second term, $p \cdot k = 0$ only if the initial Higgs is on-shell (when the process is kinematically forbidden); thus, $B \equiv 0$. However, by the transverse nature of the polarization vector the first term provides no contribution to the matrix element; therefore, $\mathcal{M}\left(h^* \to h\gamma\right) \equiv 0$. As a result, $B_H B_H \to h\gamma$ may only proceed via box diagrams with T-odd and T-even fermions in the loop, which receive no resonant enhancement. Moreover, the $B_H \tilde{Q} q$ and $B_H \tilde{L} l$ couplings are of order $g'/10 \approx 0.035$, further suppressing the cross section.

3.4.4 Continuous Photon Flux

We next consider the component of the photon flux due to hadronization and fragmentation of quarks produced in WIMP annihilation. As discussed in Section 3.3, the heavy photons predominantly annihilate into W and Z pairs; each of the vector bosons can in turn decay into a quark pair. The resulting photon spectra depend only on the initial energies of the W's and Z's, and not on the details of the WIMP

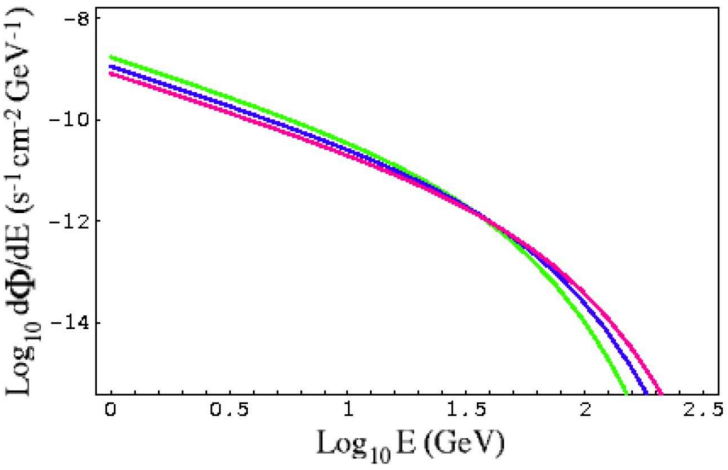

Figure 3.6: The fragmentation photon flux for $M = 150, 200, 250$ GeV (green, blue and red lines, respectively), in the pair-annihilation bands. The plot assumes $\bar{J}(\Psi, \Delta\Omega)\Delta\Omega = 1$; all fluxes scale linearly with this parameter.

annihilation process. The spectra have been studied using `PYTHIA` (in the MSSM context), and a simple analytic fit has been presented in Ref. [31]:

$$\frac{\mathrm{d}N_\gamma}{\mathrm{d}x} \approx \frac{0.73}{x^{1.5}} e^{-7.8x}. \tag{3.29}$$

where $x = E_\gamma/M$. This approximation is valid for both W^+W^- and ZZ final states. In the pair-annihilation bands, the differential flux is then given by

$$\frac{\mathrm{d}\Phi}{\mathrm{d}E} = \left(3.3 \times 10^{-12}\mathrm{s}^{-1}\mathrm{cm}^{-2}\mathrm{GeV}^{-1}\right) x^{-1.5} e^{-7.8x} \times \left(\frac{100\ \mathrm{GeV}}{M}\right)^3 \bar{J}(\Psi, \Delta\Omega)\Delta\Omega, \tag{3.30}$$

where we used the relic density constraint, $a(W^+W^-) + a(ZZ) \approx 0.8$ pb. The flux in the coannihilation region is much smaller.

The fluxes predicted by Eq. (3.30) for several values of M are plotted in Fig. 3.6. The Fermi/GLAST telescope is statistics-limited at energies above about 2 GeV [70], and would observe tens of events in this energy range for the heavy photon mass in the preferred range, assuming $\bar{J}(\Delta\Omega)\Delta\Omega = 1$. (The flux scales

linearly with this parameter combination.) One should keep in mind, however, that while the prospects for observing this signal are good, ruling out its interpretation in terms of conventional astrophysics could be challenging given the smooth, featureless nature of the fragmentation spectrum. Detailed studies of the angular distribution of these photons, in particular outside the galactic disk, will be needed.

Atmospheric Cerenkov Telescopes (ACTs) have a higher energy threshold, typically about 50 GeV, and suffer from an irreducible background from electron-induced showers, about $10^{-12} - 10^{-10}$ cm^{-2}s^{-1}GeV^{-1} in the relevant energy range ($50 \ldots 200$ GeV) for $\Delta\Omega \sim 10^{-3}$. Using the extrapolation of Ref. [31] to estimate the background, we find that the typical signal/background ratio expected at the ACTs, assuming $\Delta\Omega \sim 10^{-3}$ and $\bar{J}(\Delta\Omega)\Delta\Omega = 1$, is only about 10^{-3}. An observation of the fragmentation flux at the ACTs appears quite challenging, unless dark matter is strongly clustered at the galactic center or clumped.

3.4.5 FSR Photon Flux

The final component of the gamma-ray flux from WIMP annihilation is the final state radiation (FSR) photons. As noted in chapter 2, the FSR flux generally provides a robust signature of WIMP annihilation: it exists whenever the WIMPs have a sizable annihilation cross section into *any* charged states. The FSR photons have a continuous spectrum, in analogy to the quark fragmentation photons considered above. In fact, at low energies, the fragmentation flux dominates over the FSR component (unless WIMPs annihilate into purely leptonic states). At energies close to the WIMP mass, however, the fragmentation flux drops sharply, and the FSR component typically dominates (see chapter 2). This is particularly interesting because the FSR spectrum typically possesses a sharp edge feature,

abruptly dropping to zero at the maximal photon energy allowed by kinematics. The edge feature could help the experiments to discern this flux on top of the (a priori highly uncertain) astrophysical background, and provide a measurement of the WIMP mass (ibid). In the LHT model, the dominant charged two-body annihilation channel is W^+W^-, and correspondingly the reaction $B_H B_H \to W^+W^-\gamma$ provides the most important component of the FSR photon flux. The differential cross section for this process is given by

$$\frac{\mathrm{d}\sigma}{\mathrm{d}x}\left(B_H B_H \to W^+W^-\gamma\right) = \sigma\left(B_H B_H \to W^+W^-\right)\,\mathcal{F}(x;\mu_w), \tag{3.31}$$

where $x = 2E_\gamma/\sqrt{s} \approx E_\gamma/M$, $\mu_w = (m_W/M)^2$ and

$$\mathcal{F}(x;\mu) = \frac{\alpha}{\pi}\frac{1}{\sqrt{1-\mu}}\frac{1}{x}\times\Big[(2x-2+\mu)\log\frac{2(1-x)-\mu-2\sqrt{(1-x)(1-x-\mu)}}{\mu} + 2\left(\frac{8x^2}{4-4\mu+3\mu^2}-1\right)\sqrt{(1-x)(1-x-\mu)}\Big], \tag{3.32}$$

for $0 \le x \le 1-\mu$ and 0 for $1-\mu \le x \le 1$. In the limit of large heavy photon mass, $s \gg M_W^2$, this expression reduces to

$$\mathcal{F}(x) = \frac{2\alpha}{\pi}\frac{1-x}{x}\Big[\log\frac{s(1-x)}{m_W^2} + 2x^2 - 1 + \mathcal{O}(\mu)\Big]. \tag{3.33}$$

The leading (logarithmically enhanced) term agrees with the result obtained in chapter 2 using the Goldstone boson equivalence theorem. Note that the form of the photon emission factor $\mathcal{F}$, even in the large-s limit, depends on the theory being considered and on the initial state. For example, the $\tilde{\chi}_1^0\tilde{\chi}_1^0 \to W^+W^-\gamma$ cross section in the MSSM, computed in Ref. [71], has a different leading logarithm behavior; this is related to the fact that the W bosons effectively become massless in this limit, inducing new infrared singularities. Thus, even though we chose to write the cross section (3.31) in a "factorized" form, there is no true factorization in the $WW\gamma$ final state, in contrast to the $f\bar{f}\gamma$ final states.

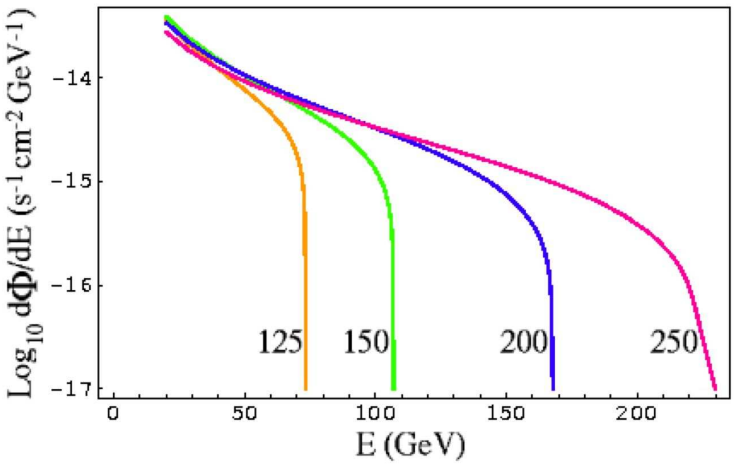

Figure 3.7: The FSR photon flux for $M = 125, 150, 200, 250$ GeV (left to right), in the pair-annihilation bands. (The fluxes for "high" and "low" solutions are essentially identical.) The plot assumes $\bar{J}(\Psi, \Delta\Omega)\Delta\Omega = 1$; all fluxes scale linearly with this parameter.

The flux of the FSR photons is given by

$$\frac{\mathrm{d}\Phi}{\mathrm{d}E} = \left(5.6 \times 10^{-12}\mathrm{s}^{-1}\mathrm{cm}^{-2}\mathrm{GeV}^{-1}\right) \times \left(\frac{a(W^+W^-)}{1\ \mathrm{pb}}\right)\left(\frac{100\ \mathrm{GeV}}{M}\right)^3 \mathcal{F}(x;\mu_w)\bar{J}(\Psi,\Delta\Omega)\Delta\Omega, \quad (3.34)$$

where $a(W^+W^-)$ is given in Eq. (3.6). Flux predictions for several representative values of M are shown in Fig. 3.7. In each case, the flux drops abruptly at the maximal photon energy,

$$E^{\gamma}_{\mathrm{max}} = \frac{M^2 - m_W^2}{M}. \quad (3.35)$$

If this edge feature is observed, it would provide a robust signature of heavy photon annihilation, as well as a measurement of its mass. Note that the FSR and fragmentation components of the flux are comparable near the edge, so that the fractional drop in the "signal" flux at the edge is significant. Just as for the fragmentation photons, the sensitivity to the FSR flux at ACTs is limited by the background from electron-induced showers. Assuming a 10% uncertainty on the

total flux measurement, the drop in the total flux associated with the edge feature of the FSR spectrum can be observed if $\bar{J} \gtrsim 10^5 - 10^6$. The sensitivity at Fermi/GLAST is limited by statistics, and an observation of the FSR edge requires even higher values of $\bar{J}$.

3.4.6 Pre-existing Constraints on the Photon Flux

Thus far, we have taken the galactic model parameter $\bar{J}$ to be constrained only by the results of numerical simulations. However, the prospects of the future searches are further restricted by the constraints on the *continuous* component of the photon flux from the observations of the gamma rays from the galactic center in the energy range up to 30 GeV by EGRET [72, 73]. Essentially, the observed gamma ray flux imposes an upper limit to $\bar{J}$, that in turn corresponds to an upper limit on the fluxes allowable in this model. Since the FSR spectrum is sub-dominant at these energies, the limit is determined by the component of the flux computed in section 3.4.4.

Examining Figs. 3.4, 3.5 and 3.7, we see that the $Z\gamma$ photon flux is always the dominant part of the spectrum that contains a sharp feature. The *maximum* value of the $Z\gamma$ photon flux compatible with the EGRET constraint (independently of the galactic halo profile) is shown in Fig. 3.8. It is clear that this maximum flux is substantially below the sensitivity of the current and near-future telescopes throughout the parameter space; it follows that the chances of seeing any of the clear signals of a non-astrophysical gamma ray source in this model are poor.

Given the presence of a point-like background source at the galactic center, other regions with possible dark matter overdensity were suggested as potential targets for a search for anomalous gamma rays. These include dwarf spheroidal companion galaxies to the Milky Way such as Sagittarius, Draco and Canis Ma-

jor [74, 75], as well as the Large Magellanic Cloud and the M87 galaxy [28]. In addition, in models where the galaxy is built up from hierarchical dark matter clustering one should expect localized clumps of dark matter inside the Milky Way halo. The values of $\bar{J}\Delta\Omega$ expected for these objects are model-dependent. For example, the dark matter profiles in dwarf spheroidals surveyed in Ref. [74] give $\bar{J}\Delta\Omega \approx 10^{-3}-1$ for $\Delta\Omega = 10^{-3}, 10^{-5}$. For dark matter clumps in the halo, Baltz *et. al.* [76] estimate that a typical clump would have $\bar{J}\Delta\Omega \approx 0.4$ at $\Delta\Omega = 1.5 \times 10^{-4}$. (This estimate uses the data from a simulation by Taylor and Babul [77].) For a space-based telescope such as GLAST, the background flux for these targets can be estimated by a simple power-law extrapolation of the extragalactic gamma ray flux measured by EGRET [78]:

$$\frac{\mathrm{d}^2\Phi}{\mathrm{d}E\mathrm{d}\Omega} = k \left(\frac{E}{100\ \mathrm{GeV}}\right)^{-2.1}, \tag{3.36}$$

where $k = 8.2 \times 10^{-11}\ \mathrm{cm}^{-2}\mathrm{s}^{-1}\mathrm{sr}^{-1}\mathrm{GeV}^{-1}$. Assuming a telescope with energy resolution $\delta E/E = 0.1$, the signal/background ratio is close to 1 for sources with $\bar{J}\Delta\Omega \sim 1$ in a model with $M \sim 100$ GeV. (The signal/background ratio decreases with increasing M and/or decreasing $\bar{J}$.) However, the number of $Z\gamma$ events expected at GLAST ($A = 10^4\ \mathrm{cm}^2$) is well below 1 event/year, so that no discovery is possible. Of course, this pessimistic prediction could be proven wrong if dark matter turned out to be significantly stronger clumped at short scales than presently thought, resulting in larger values of $\bar{J}$. Barring this possibility, a telescope with a larger effective area ($A \gtrsim 10^7\ \mathrm{cm}^2$) would be required to begin probing the heavy photon dark matter model in this channel.

3.4.7 Summary of Photon Flux

To summarize, we found that the best prospects for a discovery of anomalous gamma rays due to heavy photon annihilation in the Milky Way are offered by the

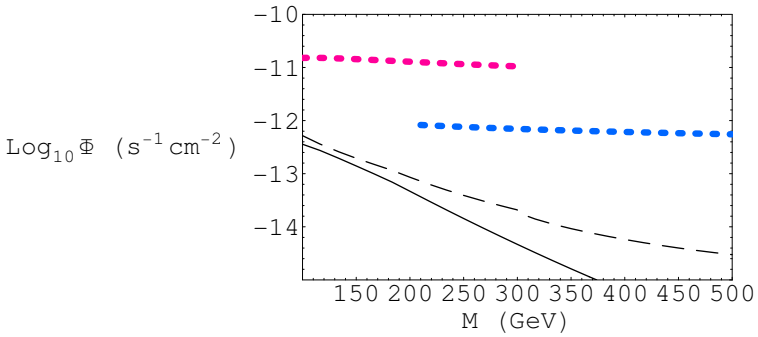

Figure 3.8: Maximum $Z\gamma$ photon fluxes consistent with the EGRET bound on the continuous photon flux from WIMP annihilation. Solid line: "high" pair-annihilation region; dashed line: coannihilation region with $m_h = 300$ GeV. Also shown are the sensitivities of GLAST (dotted red line) and HESS (dotted blue line) [73].

GLAST telescope, which should be able to observe tens of fragmentation photons in the multi-GeV energy range. The fluxes of monochromatic and FSR photons, whose spectra would provide clear signatures for galactic WIMP annihilation (a bump and an edge, respectively), are significantly smaller. These sources probably can not be detected from the galactic center, once the existing observations are used to constrain the dark matter profile. The possibility of detecting monochromatic and FSR photons from dwarf spheroidals depends on dark matter being more strongly clumped at short scales than presently thought, so that $\bar{J}\Delta\Omega \gg 1$ for these sources.

3.5 Direct Detection

Direct dark matter detection experiments attempt to observe the recoil energy transferred to a target nucleus in an elastic collision with a WIMP. The null result of the current experiments places an upper bound on the cross section of elastic WIMP-nucleon scattering. In this section, we will discuss the implications of this

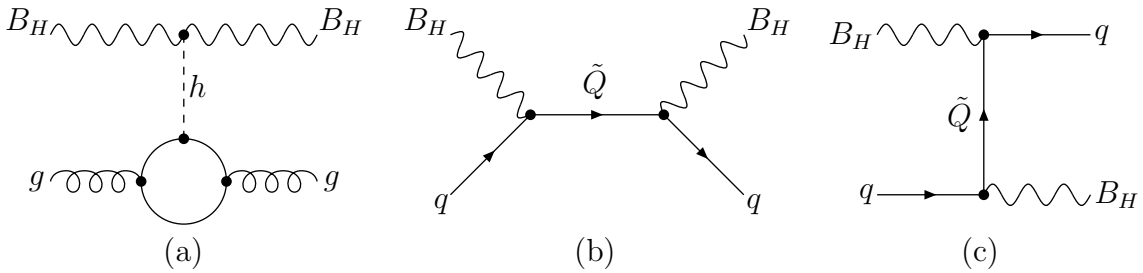

Figure 3.9: The leading processes which contribute to the heavy photon–nucleon elastic scattering cross section relevant for direct dark matter detection experiments.

bound for the LHT dark matter, and prospects for future discovery.

The elastic scattering of the heavy photon on a nucleus receives contributions from several processes shown in Fig. 3.9. Consider first the scattering off gluons, which occurs via the Higgs exchange diagram (a). The Higgs-gluon coupling arises predominantly via a top quark loop, and has the form [79]

$$\mathcal{L}_{hgg} \;=\; \frac{\alpha_s}{12\pi v}\, h G^a_{\mu\nu} G^{a\mu\nu}. \tag{3.37}$$

where $v = 246$ GeV is the Higgs vev, and $G^a_{\mu\nu}$ is the color field strength. The halo WIMPs are highly nonrelativistic ($\beta \sim 10^{-3}$), and the momentum transfer in the reaction at hand is negligible compared to m_h. The WIMP-gluon interaction can then be described by an effective operator

$$\frac{\alpha_s \alpha}{6\cos^2\theta_W}\frac{1}{m_h^2} B_{\mathrm{H}\alpha} B^\alpha_{\mathrm{H}}\, G^a_{\mu\nu} G^{a\mu\nu}. \tag{3.38}$$

In the chiral limit, the matrix element $\langle n|G^2|n\rangle$ can be related to the nucleon mass m_n [79], leading to an effective WIMP-nucleon vertex of the form

$$\mathcal{L}_{\mathrm{eff}} \;=\; \frac{e^2}{27\cos^2\theta_W}\frac{m_n}{m_h^2}\, B_{\mathrm{H}\alpha} B^\alpha_{\mathrm{H}}\, \bar{\Psi}_n \Psi_n, \tag{3.39}$$

where Ψ_n is the nucleon (neutron or proton) field. It is clear that this interaction only contributes to the spin-independent (SI) part of the WIMP-nucleon scattering cross section. Neglecting other contributions to the SI cross section (which, as we

will argue below, are expected to be subdominant), we obtain

$$\sigma_{\rm SI} \;=\; \frac{4\pi\alpha^2}{729\cos^4\theta_W}\,\frac{m_n^4}{m_h^4}\,\frac{1}{(M+m_n)^2}, \tag{3.40}$$

for both neutrons and protons. Since the scattering off nucleons in a given nucleus is coherent and the matrix elements for neutrons and protons are identical, the SI cross section for scattering off a nucleus of mass m_N is simply obtained from Eq. (3.40) by a substitution $m_n \to m_N$.

The interaction of WIMPs with quarks is dominated by the T-odd quark exchange diagrams, see Fig. 3.9 (b) and (c). (The Higgs exchange diagrams are suppressed due to small Yukawa couplings of quarks. In fact, it is well known that the Higgs-nucleon interaction is dominated by the Higgs-gluon coupling considered above.) The scattering amplitude is given by

$$-i\frac{e^2\tilde{Y}^2}{\cos^2\theta_W}\varepsilon^*_\mu(p_3)\varepsilon_\nu(p_1)\;\bar{u}(p_4)\left[\frac{\gamma^\mu\,\not{k}_1\gamma^\nu}{k_1^2-\tilde{M}^2}+\frac{\gamma^\nu\,\not{k}_2\gamma^\mu}{k_2^2-\tilde{M}^2}\right]P_L\,u(p_2)\;, \tag{3.41}$$

where $k_1 = p_1 + p_2,\ k_2 = p_2 - p_3$. The $q\tilde{q}B_H$ coupling is flavor-independent, $\tilde{Y} = 1/10$, and the expression (3.41) is valid for every quark species. The amplitude contains two important physical scales: the weak scale, $M \sim \tilde{M} \sim 100$ GeV, and the QCD scale, $\Lambda_{\rm QCD} \sim 100$ MeV, which represents the typical energy and momentum of the quarks bound inside a stationary nucleus and, by a coincidence, the spatial momenta of the halo WIMPs: $|\mathbf{p}|_{1,3} \sim \beta M \sim \Lambda_{\rm QCD}$. We will work to leading order in the ratio of these two scales. In this approximation, $k_1 \approx -k_2 \approx (M, \mathbf{0})$, and the heavy photon polarization vectors are purely spatial, $\varepsilon^\mu(p_{1,3}) = (0, \varepsilon_{1,3})$. The amplitude takes the form

$$\frac{e^2\tilde{Y}^2}{\cos^2\theta_W}\,\frac{M}{M^2-\tilde{M}^2}\,\epsilon_{ijk}\varepsilon_1^i\varepsilon_3^j\bar{u}_4\gamma^k(1-\gamma^5)u_2\,, \tag{3.42}$$

corresponding to the coupling of the B_H spin with the vector and axial-vector quark currents. The axial current interaction corresponds to the coupling between

the WIMP and quark spins, and gives rise to the spin-dependent (SD) part of the WIMP-nucleus scattering cross section. By the Wigner-Eckardt theorem, the quark axial current can be replaced by the nuclear spin operator s_N^μ:

$$\left\langle N|\bar{q}\gamma^\mu\gamma^5 q|N\right\rangle \,=\, 2s_N^\mu\lambda_q. \tag{3.43}$$

For a nucleus of spin J_N, the coefficients are given by

$$\lambda_q = \Delta q_p \frac{\langle S_p\rangle}{J_N} + \Delta q_n \frac{\langle S_n\rangle}{J_N}, \tag{3.44}$$

where $\langle S_{p,n}\rangle / J_N$ is the fraction of the total nuclear spin carried by protons and neutrons, respectively, and the quantities Δq_n can be extracted from deep inelastic scattering data. We will use $\Delta u_p = \Delta d_n = 0.78 \pm 0.02$, $\Delta d_p = \Delta u_n = -0.48 \pm 0.02$, $\Delta s_n = \Delta s_p = -0.15 \pm 0.02$ [80]. The effective WIMP-nucleus spin-spin interaction can then be written as

$$\frac{2e^2\tilde{Y}^2 M}{\cos^2\theta_W(M^2-\tilde{M}^2)}\,\epsilon_{ijk}B_H^i B_H^j \bar{\Psi}_N s_N^k \Psi_N \sum_{q=u,d,s}\lambda_q, \tag{3.45}$$

yielding the SD cross section

$$\sigma_{\rm SD} \,=\, \frac{16\pi\alpha^2\tilde{Y}^4}{3\cos^4\theta_W}\frac{m_N^2}{(M+m_N)^2}\,\frac{M^2}{(M^2-\tilde{M}^2)^2}\,J_N(J_N+1)\left(\sum_{q=u,d,s}\lambda_q\right)^2. \tag{3.46}$$

Now, consider the part of the amplitude (3.42) involving the quark vector current. Since the current is conserved, the contributions of each valence quark in a nucleon add coherently, and sea quarks do not contribute. The resulting WIMP-nucleon coupling is

$$\frac{3e^2\tilde{Y}^2 M}{\cos^2\theta_W(M^2-\tilde{M}^2)}\,\epsilon_{ijk}B_H^i B_H^j \bar{\Psi}_n\gamma^k\Psi_n\,. \tag{3.47}$$

This interaction is suppressed in the nonrelativistic limit, since $\bar{u}_n\gamma^k u_n \sim v_n^k$. In fact, it is of the same order as other contributions to the WIMP-quark scattering amplitude, suppressed by WIMP velocities or powers of $\Lambda_{\rm QCD}/M$, which were neglected in our analysis. Therefore, its effect will be neglected.

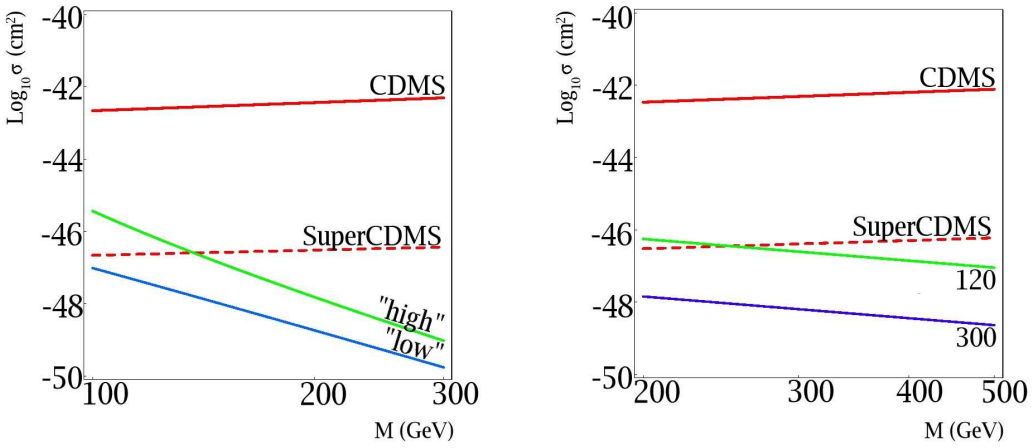

Figure 3.10: The spin-independent (SI) WIMP-nucleon elastic scattering cross section in the pair-annihilation bands (left panel) and in the coannihilation region, for two values of m_h, 120 and 300 GeV (right panel). The present [81] and projected [82] sensitivities of the CDMS experiment are also shown.

It should be noted that the SI interaction in Eq. (3.39), is parametrically suppressed with respect to the leading SD coupling, Eq. (3.45), by a factor of $m_N/m_h \sim \Lambda_{\rm QCD}/M$, and is formally of the same order as the contributions to the WIMP-quark interaction that were neglected in our analysis. Since the neglected terms contribute to the SI as well as SD interactions, one may question the validity of the SI cross section obtained in Eq. (3.40). Note, however, that the WIMP-quark interactions are additionally suppressed by a factor of $\tilde{Y}^2 = 0.01$, not present in the WIMP-gluon couplings. Thus, while of the same order as (3.39) in terms of power counting, the neglected SI corrections from WIMP-quark interactions are expected to be numerically small. One interesting potential exception occurs in the coannihilation region, where the $\tilde{Y}$ suppression could be compensated by the factor of $\tilde{M} - M \ll M$ in the propagator, and the WIMP-quark interactions could provide a significant correction to Eq. (3.40). A detailed analysis of this issue is reserved for future study.

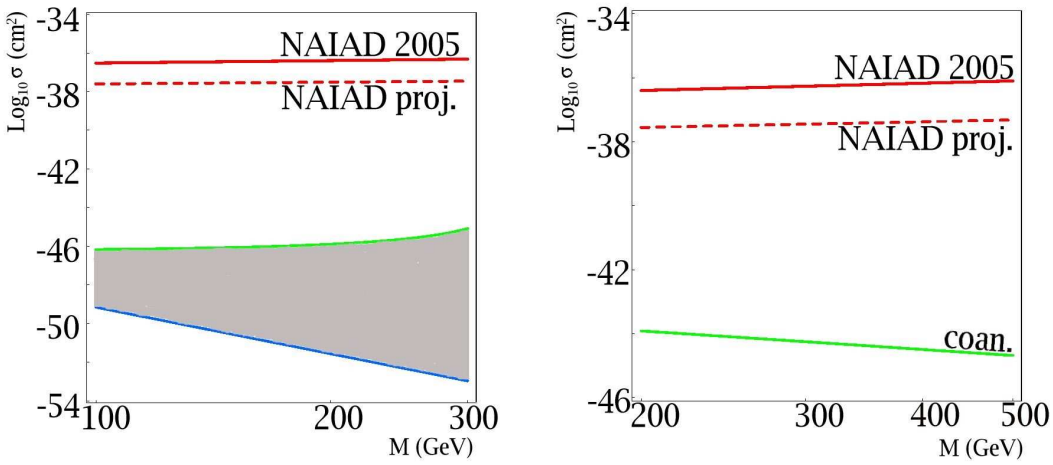

Figure 3.11: The spin-dependent (SD) WIMP-proton elastic scattering cross section in the pair-annihilation bands (left panel) and in the coannihilation region (right panel). In the pair-annihilation bands, the scale $\tilde{M}$ is allowed to vary between 350 GeV and the upper bound given in Eq. (3.3). The present [83] and projected [84] sensitivities of the NAIAD experiment are also shown.

The SI elastic WIMP-nucleon scattering cross sections expected in the LHT models are plotted in Fig. 3.10, along with the current bound from the CDMS collaboration [81] (solid red lines) and the projected future sensitivity of SuperCDMS, stage C [82] (dashed red lines). We assume that the heavy photons account for all of the observed dark matter, and the two panels correspond to the two regions of parameter space which satisfy this constraint. The left panel shows the cross section expected in the pair-annihilation bands, with the two lines corresponding to the high and low solutions in Eq. (3.11). The right panel shows the cross section expected in the coannihilation tail for two values of the Higgs mass, 120 GeV and 300 GeV. The two lines can be thought of as the upper and lower bounds on the expected cross section.[15] While the predicted cross sections are two-three

[15]Note, however, that in the LHT model a heavy Higgs, $m_h > 300$ GeV, may be consistent with precision electroweak data in certain regions of parameter space where its contribution to the T

orders of magnitude below the present sensitivity, the expected improvements of the CDMS experiments will allow it to begin probing the interesting regions of the model parameter space in both pair-annihilation and coannihilation regions.

Fig. 3.11 shows the spin-dependent cross sections predicted by the LHT model, along with the current bound from the NAIAD experiment [83] and its projected sensitivity [84]. In the pair-annihilation bands, the scale $\tilde{M}$ is allowed to vary between 350 GeV and the upper bound given in Eq. (3.3). (Recall that for a given value of M, the scale f is fixed unambiguously by Eq. (3.1).) Unfortunately, the predicted SD cross sections are several orders of magnitude below the NAIAD sensitivity.

3.6 Neutrino Fluxes from B_H Annihilations

Neutrinos produced in annihilations of heavy photons collected in the gravitational wells of the Sun and the Earth provide another potentially observable indirect signature of Little Higgs dark matter. The procedure for evaluating the neutrino fluxes in a given model is well established; a thorough review (in the context of SUSY) is given in [26]. Here we will follow this procedure to compute the neutrino fluxes expected in the LHT model.

The number of WIMPs N collected in the Sun or the Earth obeys

$$\dot{N} = C - A\,N^2, \tag{3.48}$$

where C is the capture rate and A is the annihilation rate per WIMP. Schematically, the capture rate is given by

$$C \sim c\frac{\left\langle \sigma_{\rm pb}^{\rm el} \right\rangle}{M_{\rm GeV}^2} \tag{3.49}$$

parameter is partially canceled by new physics contributions [55]. A heavier Higgs corresponds to smaller SI cross section.

where $M_{\rm GeV}$ is the WIMP mass in units of GeV, the quantity $\left\langle \sigma_{\rm pb}^{\rm el} \right\rangle$ is essentially the weighted average of the elastic WIMP-nucleus scattering cross sections (in pb) over the atomic composition of the Sun or the Earth, and c is a coefficient determined by the properties of the astronomical body in question: $c \sim 10^{30}$ s^{-1} for the Sun and $c \sim 10^{20}$ s^{-1} for the Earth. (See Ref. [26] for a more detailed discussion.) The only input from particle physics required to compute C is the elastic scattering cross sections, which were computed in the previous section for the LHT model. The annihilation rate per WIMP A is schematically given by

$$A = \frac{\langle \sigma_{\rm an} u \rangle}{V_{\rm eff}}, \tag{3.50}$$

where $\sigma_{\rm an}$ is the total WIMP annihilation cross section, the average is over the thermal distribution of the WIMPs captured in the Sun or the Earth, and $V_{\rm eff}$ is the effective volume of the "WIMP-sphere" inside the astronomical body. (For details, see Ref. [26].)

Having computed C and A, we solve Eq. (3.48) to obtain the total WIMP annihilation rate:

$$\Gamma_A = \frac{1}{2}\, C\, \tanh^2\left(t\sqrt{A\,C}\right)\,, \tag{3.51}$$

where $t \approx 4.5{\cdot}10^9$ years is the age of the Solar System. The experimental technique best suited to searching for high-energy neutrinos from WIMP annihilation relies on observing an upward-going muon created by a charged-current interaction of a muon neutrino in the rock below the detector. The rate of such muons per unit detector area is given by [26]

$$\Gamma_{\rm detect} \;=\; (2.54\times 10^{-29}\ {\rm m}^{-2}{\rm yr}^{-1})\,\frac{\Gamma_A}{{\rm s}^{-1}}\,M_{\rm GeV}^2\,\sum_i a_i b_i \sum_F B_F \left\langle N z^2 \right\rangle_{F,i}(M)\,, \tag{3.52}$$

where i are the possible neutrino types, a_i and b_i are (known) coefficients describing the neutrino scattering and muon propagation in the rock, and F are the possible final states of WIMP annihilation with branching fractions B_F. In the LHT model,

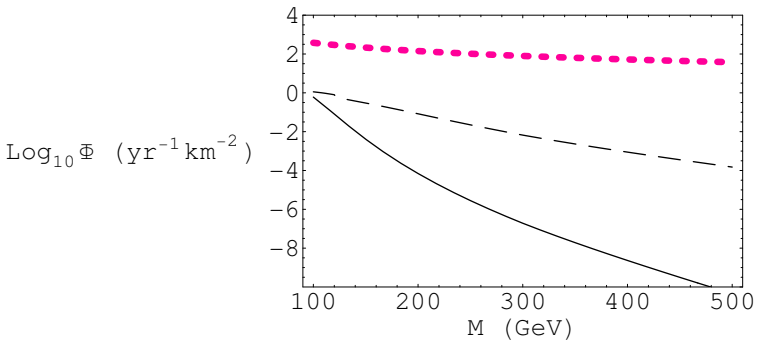

Figure 3.12: The rate of neutrino-induced upward-going muon events expected from the heavy photon annihilation in the Sun. Solid line: "low" pair-annihilation region (the flux in the "high" pair-annihilation region is similar); dashed line: coannihilation region with $m_h = 300$ GeV. Also shown is the expected sensitivity of the IceCube detector (red/dotted line).

the dominant annihilation channels are W^+W^- and ZZ. The quantity

$$\left\langle Nz^2 \right\rangle_{F,i}(M) \equiv \int_{E_{th}/M}^{1} \frac{\mathrm{d}N_{F,i}}{\mathrm{d}z}(E_i, z) z^2 \mathrm{d}z \tag{3.53}$$

is the second moment of the spectrum of neutrino type i from final state F. Here E_{th} is the threshold energy of the detector, and $dN_{F,i}/dz$ is the neutrino spectrum, normalized per single WIMP annihilation into the final state F. This spectrum is a convolution of the initial neutrino spectrum at the production point with the propagation effects (including neutrino oscillations and absorbtion) on the way to the detector. In this analysis we used the neutrino spectra computed by Cirelli *et. al.* [85],[16] and assumed a detector with a threshold energy of 50 GeV, representative of the IceCube experiment [86]. Note however that lowering this threshold would not have a substantial effect on the rates, since the sub-threshold contribution to the rate scales as $(E_{\rm th}/M)^3$ and is at most of order 10% throughout the interesting parameter range in the LHT model.

The rate of neutrino-induced upward-going muon events expected from the

[16]We thank Marco Cirelli for providing us with the updated version of the spectra.

heavy photon annihilation in the Sun is shown in Fig. 3.12. The expected sensitivity of the IceCube detector is shown for comparison. The maximum possible rate (achieved at the low end of the allowed LTP mass range, $M \approx 100$ GeV) is about 1 event/yr/km^2 in the coannihilation region and about 0.5 events/yr/km^2 in pair-annihilation regions. Unfortunately these rates are well below the sensitivity of the IceCube. The sensitivity would need to be improved by a factor of a few hundred to a thousand before the fluxes predicted in the LHT models can be probed. The rates of events due to heavy photon annihilation in the Earth are even smaller, of the order 10^{-5} events/yr/km^2 or below throughout the parameter space.

3.7 Summary of Little Higgs Dark Matter

Little Higgs models provide an interesting alternative scenario for physics at the TeV scale, with a simple and attractive mechanism of radiative electroweak symmetry breaking. Many realistic models implementing the Little Higgs mechanism have been proposed; however, generically these models are ruled out by precision electroweak data, unless the scale f is in a few-TeV range which reintroduces fine-tuning. Little Higgs models with T parity avoid this difficulty. In this chapter, we focused on the Littlest Higgs model with T parity (LHT), one of the simplest models in this class. T parity makes the lightest of the T-odd particles, the LTP, stable, enabling it to have a substantial abundance in today's universe in spite of its weak-scale mass. In the LHT model, the LTP is typically the heavy photon B_H, which can play the role of WIMP dark matter. We have computed the relic abundance of this particle, including coannihilation effects, and mapped out the regions of the parameter space where it has the correct relic abundance to account for all, or a substantial part, of the observed dark matter. These regions can be

divided into the pair-annihilation bands, where the abundance is set by the B_H pair annihilation via s-channel Higgs resonance, and the coannihilation tail, where coannihilations of B_H with T-odd quarks $\tilde{Q}$ and leptons $\tilde{L}$ play the dominant role.

In the second part of the chapter, we evaluated the prospects for observing the heavy photon dark matter of the LHT model using direct and indirect detection techniques. Direct detection is quite difficult, due to the fact that the heavy photon predominantly couples to the Standard Model states via the Higgs boson whose interactions with nucleons are weak. The elastic cross section of the B_H scattering on a nucleus in the region of parameter space consistent with the relic density constraint was found to be several orders of magnitude below the current sensitivity of direct detection searches such as CDMS.

For indirect detection, we discussed both the anomalous high-energy gamma ray signature, and the flux of high-energy neutrinos from the annihilation of the heavy photons trapped in the Sun and the Earth. Unfortunately, the near-term prospects for observing both signatures are rather poor. The predicted gamma ray flux depends sensitively on the distribution of dark matter in the halo. The best discovery prospect is offered by the Fermi telescope, which can observe the photons arising from the fragmentation of the W and Z bosons produced in the heavy photon annihilation. If dark matter distribution in the halo is favorable (in particular, if it is highly clumpy on short scales), it might also be possible to observe the monochromatic and the FSR components of the photon flux. These spectra exhibit well-defined features (a line and an edge, respectively) and would provide a smoking-gun evidence for the WIMP-related nature of the signal. Finally, in the neutrino case, the predicted flux is too small to be observed at the IceCube.

This study complements previous analyses of the discovery prospects for the LHT dark matter. While all predictions are subject to significant astrophysical un-

certainties, it appears that the most promising search channels are the "secondary" gamma rays produced in hadronization and fragmentation of the primary WIMP annihilation products, and anomalous high-energy positrons [21]. In these channels, the signal may be observed by the near-future instruments, GLAST in the case of gamma rays and PAMELA and AMS-02 in the case of positrons. On the other hand, the LHT model predicts that no signal will be observed in the near-future direct detection and high-energy neutrino searches, while the monochromatic gamma ray signal is very unlikely. By testing the predicted pattern of signals, astroparticle experiments will provide an important test of the LHT dark matter hypothesis, complementary to the more direct searches for the new particles predicted by the LHT model at the Large Hadron Collider.

CHAPTER 4

TENSOR REGGEONS FROM WARPED SPACE AT THE LHC

4.1 Introduction

In the previous two chapters, we considered possible extensions of the SM through the lens of dark matter searches. We worked both in a model-independent context, and within the boundaries of a pre-existing model. However, as the arrival of experimental data draws near, it behooves us to ensure that as many models of new physics as possible are studied. Within *this* chapter, we therefore consider a previously unconsidered possibility, combining string theory with warped extra dimensions. Our motivation is also different from before, resting in the hierarchy problem and one class of its possible solutions.

In the last decade, a number of interesting new physics scenarios involving extra dimensions of space relevant at the TeV scale have been proposed. Two of the best-known examples are the models with flat Large Extra Dimensions (LED), due to Arkani-Hamed, Dimopoulos, and Dvali [87], and the models with a single extra dimension with a non-factorizable ("warped") metric, suggested by Randall and Sundrum (RS) [22]. Both classes of models address the gauge hierarchy problem, motivating them as complements for the SM at the weak scale (although in the LED model, an additional mechanism is needed to stabilize the radii of the extra dimensions at large values in natural units). In the case of LED, this is achieved by bringing the fundamental scale of quantum gravity down into the TeV domain. If the LED scenario is realized, and if string theory serves as the ultraviolet completion of Einstein's general relativity, the stringy nature of the SM particles should become apparent at the TeV scale. In particular, the upcoming experiments at the Large Hadron Collider (LHC) could observe inherently stringy

Regge excitations of the familiar SM states. A phenomenological study of collider signatures of these states, based on simple toy models embedding parts of the SM into string theory, was initiated by Cullen, Perelstein and Peskin, in Ref. [88]. A large body of literature exists on this subject; see, e.g., Refs. [89] for some examples, and Ref. [90] for a recent review.

The RS model, viewed as a five-dimensional theory, resolves the hierarchy problem in a similar way: while the fundamental 5D Planck scale $M_{\rm Pl}^*$ is close to its 4D value (of the order of 10^{19} GeV), the actual scale where gravitational physics becomes strongly coupled depends on the position in the extra dimension, due to the non-trivial dependence of the metric on this coordinate. In particular, the scale near the "infrared (IR) brane", where the Higgs field is localized, is in the TeV domain, and that is where the Higgs loop divergences are cut off. If the RS setup emerges as part of the compactification manifold in a weakly-coupled string theory, the fundamental 5D[1] string scale, M_S^*, should lie parametrically below $M_{\rm Pl}^*$, and parametrically above the curvature scale k:

$$k \ll M_S^* \ll M_{\rm Pl}^*. \tag{4.1}$$

Phenomenologically, no large hierarchy can exist between k and $M_{\rm Pl}^*$ (increasing their ratio would exacerbate the already non-trivial tension between experimental constraints on the model and the fine-tuning in the Higgs mass); values of order 10 are preferred. The inequality (4.1) then implies $M_S^* \sim 10^{18} - 10^{19}$ GeV.[2] The Regge excitations of the states that are free to propagate in the full 5D space will appear as 5D fields, with mass terms in the 5D lagrangian of order M_S^*. However,

[1] We will not be concerned with the compactification of the other 5 dimensions at this point, assuming for simplicity that their radii are of order inverse $M_{\rm Pl}^*$ and thus they can be safely integrated out.

[2] Another obvious implication is that no large separation of scales is possible, and the approximation of weakly-coupled strings propagating on a smooth geometric background is probably subject to sizable corrections. Since in this chapter our goal is to build a toy model to describe the major features of Reggeon phenomenology, rather than a rigorous calculation, we will not be concerned about this point.

in the neighborhood of the IR brane, the masses will be warped down to the TeV scale, and upon Kaluza-Klein (KK) decomposition we should expect to see 4D Reggeons with masses in the TeV domain. Although the original RS model had all of the SM fields confined on the IR brane, it was subsequently realized that a model with the full SM (with the possible exception of the Higgs) propagating in the full 5D space is more interesting: it can naturally explain the apparent unification of gauge couplings [91], avoid precision electroweak constraints [92], and has attractive mechanisms to explain the fermion mass hierarchy [93] and suppression of flavor-changing neutral currents [94]. This setup has also been used to construct "Higgsless" models [95], where electroweak symmetry is broken by boundary conditions on the 5D gauge fields. In these models, one expects a rich Reggeon sector to appear around the warped-down string scale. The goal of this chapter is to construct a simple toy model incorporating some of the main features of this sector relevant for collider searches, and to discuss the resulting phenomenology.

Before proceeding, let us comment on how the Regge physics appears in the dual four-dimensional picture. In this picture, the warped-down Planck scale is the scale at which conformal invariance of the fundamental gauge theory is broken. The Higgs and all other states localized at, or near, the IR brane of the 5D model, can be understood as bound states of the fundamental gauge degrees of freedom, with binding energies of order TeV. The Regge states described by our toy model are no exception: from the dual point of view, they are simply higher-spin bound states (e.g., the first Regge excitations of gauge bosons are spin-2 "glueballs"). In principle, both descriptions can provide interesting information. However, for the low-lying Regge states (below the warped-down Planck scale) that are our focus here, the five-dimensional description is clearly advantageous, since in it these

states are weakly coupled.

The studies of Regge phenomenology in LED models are based on a well-known result in string theory: the Veneziano amplitudes for tree-level scattering of open-string states. Factorizing these amplitudes on their poles determines the Reggeon masses and their (on-shell) couplings to the SM states, which is sufficient to model their collider signatures. Unfortunately, the Veneziano amplitudes only apply to strings propagating on backgrounds with flat (Minkowski) metric, and their generalization to warped spaces such as the RS model is presently unknown. Therefore, we will pursue a different approach. We will restrict our attention to a small subset of the Regge states, namely, the lowest-lying spin-2 Regge excitations of the SM gauge bosons, in particular SM gluon. These states present most realistic targets for collider searches, due to a possibility of relatively large production cross sections at hadron colliders, and their higher-spin nature would make them striking signatures for low-scale string theory. We will begin, in section 4.2, by constructing a Lagrangian which reproduces their masses and on-shell couplings to SM in flat space, as obtained from Veneziano amplitudes in previous work. We will then generalize this Lagrangian, in sections 4.3 and 4.4, to spaces with arbitrary metric, using the standard trick of introducing metric factors and covariant derivatives to restore general covariance. (In fact, a slightly non-minimal extension will be preferred, in order to maintain a simple form of the gauge invariance for spin-2 states.) In section 4.3.2, we will also study the KK decomposition of a massive 5D spin-2 field, which to the best of our knowledge has not yet been considered in the literature. In section 4.5, we will outline the predictions of our model for the LHC phenomenology of the 4D tensor Regge excitation of the gluon.[3]

[3]High-energy behavior of scattering amplitudes in RS space has been considered in Ref. [96]. An approach similar to ours has been applied recently in Ref. [97] to spin-3/2 Regge excitations of the top quark.

4.2 A Model for Reggeons in Flat 4D Space

Our starting point is the toy model proposed by Cullen, Perelstein and Peskin (CPP) in Ref. [88]. This toy model embeds QED of electrons and photons and QCD of quarks and gluons into string theory as zero modes of open strings living on coincident D3 branes. Factorizing the tree-level scattering amplitudes between these states at their s-channel poles at $s = M_S^2$ provides their (on-shell) couplings to the first-level Reggeons. Our goal in this section is to encode these couplings in a Lagrangian, which can then be generalized to the Randall-Sundrum model.

4.2.1 Stringy Toy Model of Electrons and Photons

To describe a string embedding of electrons and photons, the CPP model introduces two coincident D3 branes. The low-energy physics of this configuration is given by an $\mathcal{N} = 4$ supersymmetric theory with a $U(2)$ gauge group. However, if the external states are chosen from a restricted set consisting of a single (diagonal) gauge boson and two (off-diagonal) gauginos, the internal propagators in any tree-level diagram must also come from this set. The gauge boson is identified with the photon and the two gauginos with the two helicity states of the electron. Taking the low-energy limit of the tree-level scattering amplitudes of this string theory reproduces the familiar helicity amplitudes of QED, while at high energies the amplitudes exhibit the Regge poles characteristic of string theory. In particular, on-shell couplings of the string Regge resonances to the SM (zero-mode) fields can be obtained by factorizing the amplitudes on the s-channel Regge poles.

Since the kinematic reach of near-future collider experiments is unlikely to extend deep into the Regge domain, we will focus our analysis on modelling the phenomenology of the first Regge level. Moreover, as the first step, we will restrict ourselves to the excitations of the SM gauge bosons. These states can be singly

produced in the collision of SM fermion-antifermion pairs, as well as, in the case of the $SU(3)$ Reggeons, SM gluons. In the CPP model, the bosonic states at the first Regge level are a spin-2 state γ_2^*, a spin-1 state γ_1^*, and four spin-0 states $\gamma_0^{*(i)}$. We will focus on the spin-2 states in this chapter, since they would provide the most unambiguous signature of stringy physics if discovered; the approach of this chapter, however, can be easily generalized to include the lower-spin states. Our first task is to construct a field theory model to reproduce the Feynman rules for the couplings of these states to SM, derived in Ref. [88]. We introduce Reggeon field $B_{\mu\nu}(x)$. (Since open strings are confined to D3 branes, it is a 4D field.) The quadratic action has the usual form:

$$\mathcal{L}_{S=2} \;=\; \frac{1}{4}H^{\lambda\mu\nu}H_{\lambda\mu\nu} - \frac{1}{2}H^{\lambda\mu}{}_{\mu}H_{\lambda\nu}{}^{\nu} + \frac{1}{2}m^2\left\{\left(B_{\mu}{}^{\mu}\right)^2 - B^{\mu\nu}B_{\mu\nu}\right\}\,, \tag{4.2}$$

where we introduced the field-strength tensor $H_{\lambda\mu\nu} \equiv \partial_\lambda B_{\mu\nu} - \partial_\mu B_{\lambda\nu}$, and $m \equiv M_S$ is the Reggeon mass. The kinetic term is, up to a factor, the same as the standard graviton action found by expanding the Einstien-Hilbert action to quadratic order in $h_{\mu\nu} \equiv g_{\mu\nu} - \eta_{\mu\nu}$. The mass term has the Fierz-Pauli form [98] that is necessary for unitarity.

The interactions of SM electrons and photons (string zero-modes) with the Regge states can be described by the following lagrangian:

$$\begin{aligned}\mathscr{L}_{\rm int} = {}& \frac{i\,e}{\sqrt{2}M_S}\left(\partial^\mu\bar{\psi}\gamma^\nu\psi - \bar{\psi}\gamma^\nu\partial^\mu\psi\right)B_{\mu\nu} \\ & + \frac{e}{\sqrt{2}M_S}\left(F^{\rho\mu}F^{\nu}{}_{\rho} - \frac{1}{4}F^{\rho\sigma}F_{\rho\sigma}\eta^{\mu\nu}\right)B_{\mu\nu} + \text{ (vectors, scalars)}\end{aligned} \tag{4.3}$$

where ψ is the electron field and F is the electromagnetic field strength. This lagrangian can be read off from the Feynman rules in Fig. 7 of Ref. [88]. Note that the Feynman rules were derived by factorizing the Veneziano amplitudes on the Regge poles, and thus only contain information about interactions of on-shell particles. So, the model (4.3) is only valid on-shell: there may be additional operators

not included here that vanish for on-shell particles. It is adequate for describing resonant production of Regge states in SM collisions at tree level, which should be sufficient for understanding the main features of their collider phenomenology.

4.2.2 Stringy Toy Model of Quarks and Gluons

The Regge gluon is of great interest phenomenologically, since it is strongly interacting and could have a large production cross section at hadron colliders. The quark-antiquark-Regge gluon coupling is simply obtained from the $e^+e^-\gamma^*$ vertex by replacing $e \to g$, promoting derivatives ∂_μ to covariant derivatives D_μ, and introducing the usual color structure [88]:

$$\mathcal{L}_{q\bar{q}g^*} = \frac{ig}{\sqrt{2}M_S}\left((D^\mu\bar{q})\gamma^\nu\tilde{B}_{\mu\nu}q - \bar{q}\gamma^\nu\tilde{B}_{\mu\nu}D^\mu q\right) + (\text{vectors}, \text{scalars})\,. \tag{4.4}$$

Here we defined $\tilde{B}_{\mu\nu} = B^a_{\mu\nu}t^a$, where $B^a_{\mu\nu}$ $(a = 1\ldots 8)$ is the Regge gluon field, and t^a are the fundamental representation generators of QCD $SU(3)$, normalized by $\mathrm{tr}(t^at^b) = \delta^{ab}/2$. Note that the Regge gluon field transforms linearly in the adjoint representation of $SU(3)$:

$$\tilde{B}_{\mu\nu} \to \mathcal{U}\,\tilde{B}_{\mu\nu}\mathcal{U}^{-1}, \quad \mathcal{U} = \exp\left(it^a\theta^a\right)\,. \tag{4.5}$$

Since $q \to \mathcal{U}q$, this ensures the gauge invariance of the coupling (4.4).

In the Randall-Sundrum model, the Regge gluon wavefunctions are localized near the TeV brane (as will be shown below), while the wavefunctions of light fermions may be localized at the opposite "Planck" boundary. In this case, the coupling of the Regge gluon to light SM quarks is strongly suppressed, and the most important production channel for g^* is via gluon fusion. (The zero-mode gluon wavefunction is constant across the extra dimension.) To model this interaction, we need to obtain the gluon-gluon-Regge gluon vertex in the CPP model. Since this was not done in Ref. [88], let us briefly outline the derivation here. The CPP

model identifies gluons with open strings ending on a stack of 4 coincident D3 branes. The 4-gluon scattering amplitude is given by

$$\begin{aligned}\mathcal{A}(1,2,3,4) \;=\; & g^2 A(1,2,3,4)\,\mathcal{S}(s,t)\,\mathrm{tr}[t^1t^2t^3t^4 + t^4t^3t^2t^1] \\ & + g^2 A(1,3,2,4)\,\mathcal{S}(u,t)\,\mathrm{tr}[t^1t^3t^2t^4 + t^4t^2t^3t^1] \\ & + g^2 A(1,2,4,3)\,\mathcal{S}(s,u)\,\mathrm{tr}[t^1t^2t^4t^3 + t^3t^4t^2t^1]\,, \quad (4.6)\end{aligned}$$

where $t^i \equiv t^{a_i}$ are the generators of the fundamental representation of $SU(3)$ ("Chan-Paton factors"), while

$$\mathcal{S}(s,t) = \frac{\Gamma(1-\alpha' s)\Gamma(1-\alpha' t)}{\Gamma(1-\alpha' s-\alpha' t)} \quad (4.7)$$

is the string formfactor (essentially the Veneziano amplitude), and the A's denote the color-ordered four-point gauge theory amplitudes. (Note that $\alpha' = 1/M_S^2$.) At tree level, all non-vanishing color-ordered helicity amplitudes for four-gluon scattering can be obtained from the two basic ones by index permutations. The basic amplitudes are

$$A(1^+,2^-,3^-,4^+) = -4\frac{t}{s}\,, \quad A(1^+,2^-,3^+,4^-) = -4\frac{u^2}{st}\,, \quad (4.8)$$

where helicities are directed inward. Using these amplitudes in Eq. (4.6) and factorizing the amplitudes on the Regge pole, $s = M_S^2$, we obtain

$$\mathcal{A}(g^+g^+ \to g^+g^+) = -g^2\frac{s}{s-M_S^2}\cdot\mathcal{C}^{1234}\,, \quad (4.9)$$

$$\mathcal{A}(g^+g^- \to g^+g^-) = -g^2\frac{u^2}{s^2}\,\frac{s}{s-M_S^2}\cdot\mathcal{C}^{1234}\,, \quad (4.10)$$

All other non-vanishing amplitudes are related to these two by parity. Note that the kinematic dependence of the factorized four-gluon amplitudes exactly matches that of the four-photon amplitudes studied in Ref. [88], implying that the Lorentz structure of the ggg^* vertices is the same as for the $\gamma\gamma\gamma^*$ vertices. The color factor

is given by

$$\mathcal{C}^{1234} = \mathrm{tr}[t^1 t^2 t^3 t^4] + \mathrm{tr}[t^4 t^3 t^2 t^1] + \mathrm{tr}[t^1 t^2 t^4 t^3] + \mathrm{tr}[t^3 t^4 t^2 t^1]\,, \tag{4.11}$$

where as before $t^i \equiv t^{a_i}$. To factorize this, we use the well-known $SU(N)$ identity

$$2\sum_{a=1}^{N^2-1} (t^a)^i_j (t^a)^k_l = \delta^i_l \delta^k_j - \frac{1}{N}\delta^i_j \delta^k_l\,. \tag{4.12}$$

We obtain

$$\mathcal{C}^{1234} = 2\sum_{a=1}^{N^2-1} \left(\mathrm{tr}[t^1 t^2 t^a] + \mathrm{tr}[t^2 t^1 t^a]\right) \cdot \left(\mathrm{tr}[t^3 t^4 t^a] + \mathrm{tr}[t^4 t^3 t^a]\right) + \frac{4}{3}\mathrm{tr}[t^1 t^2] \cdot \mathrm{tr}[t^3 t^4]\,. \tag{4.13}$$

This suggests that there are in fact 9 Regge gluons propagating in the s channel in four-gluon scattering: a color-octet, coupled with strength g, and a color-singlet, coupled with strength $g/\sqrt{3}$. The appearance of the color singlet Reggeon in the CPP model was already noted in Ref. [88]; in fact, there is an additional *massless* color-singlet vector boson in this model as well, due to an extra $U(1)$ factor in the low-energy theory of strings on D3-branes. In realistic string models, such $U(1)$ factors are typically anomalous, and the corresponding gauge bosons obtain masses at the string scale via Green-Schwartz mechanism. This mechanism will probably also affect the mass of the color-singlet Reggeon. In general, the fate of this state appears model-dependent, and even if it is present at M_S, its effect on phenomenology would be subdominant to the color-octet state due a smaller number of degrees of freedom and a suppressed coupling. Thus, we will focus on the color-octet Reggeon. To obtain the Feynman rules for the interactions of this state with SM gluons, one needs to simply multiply the photon-Regge photon vertices in Fig. 7 of Ref. [88] by a color factor

$$C^{abc} = \left(\mathrm{tr}[t^a t^b t^c] + \mathrm{tr}[t^a t^c t^b]\right)\,, \tag{4.14}$$

and substitute $e \to g$. The corresponding term in the Lagrangian is

$$\mathcal{L}_{ggg^*} = \frac{g}{\sqrt{2}M_S} C^{abc} \left(F^{a\rho\mu} F^{b\nu}_{\rho} - \frac{1}{4} F^{a\rho\sigma} F^{b}_{\rho\sigma} \eta^{\mu\nu} \right) B^{c}_{\mu\nu} + (\text{vectors}, \text{scalars}) \,, \quad (4.15)$$

where $F^a_{\mu\nu} = \partial_\mu A^a_\nu - \partial_\nu A^a_\mu + igf^{abc} A^b_\mu A^c_\nu$ is the gluon field strength. As before, it is important to keep in mind that this Lagrangian is only valid for on-shell production of Regge gluons in SM gluon collisions. Using

$$F^a_{\mu\nu} t^a \to \mathcal{U} \left(F^a_{\mu\nu} t^a \right) \mathcal{U}^{-1}, \quad (4.16)$$

together with Eq. (4.5), it is easy to show that the coupling (4.15) is $SU(3)$ invariant. Note that in order to preserve gauge invariance, the derivatives in the kinetic lagrangian of the Reggeon, Eq. (4.2), need to be promoted to covariant derivatives, leading to additional couplings between gluons and the Reggeon. However, these vertices always involve two Reggeon fields, and thus do not contribute to on-shell single-Reggeon production, making them irrelevant for the analysis of this chapter.

4.3 A Model for Warped-Space Reggeons

In this section, we generalize the above toy model to Reggeons propagating in the Randall-Sundrum (RS) space, and present the Kaluza-Klein decomposition of a massive spin-2 field in RS.

4.3.1 The Randall-Sundrum Orbifold

Let us first review the relevant features of the Randall-Sundrum (RS) orbifold. Topologically, the RS space is the direct product of Minkowski space and the $S^1/\mathbb{Z}_2$ orbifold. We use coordinates (x^μ, y) where y spans the extra dimension:

$$y \in (-\pi R, \pi R]; \qquad y \sim y + 2\pi R. \quad (4.17)$$

The orbifold symmetry takes $y \to -y$; the orbifold fixed points are at $y = 0, \pi R$. The interval in these coordinates is

$$\mathrm{d}s^2 = \mathrm{e}^{-2k|y|}\,\mathrm{d}x^\mu\,\mathrm{d}x_\mu - \mathrm{d}y^2\,. \tag{4.18}$$

The RS space is a solution of the Einstein equations with a 5D cosmological constant and 3-branes at the orbifold fixed points. The brane at $y = 0$ is referred to as the ultraviolet (UV) brane, while the brane at $y = \pi R$ is the infrared (IR) brane. The curvature scale k is of order (though somewhat below) the 5D Planck scale M_{Pl}^*, which in turn is essentially identical to the 4D Planck scale M_{Pl}. To solve the hierarchy problem, the model parameters must obey

$$\mathrm{e}^{k\pi R} \sim \frac{M_{\mathrm{Pl}}}{\mathrm{TeV}} \sim 10^{16}\,. \tag{4.19}$$

Away from the orbifold fixed points ("in the bulk") the RS space is isomorphic to AdS^5. The non-vanishing Christoffel symbols are

$$\Gamma^\mu_{\nu 5} \;=\; -k\,\mathrm{sgn}(y)\,\delta^\mu_\nu, \quad \Gamma^5_{\mu\nu} \;=\; -k\,\mathrm{sgn}(y)\,\mathrm{e}^{-2k|y|}\eta_{\mu\nu}\,. \tag{4.20}$$

In the bulk, the Riemann tensor has the form

$$R^M{}_{NKL} = k^2\left(\delta^M_K g_{NL} - \delta^M_N g_{KL}\right)\,. \tag{4.21}$$

The discontinuities of the Christoffel symbols on the boundaries introduce additional, localized contributions:

$$\Delta R^5{}_{5\mu\nu} = -\Delta R^5{}_{\mu 5\nu} \;=\; 2k\,\mathrm{e}^{-2k|y|}\,\eta_{\mu\nu}\big[\delta(y) - \delta(y-\pi R)\big]; \tag{4.22a}$$

$$\Delta R^\mu{}_{5\nu 5} = -\Delta R^\mu{}_{\nu 55} \;=\; 2k\,\delta^\mu_\nu\big[\delta(y) - \delta(y-\pi R)\big]\,. \tag{4.22b}$$

While these contributions are irrelevant for particles of lower spin (for example, all factors involving Christoffel symbols vanish in the Lagrangian for vector particles by antisymmetry), they have consequences for spin-two fields.

Finally, we note a convention we will use throughout: Roman indices $M, N, \ldots$ span the full five-dimensional space, and are raised and lowered with the full metric g, while Greek indices $\mu, \nu, \ldots$ span the four large dimensions only and are raised and lowered with the *flat* metric $\eta_{\mu\nu}$.

4.3.2 Kaluza-Klein Decomposition of Massive Spin-2 Field

To model Regge excitations of the SM fields propagating in the RS bulk, we generalize the field theory of section 4.2 in a straightforward way: First, we promote both the Regge and SM fields to five-dimensional fields, and introduce the appropriate metric factors, Christoffel symbols, etc. into the Lagrangian to restore general covariance. For SM fermions, bulk masses are introduced, and chiral 4D zero modes are obtained by imposing appropriate boundary conditions [93, 99]. Then, we perform the Kaluza-Klein (KK) decomposition of the theory, and derive the interactions between the 4D fields. For spin-1 and spin-1/2 fields, the KK decomposition is straightforward. The KK decomposition for a massive spin-2 field in RS space is somewhat complicated, and to the best of our knowledge this problem has not yet been addressed in the literature. In this subsection, we will outline the required steps.

A free (non-interacting) massive spin-2 field in curved 5D space is described by the covariant generalisation of (4.2):

$$\mathscr{L} = \frac{1}{4} H^{LMN} H_{LMN} - \frac{1}{2} H^{LM}{}_{M} H_{LN}{}^{N} + \frac{1}{2} m^2 \left\{ \left(B_M{}^{M} \right)^2 - B^{MN} B_{MN} \right\}, \quad (4.23)$$

where $H_{LMN} \equiv \nabla_L B_{MN} - \nabla_M B_{LN}$ is the field strength tensor. Under the 4D Lorentz group, the field decomposes into tensor, vector and scalar components, $B_{\mu\nu}$, $B_{\mu 5}$, and B_{55}, respectively. However, the Lagrangian (4.23) contains terms which mix these components. To obtain a consistent KK decomposition, these

mixed terms need to be cancelled. To do this, first note that in flat space, the kinetic part of Eq. (4.23) is invariant (up to a total derivative) under the gauge transformation

$$\delta B_{MN} = \partial_M \beta_N + \partial_N \beta_M \,. \tag{4.24}$$

The mass terms can be thought of as spontaneous breaking of this gauge invariance. One can formally restore the gauge invariance to this Lagrangian by introducing pion fields:[4]

$$\begin{aligned}\mathscr{L} = \frac{1}{4} H^{LMN} H_{LMN} - \frac{1}{2} H^{LM}{}_{M} H_{LN}{}^{N} + \frac{1}{2} \Big\{ \left(m\, B_M{}^M - 2\partial_M \pi^M \right)^2 \\ - \left(m\, B^{MN} - \partial^M \pi^N - \partial^N \pi^M \right) \left(m\, B_{MN} - \partial_M \pi_N - \partial_N \pi_M \right) \Big\}. \end{aligned} \tag{4.25}$$

If the pion fields transform as

$$\delta \pi_M = m\, \beta_M \tag{4.26}$$

the Lagrangian (4.25) is gauge invariant. Setting the pion fields to zero corresponds to the unitary gauge, where the Lagrangian has the familiar form, Eq. (4.23). Following the standard prescription of the R_ξ gauges, one can choose a gauge in which the mixings between fields of different 4D spins disappear. This gauge is a natural basis for KK decomposition.

To apply this procedure in RS space, we must first determine the correct form of the gauge transformations, since the kinetic terms in (4.23) are *not* invariant under (4.24) in the presence of curvature. We take the gauge transformations in warped space to be

$$\begin{aligned}\delta B_{MN} &= \nabla_M \beta_N + \nabla_N \beta_M; \\ \delta \pi_M &= m\, \beta_M \,. \end{aligned} \tag{4.27}$$

Invariance under these transformations requires additional terms in the Lagrangian, which are proportional to curvature and disappear in flat-space limit. These

[4]This idea is based on the non-linear sigma model for gravity constructed in Ref. [100].

terms are of two kinds: corrections to the bulk Lagrangian, and boundary-localized corrections. (The appearance of the boundary-localized terms is due to the boundary contributions to the curvature tensor, Eq. (4.22).) The bulk term is

$$\Delta\mathcal{L}_{\rm bulk} = \frac{3k^2}{2}\left\{\left(B_M{}^M\right)^2 - B^{MN}B_{MN}\right\}. \tag{4.28}$$

The form of the boundary terms depends on the transformations of the B_{MN} components under the action of the orbifold symmetry. We choose the 4D tensor field to be *even* under $y \to -y$; consistency then implies

$$B_{\mu\nu}(y) = +B_{\mu\nu}(-y), \quad B_{\mu 5}(y) = -B_{\mu 5}(-y), \quad B_{55}(y) = +B_{55}(-y)\,. \tag{4.29}$$

These conditions in turn imply the following boundary conditions for the gauge functions β_M:

$$\partial_5\left(\beta_\mu(x,y)\mathrm{e}^{-2k|y|}\right)|_{y=0,\pi R} = 0, \quad \beta_5(x,y)|_{y=0,\pi R} = 0\,. \tag{4.30}$$

To restore gauge invariance on the boundary, for gauge transformations satisfying (4.30), we add

$$\Delta\mathcal{L}_{\rm brane} = -k\left[\delta(y) - \delta(y-\pi R)\right]\left(\left(B_\mu{}^\mu\right)^2 - B^{\mu\nu}B_{\mu\nu}\right). \tag{4.31}$$

Summarizing, the gauge-invariant warped-space generalization of Eq. (4.25) is

$$\begin{aligned}\mathscr{L} = \frac{1}{4}H^{LMN}H_{LMN} - \frac{1}{2}H^{LM}{}_M H_{LN}{}^N + \frac{1}{2}\Big\{&\left(mB_M{}^M - 2\nabla_M\pi^M\right)^2 \\ &- \left(mB^{MN} - \nabla^M\pi^N - \nabla^N\pi^M\right)\left(mB_{MN} - \nabla_M\pi_N - \nabla_N\pi_M\right)\Big\} \\ &+ \Delta\mathcal{L}_{\rm bulk} + \Delta\mathcal{L}_{\rm brane}.\end{aligned} \tag{4.32}$$

Finally, we comment on the connection between Eq. (4.32) and general relativity. It is well known that in curved spacetimes, the graviton Lagrangian is invariant under a gauge transformation of the form (4.27) that arises from coordinate invariance. Quadratic expansion of the Einstein-Hilbert action in curved space includes terms

of the form $R\,h\,h$ (where R is a curvature tensor) in the bulk, and $T\,h\,h$ (where T is the brane tension, related to R via Einstein's equations) on the branes. For the RS space, those terms are in fact identical to the terms added by hand in our approach, Eqs. (4.28) and (4.31).

Most of the terms mixing fields of different 4D spin in this Lagrangian can be eliminated with judiciously chosen gauge-fixing terms. However, there are terms mixing spin-2 and spin-0 fields in (4.32) that cannot be removed within the R_ξ-gauge approach; they have the form

$$\mathrm{e}^{-2k|y|}\big(-3k\,\mathrm{sgn}(y)\,(\partial_y B_\mu{}^\mu)B_{yy} - (6k^2+m^2)B_\mu{}^\mu B_{yy} + 2mB_\mu{}^\mu\,(\partial_y\pi_y - 3k\,\mathrm{sgn}(y)\,\pi_y)\big). \quad (4.33)$$

This mixing can be eliminated by shifting the spin-2 field,

$$B_{\mu\nu} \to B_{\mu\nu} - \frac{1}{3}g_{\mu\nu}\phi\,. \quad (4.34)$$

The shift ϕ is a function of the fields B_{yy} and π_y, defined as a solution to the differential equation

$$\begin{aligned}\left(-\partial_y^2 + 4k^2 + m^2\right)\,\mathrm{e}^{-2k|y|}\,\phi - 4k\left[\delta(y) - \delta(y-\pi R)\right]\mathrm{e}^{-2k|y|}\phi \\ = \mathrm{e}^{-2k|y|}\left(3k\,\mathrm{sgn}(y)\,\partial_y B_{yy} - (12k^2+m^2)B_{yy} + 2m\,\partial_y\pi_y \right. \\ \left. - 6mk\,\mathrm{sgn}(y)\,\pi_y\right) + 6k\left[\delta(y) - \delta(y-\pi R)\right]\mathrm{e}^{-2k|y|}B_{yy}. \quad (4.35)\end{aligned}$$

The operator acting on $\mathrm{e}^{-2k|y|}\,\phi$ arises from the terms that are quadratic in $B_{\mu\nu}$. Since it is a self-adjoint operator with strictly positive eigenvalues, it can be inverted and thus ϕ exists. The shift must be done *before* gauge fixing as it introduces terms mixing $B_{\mu\nu}$ and ϕ which must be cancelled by the gauge-fixing terms.

To cancel the remaining mixing between the 4D tensor mode and 4D vectors and scalars, we introduce the gauge-fixing term

$$\mathscr{L}_{\mathrm{gf1}} = \frac{1}{\xi}\mathrm{e}^{2k|y|}G^\mu G_\mu\,, \quad (4.36)$$

where

$$G_\mu \equiv \mathrm{e}^{2k|y|}\left(\partial_\mu B_\nu{}^\nu - \partial^\nu B_{\mu\nu}\right) - \frac{1}{2}\xi\big(-2\partial_y B_{\mu y} + 4k\,\mathrm{sgn}(y)\,B_{\mu y} + 2m\,\pi_\mu + \partial_\mu B_{yy} + \frac{2}{3}\partial_\mu\phi\big)\,. \quad (4.37)$$

This results in the action of the form

$$S = S_{\text{spin-2}} \oplus S_{\text{spin-1, spin-0}}\,, \quad (4.38)$$

where

$$S_{\text{spin-2}} = \int \mathrm{d}^5x\Bigg[\mathrm{e}^{2k|y|}\left(\frac{1}{4}H^{\lambda\mu\nu}H_{\lambda\mu\nu} - \frac{1}{2}\left(1-\frac{2}{\xi}\right)H^{\lambda\mu}{}_\mu H_{\lambda\nu}{}^\nu\right) + \frac{1}{2}B_\mu{}^\mu\left(-\partial_y^2 + 4k^2 + m^2\right)B_\nu{}^\nu - \frac{1}{2}B^{\mu\nu}\left(-\partial_y^2 + 4k^2 + m^2\right)B_{\mu\nu} + 2k\left(\delta(y) - \delta(y-\pi R)\right)\left(B^{\mu\nu}B_{\mu\nu} - (B^\mu_\mu)^2\right)\Bigg]\,. \quad (4.39)$$

Additional gauge-fixing terms must be introduced to separate the vector and scalar fields in the action. Since the procedure is rather complicated, and since phenomenologically the tensor field provides the most interesting and unambiguous signature for stringy physics, we will not pursue a complete description of the vector and scalar sectors in this chapter.

Once the tensor field is isolated in the action, KK decomposition is straightforward. We make the standard KK ansatz

$$B_{\mu\nu}(x,y) = \frac{1}{\sqrt{\pi R}}\sum_{n=1}^{\infty} B^{(n)}_{\mu\nu}(x) f^{(n)}(y). \quad (4.40)$$

The defining equation for the $\{f^{(n)}\}$ are found easily from either the equations of motion or the action:

$$-f^{(n)\prime\prime} + \left(4k^2 + m^2\right)f^{(n)} - 2k\left(\delta(y) - \delta(y-\pi R)\right)f^{(n)} = {\mu^{(n)}}^2\mathrm{e}^{2k|y|}f^{(n)}. \quad (4.41)$$

This equation is self-adjoint, so we can take the KK functions to be orthonormal. In this case, the associated inner product is

$$\frac{1}{\pi R}\int_0^{\pi R}\mathrm{d}y\,\mathrm{e}^{2k|y|}f^{(n)}f^{(m)} = \delta^{nm}. \quad (4.42)$$

After integrating over the extra dimension, the action (4.39) becomes

$$S_{\text{spin-2}} = \int \mathrm{d}^4x \sum_{n=1}^{\infty} \Bigg[\frac{1}{4} H^{(n)}_{\lambda\mu\nu} H^{(m)\,\lambda\mu\nu} - \frac{1}{2}\left(1 - \frac{2}{\xi}\right) H^{(n)\lambda\mu}{}_{\mu} H^{(n)\nu}_{\lambda\nu} + \frac{1}{2}\mu^{(n)^2}\left\{ \left(B^{(n)\mu}_{\mu}\right)^2 - B^{(n)\mu\nu} B^{(n)}_{\mu\nu} \right\} \Bigg], \quad (4.43)$$

which is just a tower of free 4D spin-2 fields with masses $\mu^{(n)}$ (in unitary gauge, if $\xi \to \infty$.) The general solution to (4.41) is a Bessel function:

$$f^{(n)}(y) = \frac{1}{N}\left\{ J_\nu\left(\frac{\mu^{(n)}}{\Lambda_{\text{IR}}} w\right) + c\, J_{-\nu}\left(\frac{\mu^{(n)}}{\Lambda_{\text{IR}}} w\right) \right\}, \quad (4.44)$$

where

$$\Lambda_{\text{IR}} = k\mathrm{e}^{-k\pi R}, \quad w = \mathrm{e}^{k(|y|-\pi R)} \in [e^{-\pi k R}, 1]\,. \quad (4.45)$$

The order of the Bessel function is $\nu \equiv \sqrt{4 + \mathfrak{m}^2}$, where $\mathfrak{m} = m/k$ is the string scale in units of the RS curvature. Formally, consistent treatment of the RS geometry as a smooth background for propagating strings requires $\mathfrak{m} \gg 1$; in our phenomenological study, we will consider $\mathfrak{m} \sim$ a few. N is the normalisation and c is a constant of integration; each implicitly depends upon the level n. Both c and the mass are set by the boundary conditions. Since $B_{\mu\nu}$ is even under the orbifold symmetry (see Eq. (4.29)) it (and hence the $\{f^{(n)}\}$) would normally satisfy Neumann boundary conditions. However, the presence of localized terms in (4.41) changes this, making the derivative of the KK functions discontinuous. The correct boundary conditions are

$$f^{(n)\prime}(0+) - f^{(n)\prime}(0-) = -2k f^{(n)}(0); \quad (4.46a)$$

$$f^{(n)\prime}(-\pi R+) - f^{(n)\prime}(\pi R-) = 2k f^{(n)}(\pi R). \quad (4.46b)$$

We plot the spectrum that is implied by these boundary conditions in Fig. 4.1, and the numerical values of the lightest tensor Reggeon mass for a few choices of m/k are listed in Table 4.1. The wavefunctions of the first five modes, for a specific

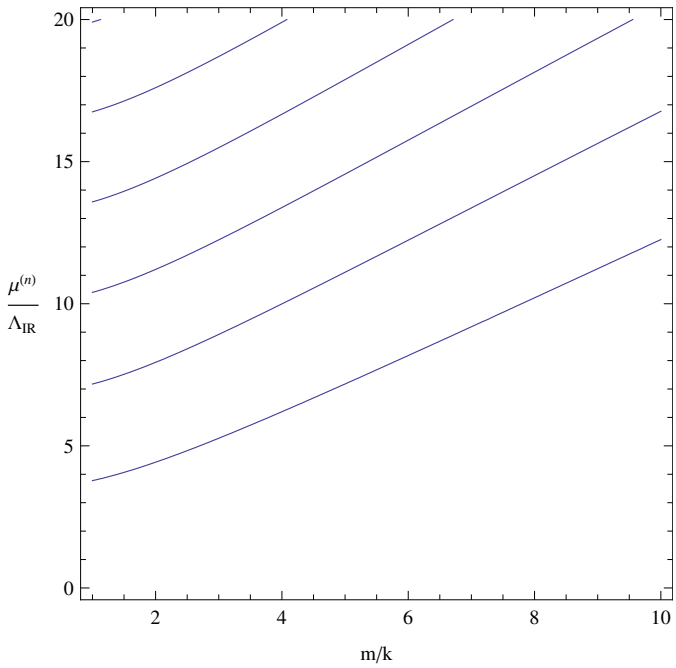

Figure 4.1: The spectrum of 4D tensor particles. We have assumed that the RS curvature $k = 10^{15}$ TeV; the results are essentially independent of this choice.

choice of $m/k = 3$, are plotted in Fig. 4.2. As expected, the mass of the spin-2 Reggeon (and its first few KK excitations) is of the order

$$\mu \sim \text{ (a few)} \times m\, \mathrm{e}^{-k\pi R} \sim \text{ a few TeV}\,, \tag{4.47}$$

and the wavefunctions are strongly localized in the vicinity of the IR brane, $y = \pi R$. It is also easy to roughly estimate the two constants appearing in the wavefunctions:

$$N \sim \frac{1}{\sqrt{\pi k R}} \mathrm{e}^{+k\pi R}\,, \quad c \sim \mathrm{e}^{-2\nu k\pi R}\,. \tag{4.48}$$

These estimates are useful in discussing the Reggeon phenomenology.

4.4 SM Couplings to the Tensor Reggeon

To model the interactions of SM quarks and gluons with the Regge gluon, we will use the minimal generally covariant extension of the interaction Lagrangian of the 4D, flat-space CPP model, discussed in Section 2.

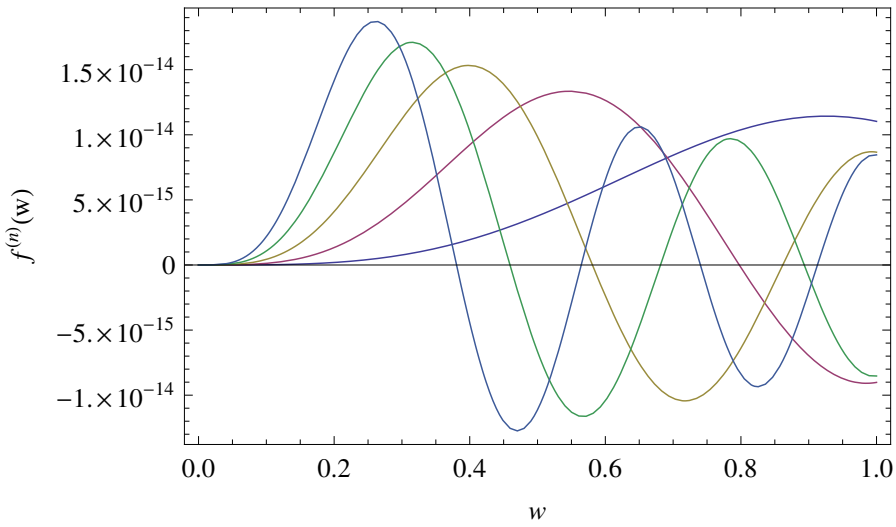

Figure 4.2: The KK functions for the five lightest KK modes. We have assumed that the RS curvature $k = 10^{15}$ TeV, $\Lambda_{\rm IR} = 1$ TeV and $m = 3k$. The qualitative form of the wavefunctions are all robust to varying these parameters.

4.4.1 Gluon-Reggeon Coupling

The gluon-Reggeon coupling is a simple generalization of Eq. (4.15):

$$\mathcal{S}_{ggg^*} = \int \mathrm{d}^5x\sqrt{-G}\,\frac{g_5}{\sqrt{2}M_S^*}\,C^{abc}\left(F^{aAC}F_C^{bB} - \frac{1}{4}\,F^{aCD}F^b_{CD}G^{AB}\right)B^c_{AB}\,. \quad (4.49)$$

The 5D coupling g_5 is related to the 4D QCD coupling g_s by

$$g_5 = \sqrt{\pi R}\,g_s\,. \quad (4.50)$$

The 5D gauge coupling has mass dimension of $-1/2$, so that the power-counting of the operator (4.49) is correct for canonically normalized fields (namely, the 5D gauge field and the Reggeon both have mass dimension 3/2). The interaction Lagrangian is invariant under the usual QCD gauge transformations (see discussion in section 4.2.2), but not under the transformations (4.27). It is easy to formally restore this symmetry by replacing $B_{MN} \to B_{MN} - \nabla_M\pi_N - \nabla_N\pi_M$; however, the terms involving pions do not contribute to the couplings of the 4D tensor mode, which is the only object of interest for us.

The Kaluza-Klein decomposition of the SM gauge field is straightforward [101]. Gauge freedom can be used to choose $A_5 = 0$, and the 4D vector zero-mode has a constant profile in the bulk:

$$A_\mu(x, y) = \frac{1}{\sqrt{\pi R}} A_\mu^{(0)}(x) + \dots . \tag{4.51}$$

This yields the following 4D Lagrangian for the interactions of the SM gluons with the tensor Reggeons:

$$\mathcal{L}_{ggg^*} = \sum_n \frac{g^{(n)}}{\sqrt{2}\tilde{M}_S} \mathcal{C}^{abc} \left(F^{a\alpha\gamma} F_\gamma^{b\,\beta} - \frac{1}{4} F^{a\gamma\delta} F_{\gamma\delta}^b \right) B_{\alpha\beta}^c \,, \tag{4.52}$$

where we defined the warped-down string scale

$$\tilde{M}_S = e^{-\pi k R} M_S^* \sim \text{ a few TeV}, \tag{4.53}$$

and the dimensionless coupling

$$g^{(n)} = \frac{g_s \, \mathrm{e}^{-k\pi R}}{\pi R} \int_0^{\pi R} \mathrm{d}y \, \mathrm{e}^{2ky} \, f^{(n)}(y) \,. \tag{4.54}$$

Since the Reggeon wavefunction is localized near $y = \pi R$, and is of order $1/N \sim \sqrt{\pi k R} e^{-\pi k R}$ in that region, we can estimate

$$g^{(n)} \sim \frac{g_s}{\sqrt{\pi k R}} \,. \tag{4.55}$$

The operator in the 4D action, Eq. (4.52), is suppressed by a scale of order $\tilde{M}_S$, as expected; however, note the additional volume suppression. Sample numerical values for the coupling of the lightest Reggeon $g^{(0)}$ are shown in Table 4.1. The coupling is approximately independent of the Reggeon mass, with a value of roughly $0.1 g_s$.

4.4.2 Quark-Reggeon Coupling

Embedding of the SM fermions as zero modes of 5D fermions in the RS background is well known [93, 99]. For each SM chiral quark, we introduce a 5D field Q_i, where

the index i includes both chirality and flavor. Generalizing Eq. (4.4), the Regge gluon couples to this field via

$$\mathcal{S}_{q\bar{q}g^*} \;=\; \int \mathrm{d}^5x\sqrt{-G}\,\frac{ig_5}{\sqrt{2}M_S^*}\,G^{LM}\,E_a^N\,\left((\overline{\mathcal{D}_M Q_i})\Gamma^a\tilde{B}_{LN}Q_i - \overline{Q}_i\Gamma^a\tilde{B}_{LN}\mathcal{D}_M Q_i\right)\,, \tag{4.56}$$

where $\Gamma^n = (\gamma^\nu, i\gamma^5)$, and $E_n^N(y) =$ diag $(e^{k|y|}, e^{k|y|}, e^{k|y|}, e^{k|y|}, 1)$ is the inverse vierbein. The covariant derivative has the form (up to terms containing gauge fields)

$$\mathcal{D}_M Q = \partial_M Q + \frac{1}{2}\,\omega_M^{ab}\sigma_{ab}\,, \tag{4.57}$$

where ω^{ab} is the spin connection, and $\sigma_{ab} = \frac{1}{4}[\Gamma_a, \Gamma_b]$. (Note that the indices $a, b, \ldots$ refer to the transformations under local Lorentz group, and as such are raised and lowered with Minkowski metric.) In RS space, the only non-vanishing components of the spin connection are

$$\omega_\mu^{\alpha 5} = -\omega_\mu^{5\alpha} = -k\;\mathrm{sgn}(y)\,\mathrm{e}^{-k|y|}\,\delta_\mu^\alpha\,. \tag{4.58}$$

It is easy to show that the terms involving spin connection in the action (4.56) are proportional to the trace of the tensor Reggeon, B_μ^μ, and thus vanish for an on-shell Reggeon. As a result, the covariant derivatives in Eq. (4.56) can be replaced with ordinary derivatives when considering an on-shell Reggeon, as will always be the case in this chapter.

The zero-mode quarks $q_i(x)$ are given by [93, 99]

$$Q_i(x,y) = N_i\mathrm{e}^{(2-c_i)k|y|}q_i(x) + \ldots \tag{4.59}$$

where the normalization constant is

$$N_i = k^{1/2}\sqrt{\frac{1-2c_i}{\mathrm{e}^{(1-2c_i)k\pi R}-1}}\,. \tag{4.60}$$

The 4D fields q_i are canonically normalized. The c parameters are related to the 5D fermion masses M_5: in the notation of Ref. [93], $c = M_5/k$ for the right-handed

fields and $c = -M_5/k$ for the left-handed fields. (The "handedness" of the 5D fields refers to the 4D chirality of their zero modes.) We work in the basis where the bulk masses are diagonal.[5] In four dimensions, we obtain

$$\mathcal{L}_{q\bar{q}g^*} = \sum_n \frac{i\tilde{g}_i^{(n)}}{\sqrt{2}\tilde{M}_S} \left(\partial^\mu \bar{q}\gamma^\nu \tilde{B}_{\mu\nu} q - \bar{q}\gamma^\nu \tilde{B}_{\mu\nu}\partial^\mu q \right) , \tag{4.61}$$

where

$$\tilde{g}_i^{(n)} = g_s e^{-\pi k R} N_i^2 \int_0^{\pi R} \mathrm{d}y \, f^{(n)}(y) \, \mathrm{e}^{(3-2c_i)k|y|} . \tag{4.62}$$

Clearly, the strength of the coupling depends crucially on the value of c_i. As a rough estimate, we obtain

$$\tilde{g}_i \sim g_s \, \mathrm{e}^{(1-2c_i)k\pi R}, \quad c_i > \frac{1}{2} ; \tag{4.63a}$$

$$\tilde{g}_i \sim \frac{g_s}{\sqrt{\pi k R}} \approx \frac{g_s}{6}, \quad c_i = \frac{1}{2} ; \tag{4.63b}$$

$$\tilde{g}_i \sim g_s, \quad c_i < \frac{1}{2} . \tag{4.63c}$$

Thus, the couplings to "elementary" fermions ($c > 1/2$) are exponentially suppressed, couplings to "mixed" fermions ($c = 1/2$) are volume-suppressed, and couplings to "composite" fermions ($c < 1/2$) are unsuppressed. This behavior is consistent with naive expectations from the dual CFT picture, where the Reggeon is a composite. Numerical values for the couplings of the lightest Reggeon to fermions with three sample values of c are shown in Table 4.1.

The values of c_i for various quark flavors are somewhat model-dependent. We will study the Reggeon phenomenology in two scenarios. The first one is the model with a light Higgs on the IR brane [92]. If the brane-localized Yukawa couplings are anarchic, the SM pattern of masses and mixings leads to the following estimates

[5] The SM fermion masses and mixings may be due to the interactions of the bulk fermions with a brane-localized Higgs boson [92], or, in Higgsless models, to modified boundary conditions [102]. We will not consider these effects in this chapter, since they do not have a major effect on the Reggeon collider phenomenology.

Table 4.1: Mass of the lightest tensor Reggeon and its couplings to gluons and quarks (with three different values of c), as a function of the bulk Reggeon mass m. We have assumed $k/\Lambda_{\rm IR} = 10^{15}$; masses and couplings only depend on k and R through a logarithm of this ratio.

$\frac{m}{k}$	$\frac{\mu^{(0)}}{\Lambda_{\rm IR}}$	$\frac{g^{(0)}}{g_s}$	$\frac{\tilde{g}^{(0)}}{g_s}(c=0.65)$	$\frac{\tilde{g}^{(0)}}{g_s}(c=0.5)$	$\frac{\tilde{g}^{(0)}}{g_s}(c=0)$
2.0	4.43	0.109	3.9×10^{-5}	0.109	2.9
3.0	5.27	0.106	3.8×10^{-5}	0.106	2.9
4.0	6.20	0.102	3.6×10^{-5}	0.102	2.9
5.0	7.18	0.099	3.5×10^{-5}	0.099	2.8

for these coefficients [94]:

$$c_{Q^1} \approx 0.63, \quad c_{u^1} \approx 0.675, \quad c_{d^1} \approx 0.675\,; \tag{4.64a}$$

$$c_{Q^2} \approx 0.575, \quad c_{u^2} \approx 0.5, \quad c_{d^2} \approx 0.64\,; \tag{4.64b}$$

$$c_{Q^3} \approx 0.39, \quad c_{u^3} \approx -0.19, \quad c_{d^3} \approx 0.62\,. \tag{4.64c}$$

In this scenario, the first two generations of quarks are mostly elementary, and their couplings to the tensor Reggeon are exponentially suppressed (numerically, the suppression factor is of order $10^{-5} - 10^{-6}$). The couplings to the third generation doublet and the right-handed top quark are unsuppressed.

Our second scenario is the "Higgsless" model [95, 102]. In this model, consistency with precision electroweak constraints requires [103]

$$c_i \approx \frac{1}{2} \tag{4.65}$$

for all flavors, with the exception of the third-generation doublet and the right-handed top, which have approximately the same c values as in Eq. (4.64c). In this scenario, the tensor Reggeon couples to light quarks, with a coupling suppressed only by the volume factor.

4.5 Phenomenological Implications

The most important parameter that determines the sensitivity of the LHC experiments to a new particle is its mass. The tensor Reggeon mass in our model depends on two parameters, $\Lambda_{\rm IR}$ and m/k; for fixed m/k, the Reggeon mass is, to an excellent approximation, a linear function of $\Lambda_{\rm IR}$. The scale $\Lambda_{\rm IR}$ is subject to a number of significant constraints from existing experiments. Bounds from precision electroweak measurements and flavor physics have been considered by many authors, both in models with the Higgs and in the Higgsless approach. Among these, precision electroweak bounds, in particular the bound from the S parameter, are considered to be more robust, since no known symmetry can be used to avoid it. In the model with the Higgs, the bound on the first KK excitation mass is of order 3 TeV [92], translating into roughly $\Lambda_{\rm IR} \gtrsim 1$ TeV. In the Higgsless model, the KK excitations of the W bosons must lie below 1 TeV for unitarity, corresponding to $\Lambda_{\rm IR} \lesssim 0.5$ TeV. This is only consistent with precision electroweak constraints if all SM fermions, with the exception of the right-handed top quark, have approximately flat profiles in the extra dimension, $c_i \approx 1/2$ [103]. Since lower KK masses generally require more finely-tuned fermion profiles, we will adapt the value $\Lambda_{\rm IR} = 0.5$ TeV for this model. As we already remarked in the Introduction, the description of physics in the RS model as strings propagating on a smooth geometric background formally requires $m/k \gg 1$; however, as in many examples in various areas of physics, $m/k \sim$ a few may in fact be sufficient, depending on the behavior of the leading corrections to the geometric limit, as well as on desired accuracy. Precise determination of the domain of validity of geometric description is beyond the scope of this chapter. The lower the allowed value of m/k, the lighter the tensor Reggeon can be; for example, assuming that $m/k \geq 3$ is acceptable, we find that the lowest tensor Reggeon mass is about $5\Lambda_{\rm IR}$ (see Fig. 4.1), corre-

sponding to 2.5 TeV in the Higgsless model and above 5 TeV in the model with the Higgs.

The second crucial quantity for experimental searches for the tensor Reggeon is its production cross section. For the lightest Reggeon, parton-level cross sections are given by

$$\hat{\sigma}(q_i\bar{q}_i \to g^*) = \frac{2\pi^2\alpha_s}{9}\left(\frac{\tilde{g}_i^{(0)}M}{g_s\tilde{M}_S}\right)^2 \delta(\hat{s}-M^2)\,; \tag{4.66a}$$

$$\hat{\sigma}(gg \to g^*) = \frac{5\pi^2\alpha_s}{24}\left(\frac{g^{(0)}M}{g_s\tilde{M}_S}\right)^2 \delta(\hat{s}-M^2)\,, \tag{4.66b}$$

where $M \equiv \mu^0$ is the Reggeon mass, and q_i are Weyl (2-component) SM quarks. (Note that in the model with the Higgs, Regge gluon couplings to light quarks violate parity due to different 5D profiles of left-handed and right-handed SM quarks.) The total production cross section at the LHC ($\sqrt{s} = 14$ TeV), evaluated using the MSTW NLO parton distribution function set [104], is shown as a function of the Reggeon mass in Fig. 4.3. In this plot, we have assumed $m = M_S^*$ (as is in fact required for our Lagrangian to reproduce the Veneziano amplitudes in the flat-space limit). We further assumed $\Lambda_{\rm IR} = 1$ TeV in the model with the Higgs, $\Lambda_{\rm IR} = 500$ GeV in the Higgsless model, and $k/\Lambda_{\rm IR} = 10^{15}$ in both models. The range of Reggeon masses plotted in Fig. 4.3 corresponds to $m/k \gtrsim 1$; we remind the reader that the results for small m/k should be interpreted with caution since our framework may not be applicable.

We conclude that a significant sample (possibly thousands or even tens of thousands) of tensor Regge gluons could be produced at the LHC, for favorable model parameters. The Reggeon production cross sections is similar to that of a KK gluon [105] in the $2-3$ TeV range, but decreases faster with mass. It appears from the plot that large production cross sections are only possible in the Higgsless model; this is mainly due to the higher value of $\Lambda_{\rm IR}$ assumed for the model with

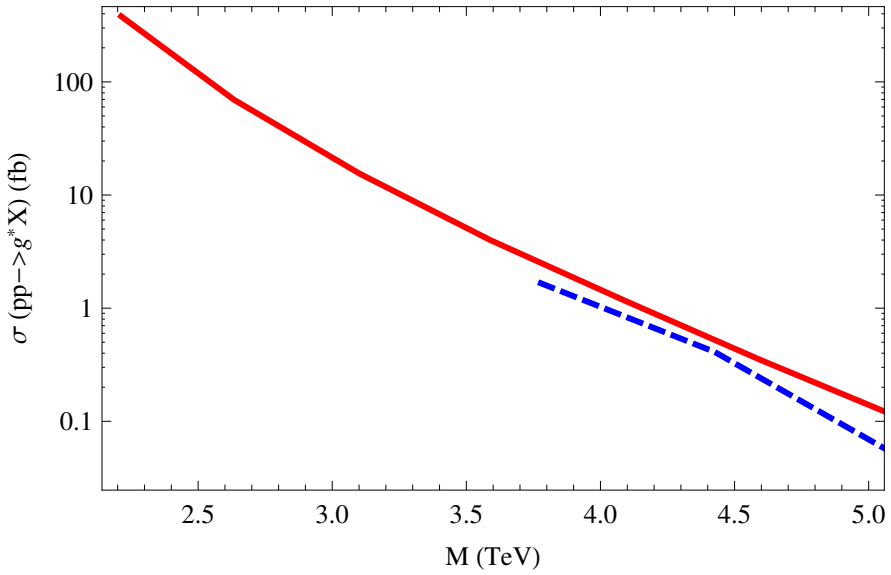

Figure 4.3: Production cross section of the lowest-lying tensor Regge gluon at the LHC, $\sqrt{s} = 14$ TeV. Red/solid line: Higgsless model. Blue/dashed line: Model with a Higgs. (See text for detailed definition of the two models.)

the Higgs. While this value is suggested as a lower bound by precision electroweak constraints in this model, it could in principle be lowered at a price of fine-tuning, in which case lower Reggeon mass, and higher production cross section, would be possible. For the same value of the Reggeon mass, the two models predict similar cross sections to within a factor of two. The slightly higher value in the Higgsless model is due to the possibility of Reggeon production in light quark collisions, in addition to gluon-initiated production which occurs in both models.

Finally, the experimental signatures of the Reggeon production depend on its decay pattern. The partial widths are

$$\Gamma(g^* \to q_i \bar{q}_i) = \frac{\alpha_s M}{40} \left(\frac{\tilde{g}_i^{(0)} M}{g_s \tilde{M}_S} \right)^2 ; \tag{4.67a}$$

$$\Gamma(g^* \to gg) = \frac{\alpha_s M}{24} \left(\frac{g^{(0)} M}{g_s \tilde{M}_S} \right)^2 , \tag{4.67b}$$

where, as before, q_i are two-component quarks. The total width of the Reggeon into SM channels is shown in Fig. 4.4. Among the SM channels, decays to top-antitop

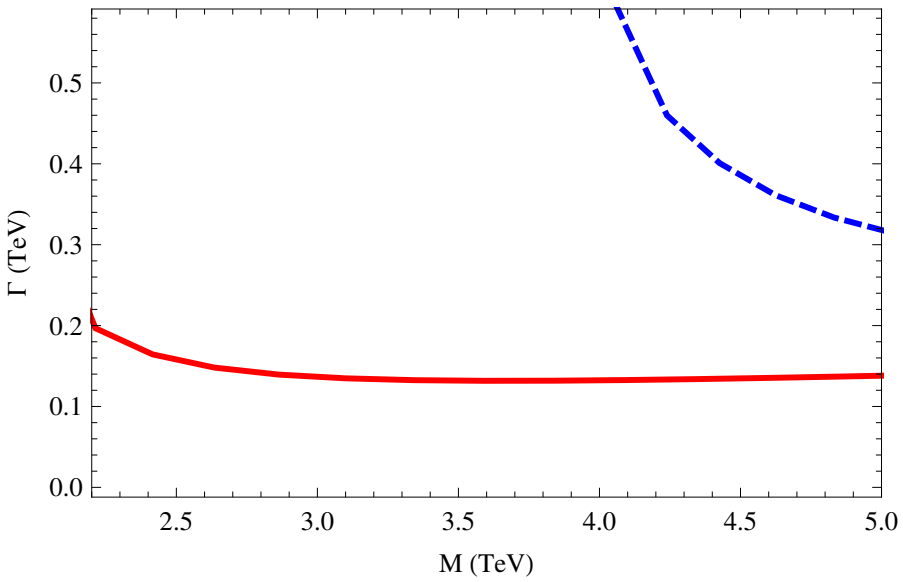

Figure 4.4: Decay width of the lowest-lying Reggeon as a function of its mass. Red/solid line: Higgsless model. Blue/dashed line: Model with a Higgs. (See text for detailed definition of the two models.)

pairs dominate in both models under consideration: the branching ratio into tops (assuming that only SM decay channels are open) is about 95% throughout the interesting mass range. Right-handed tops are preferred. Since the Reggeon mass is expected to be in the few TeV range, the tops would be highly boosted in the lab frame, so that the top decay products are strongly collimated into"top jets". Experimental and theoretical issues related to distinguishing such jets from light quark/gluon jets have been analyzed recently in a number of papers, in the context of KK gluon searches [106]. The proposed techniques would apply to Regge gluon searches as well. Since the Reggeon momentum can be fully reconstructed in events with hadronic top decays, such events could in principle be used to determine the angular distribution of the tops with respect to the beam axis, which would in turn allow one to determine the spin of the Reggeon and unambiguously distinguish it from a KK gluon.

In addition to the SM decays, the Reggeon may decay to other exotic states.

For example, if the Reggeon mass is large enough, it can decay into pairs of Kaluza-Klein excitations of the SM quarks and gluons, which would in turn decay down to SM particles. We will not attempt to analyze such cascade decays in this chapter.

4.6 Summary of Tensor Reggeons from Warped Space

In this chapter, we constructed a field-theoretic toy model to describe the lowest-lying Regge excitations of the SM gauge bosons, in a framework of the Randall-Sundrum model with all SM fields propagating in the bulk. We focused on the 4D tensor (spin-2) states, which would provide a clear signature of the underlying stringy physics if discovered. Our toy model allows us to predict the spectrum of these states (as a function of the underlying model parameters, including the fundamental string scale M_S^*), and their on-shell couplings to Standard Model fermions and gauge bosons. This is sufficient to make predictions for the processes that would dominate the Reggeon phenomenology at the LHC.

If the curvature of the RS space is taken to zero, our model by construction reproduces the spectrum and couplings of the Reggeons in the toy model of CPP [88]. The CPP results were derived by factorizing Veneziano amplitudes of string theory on s-channel poles. While the embedding of the SM into string theory in the CPP model was hardly fully realistic, the Veneziano amplitudes, and the on-shell Reggeon couplings derived from them, are very generic and do not depend on many of the details of realistic string compactifications. On the other hand, one should keep in mind that the Reggeon couplings in curved space may contain additional operators which vanish in the flat-space limit. A drawback of our approach is that it has no sensitivity to such operators, and while we do not expect their presence to result in qualitative changes to the picture obtained in our model, order-one numerical corrections seem possible. To properly handle this issue, one would need

to properly quantize full string theory on the RS background, study four-particle scattering amplitudes, and factorize them to obtain Reggeon interaction vertices.

Our model can be extended in a number of ways. First, 4D vector and scalar excitations of the SM vector bosons, as well as Regge excitations of the SM fermions, can be included. Second, higher Regge levels can in principle be considered, although it seems very unlikely that those could be within the LHC range. The contributions of the Reggeons to precision electroweak and flavor observables can be computed within our model, and may lead to additional constraints on models of this type. We leave all these issues for future work.

BIBLIOGRAPHY

[1] E. Fermi, Z. Phys. **88**, 161 (1934).

[2] E. Komatsu *et al.* [WMAP Collaboration], Astrophys. J. Suppl. **180**, 330 (2009) [arXiv:0803.0547 [astro-ph]].

[3] W. L. Freedman *et al.* [HST Collaboration], Astrophys. J. **553**, 47 (2001) [arXiv:astro-ph/0012376].

[4] For a review and a collection of references, see G. Bertone, D. Hooper and J. Silk, Phys. Rept. **405**, 279 (2005) [arXiv:hep-ph/0404175].

[5] S. L. Glashow, Nucl. Phys. **22**, 579 (1961); A. Salam, Phys. Rev. **127**, 331 (1962); and S. Weinberg, Phys. Rev. Lett. **19**, 1264 (1967).

[6] M. Gell-Mann, Phys. Lett. **8**, 214 (1964).

[7] D. J. Gross and F. Wilczek, Phys. Rev. D **8**, 3633 (1973); H. D. Politzer, Phys. Rept. **14**, 129 (1974).

[8] N. Cabibbo, Phys. Rev. Lett. **10**, 531 (1963). M. Kobayashi and T. Maskawa, Prog. Theor. Phys. **49**, 652 (1973).

[9] [ALEPH, DELPHI, L3, OPAL and SLD Collaborations and LEP Electroweak Working Group and SLD Electroweak Group and SLD Heavy Flavour Group], Phys. Rept. **427**, 257 (2006) [arXiv:hep-ex/0509008].
See also updates from the LEP Electroweak Working Group webpage, `http://lepewwg.web.cern.ch/LEPEWWG/`

[10] A. G. Riess *et al.* [Supernova Search Team Collaboration], Astron. J. **116**, 1009 (1998) [arXiv:astro-ph/9805201].

[11] Y. Fukuda *et al.* [Super-Kamiokande Collaboration], Phys. Rev. Lett. **81**, 1562 (1998) [arXiv:hep-ex/9807003].

[12] S. Weinberg, Phys. Rev. Lett. **59**, 2607 (1987); S. Weinberg, arXiv:hep-th/0511037.

[13] A. Linde, arXiv:hep-th/0211048; for a review see S. M. Carroll, arXiv:hep-th/0512148.

[14] F. Zwicky, Helv. Phys. Acta **6**, 110 (1933).

[15] S. Burles, K. M. Nollett and M. S. Turner, Phys. Rev. D **63**, 063512 (2001) [arXiv:astro-ph/0008495].

[16] D. Clowe, S. W. Randall and M. Markevitch, Nucl. Phys. Proc. Suppl. **173**, 28 (2007) [arXiv:astro-ph/0611496].

[17] G. 't Hooft, "Naturalness, Chiral Symmetry, and Spontaneous Chiral Symmetry Breaking", reprinted in "Under the Spell of the Gauge Principle", World Scientific, Singapore, 1994

[18] H. Georgi and A. Pais, Phys. Rev. D **10**, 539 (1974).

[19] C. Csaki, J. Hubisz, G. D. Kribs, P. Meade and J. Terning, Phys. Rev. D **67**, 115002 (2003) [arXiv:hep-ph/0211124]; J. L. Hewett, F. J. Petriello and T. G. Rizzo, JHEP **0310**, 062 (2003) [arXiv:hep-ph/0211218].

[20] H. C. Cheng and I. Low, JHEP **0309**, 051 (2003) [arXiv:hep-ph/0308199]; JHEP **0408**, 061 (2004) [arXiv:hep-ph/0405243].

[21] M. Asano, S. Matsumoto, N. Okada and Y. Okada, Phys. Rev. D **75**, 063506 (2007) [arXiv:hep-ph/0602157].

[22] L. Randall and R. Sundrum, Phys. Rev. Lett. **83**, 3370 (1999) [arXiv:hep-ph/9905221].

[23] D. N. Spergel *et al.*, Astrophys. J. Suppl. **148**, 175 (2003) [astro-ph/0302209].

[24] A. Birkedal, K. Matchev and M. Perelstein, Phys. Rev. D **70**, 077701 (2004) [arXiv:hep-ph/0403004].

[25] J. L. Feng, S. Su and F. Takayama, Phys. Rev. Lett. **96**, 151802 (2006) [arXiv:hep-ph/0503117].

[26] For a review, see G. Jungman, M. Kamionkowski and K. Griest, Phys. Rept. **267**, 195 (1996) [hep-ph/9506380].

[27] M. Srednicki, S. Theisen and J. Silk, Phys. Rev. Lett. **56**, 263 (1986) [Erratum-ibid. **56**, 1883 (1986)]; M. S. Turner, Phys. Rev. D **34**, 1921 (1986); F. W. Stecker and A. J. Tylka, Astrophys. J. **343**, 169 (1989); A. Bouquet, P. Salati and J. Silk, Phys. Rev. D **40**, 3168 (1989); H. U. Bengtsson, P. Salati

and J. Silk, Nucl. Phys. B **346**, 129 (1990); S. Rudaz and F. W. Stecker, Astrophys. J. **368**, 406 (1991); M. Urban, A. Bouquet, B. Degrange, P. Fleury, J. Kaplan, A. L. Melchior and E. Pare, Phys. Lett. B **293**, 149 (1992) [arXiv:hep-ph/9208255]; V. S. Berezinsky, A. V. Gurevich and K. P. Zybin, Phys. Lett. B **294**, 221 (1992); V. Berezinsky, A. Bottino and G. Mignola, Phys. Lett. B **325**, 136 (1994) [arXiv:hep-ph/9402215]; L. Bergstrom, J. Edsjo and P. Ullio, Phys. Rev. D **58**, 083507 (1998) [arXiv:astro-ph/9804050]; L. Bergstrom, J. Edsjo, P. Gondolo and P. Ullio, Phys. Rev. D **59**, 043506 (1999) [arXiv:astro-ph/9806072]; J. L. Feng, K. T. Matchev and F. Wilczek, Phys. Rev. D **63**, 045024 (2001) [arXiv:astro-ph/0008115]; J. R. Ellis, J. L. Feng, A. Ferstl, K. T. Matchev and K. A. Olive, Eur. Phys. J. C **24**, 311 (2002) [arXiv:astro-ph/0110225]; D. Merritt, M. Milosavljevic, L. Verde and R. Jimenez, Phys. Rev. Lett. **88**, 191301 (2002) [arXiv:astro-ph/0201376]. P. Ullio, L. Bergstrom, J. Edsjo and C. G. Lacey, Phys. Rev. D **66**, 123502 (2002) [arXiv:astro-ph/0207125]; D. Hooper and B. L. Dingus, Phys. Rev. D **70**, 113007 (2004) [arXiv:astro-ph/0210617]; W. de Boer, M. Herold, C. Sander and V. Zhukov, arXiv:hep-ph/0309029; D. Hooper and L. T. Wang, Phys. Rev. D **69**, 035001 (2004) [arXiv:hep-ph/0309036]; P. Binetruy, Y. Mambrini and E. Nezri, Astropart. Phys. **22**, 1 (2004) [arXiv:hep-ph/0312155]; H. Baer and J. O'Farrill, JCAP **0404**, 005 (2004) [arXiv:hep-ph/0312350]; A. Bottino, F. Donato, N. Fornengo and S. Scopel, Phys. Rev. D **70**, 015005 (2004) [arXiv:hep-ph/0401186]; S. Peirani, R. Mohayaee and J. A. de Freitas Pacheco, Phys. Rev. D **70**, 043503 (2004) [arXiv:astro-ph/0401378]; H. Baer, A. Belyaev, T. Krupovnickas and J. O'Farrill, JCAP **0408**, 005 (2004) [arXiv:hep-ph/0405210]; J. Edsjo, M. Schelke and P. Ullio, JCAP **0409**, 004 (2004) [arXiv:astro-ph/0405414]; G. Bertone, P. Binetruy, Y. Mambrini and E. Nezri, Astropart. Phys. **24**, 44 (2005) [arXiv:hep-ph/0406083]. Y. Mambrini and C. Munoz, Astropart. Phys. **24**, 208 (2005) [arXiv:hep-ph/0407158]. Y. Mambrini and C. Munoz, JCAP **0410**, 003 (2004) [arXiv:hep-ph/0407352]; W. de Boer, M. Herold, C. Sander, V. Zhukov, A. V. Gladyshev and D. I. Kazakov, arXiv:astro-ph/0408272. H. Baer, A. Mustafayev, S. Profumo, A. Belyaev and X. Tata, JHEP **0507**, 065 (2005) [arXiv:hep-ph/0504001]. L. Pieri and E. Branchini, JCAP **0505**, 007 (2005) [arXiv:astro-ph/0505058]; H. Baer, A. Mustafayev, E. K. Park and S. Profumo, JHEP **0507**, 046 (2005) [arXiv:hep-ph/0505227]. Y. Mambrini, C. Munoz, E. Nezri and F. Prada, JCAP **0601**, 010 (2006) [arXiv:hep-ph/0506204].

[28] E. A. Baltz, C. Briot, P. Salati, R. Taillet and J. Silk, Phys. Rev. D **61**, 023514 (2000) [arXiv:astro-ph/9909112]; N. Fornengo, L. Pieri and S. Scopel, Phys. Rev. D **70**, 103529 (2004) [arXiv:hep-ph/0407342].

[29] L. Bergstrom and H. Snellman, Phys. Rev. D **37**, 3737 (1988); V. S. Berezin-

sky, A. Bottino and V. de Alfaro, Phys. Lett. B **274**, 122 (1992); P. Ullio and L. Bergstrom, Phys. Rev. D **57**, 1962 (1998) [arXiv:hep-ph/9707333]; L. Bergstrom, T. Bringmann, M. Eriksson and M. Gustafsson, JCAP **0504**, 004 (2005) [arXiv:hep-ph/0412001]. F. Boudjema, A. Semenov and D. Temes, Phys. Rev. D **72**, 055024 (2005) [arXiv:hep-ph/0507127].

[30] L. Bergstrom and P. Ullio, Nucl. Phys. B **504**, 27 (1997) [arXiv:hep-ph/9706232]; Z. Bern, P. Gondolo and M. Perelstein, Phys. Lett. B **411**, 86 (1997) [arXiv:hep-ph/9706538].

[31] L. Bergstrom, P. Ullio and J. H. Buckley, Astropart. Phys. **9**, 137 (1998) [arXiv:astro-ph/9712318].

[32] H. C. Cheng, J. Feng and K. Matchev, Phys. Rev. Lett. **89**, 211301 (2002) [hep-ph/0207125];

[33] G. Bertone, G. Servant and G. Sigl, Phys. Rev. D **68**, 044008 (2003) [arXiv:hep-ph/0211342].

[34] L. Bergstrom, T. Bringmann, M. Eriksson and M. Gustafsson, Phys. Rev. Lett. **94**, 131301 (2005) [arXiv:astro-ph/0410359].

[35] T. Appelquist, H. C. Cheng and B. A. Dobrescu, Phys. Rev. D **64**, 035002 (2001) [arXiv:hep-ph/0012100]; H. C. Cheng, K. T. Matchev and M. Schmaltz, Phys. Rev. D **66**, 036005 (2002) [arXiv:hep-ph/0204342]; Phys. Rev. D **66**, 056006 (2002) [arXiv:hep-ph/0205314].

[36] A. Pukhov *et al.*, hep-ph/9908288.

[37] G. Servant and T. M. P. Tait, Nucl. Phys. B **650**, 391 (2003) [arXiv:hep-ph/0206071].

[38] M. Kakizaki, S. Matsumoto, Y. Sato and M. Senami, Phys. Rev. D **71**, 123522 (2005) [arXiv:hep-ph/0502059].

[39] T. Sjostrand, L. Lonnblad and S. Mrenna, arXiv:hep-ph/0108264.

[40] J. F. Navarro, C. S. Frenk and S. D. M. White, Astrophys. J. **490**, 493 (1997).

[41] B. Moore, F. Governato, T. Quinn, J. Stadel and G. Lake, Astrophys. J. **499**, L5 (1998) [arXiv:astro-ph/9709051]; B. Moore, T. Quinn, F. Gover-

nato, J. Stadel and G. Lake, Mon. Not. Roy. Astron. Soc. **310**, 1147 (1999) [arXiv:astro-ph/9903164].

[42] G. R. Blumenthal, S. M. Faber, R. Flores and J. R. Primack, Astrophys. J. **301**, 27 (1986); F. Prada, A. Klypin, J. Flix, M. Martinez and E. Simonneau, Phys. Rev. Lett. **93**, 241301 (2004) [arXiv:astro-ph/0401512]. O. Y. Gnedin, A. V. Kravtsov, A. A. Klypin and D. Nagai, Astrophys. J. **616**, 16 (2004) [arXiv:astro-ph/0406247].

[43] S. D. Hunger *et al.*, Astrophys. J. **481**, 205 (1997).

[44] T. C. Weekes *et al.*, Astropart. Phys. **17**, 221 (2002) [arXiv:astro-ph/0108478].

[45] W. Benbow [The HESS Collaboration], AIP Conf. Proc. **745**, 611 (2005); J. A. Hinton [The HESS Collaboration], New Astron. Rev. **48**, 331 (2004) [arXiv:astro-ph/0403052].

[46] A. Cesarini, F. Fucito, A. Lionetto, A. Morselli and P. Ullio, Astropart. Phys. **21**, 267 (2004) [arXiv:astro-ph/0305075]. See also the project's web site, `http://www-glast.sonoma.edu/`

[47] H. Bachacou, I. Hinchliffe and F. E. Paige, Phys. Rev. D **62**, 015009 (2000) [arXiv:hep-ph/9907518].

[48] A. Birkedal, A. Noble, M. Perelstein and A. Spray, Phys. Rev. D **74**, 035002 (2006) [arXiv:hep-ph/0603077].

[49] M. Perelstein and A. Spray, Phys. Rev. D **75**, 083519 (2007) [arXiv:hep-ph/0610357].

[50] N. Arkani-Hamed, A. G. Cohen and H. Georgi, Phys. Lett. B **513**, 232 (2001) [arXiv:hep-ph/0105239]; N. Arkani-Hamed, A. G. Cohen, E. Katz and A. E. Nelson, JHEP **0207**, 034 (2002) [arXiv:hep-ph/0206021].

[51] M. Schmaltz and D. Tucker-Smith, Ann. Rev. Nucl. Part. Sci. **55**, 229 (2005) [arXiv:hep-ph/0502182].

[52] M. Perelstein, Prog. Part. Nucl. Phys. **58**, 247 (2007) [arXiv:hep-ph/0512128].

[53] G. Burdman, M. Perelstein and A. Pierce, Phys. Rev. Lett. **90**, 241802 (2003) [Erratum-ibid. **92**, 049903 (2004)] [arXiv:hep-ph/0212228]; T. Han, H. E. Logan, B. McElrath and L. T. Wang, Phys. Rev. D **67**, 095004 (2003) [arXiv:hep-

ph/0301040]; M. Perelstein, M. E. Peskin and A. Pierce, Phys. Rev. D **69**, 075002 (2004) [arXiv:hep-ph/0310039].

[54] I. Low, JHEP **0410**, 067 (2004) [arXiv:hep-ph/0409025].

[55] J. Hubisz, P. Meade, A. Noble and M. Perelstein, JHEP **0601**, 135 (2006) [arXiv:hep-ph/0506042].

[56] J. Hubisz and P. Meade, arXiv:hep-ph/0411264, v3. See also Phys. Rev. D **71**, 035016 (2005); note however that the dark matter relic density plot has not been updated in the journal version.

[57] D. E. Kaplan and M. Schmaltz, JHEP **0310**, 039 (2003) [arXiv:hep-ph/0302049]; M. Schmaltz, JHEP **0408**, 056 (2004) [arXiv:hep-ph/0407143].

[58] A. Martin, arXiv:hep-ph/0602206.

[59] A. Birkedal-Hansen and J. G. Wacker, Phys. Rev. D **69**, 065022 (2004) [arXiv:hep-ph/0306161].

[60] J. Hubisz, S. J. Lee and G. Paz, JHEP **0606**, 041 (2006) [arXiv:hep-ph/0512169]; M. Blanke, A. J. Buras, A. Poschenrieder, C. Tarantino, S. Uhlig and A. Weiler, arXiv:hep-ph/0605214; M. Blanke, A. J. Buras, A. Poschenrieder, S. Recksiegel, C. Tarantino, S. Uhlig and A. Weiler, arXiv:hep-ph/0609284.

[61] H. C. Cheng, I. Low and L. T. Wang, Phys. Rev. D **74**, 055001 (2006) [arXiv:hep-ph/0510225].

[62] A. Pukhov, arXiv:hep-ph/0412191.

[63] G. Belanger, F. Boudjema, A. Pukhov and A. Semenov, Comput. Phys. Commun. **174**, 577 (2006) [arXiv:hep-ph/0405253].

[64] B. C. Allanach *et al.*, arXiv:hep-ph/0602198, pp. 146–149.

[65] R. J. Scherrer and M. S. Turner, Phys. Rev. D **33**, 1585 (1986) [Erratum-ibid. D **34**, 3263 (1986)].

[66] M. A. Shifman, A. I. Vainshtein, M. B. Voloshin and V. I. Zakharov, Sov. J. Nucl. Phys. **30**, 711 (1979) [Yad. Fiz. **30**, 1368 (1979)].

[67] J. F. Gunion, H. E. Haber, G. L. Kane and S. Dawson, *The Higgs Hunter's Guide,* Perseus, Cambridge, MA, 1990; see also arXiv:hep-ph/9302272.

[68] C. R. Chen, K. Tobe and C. P. Yuan, Phys. Lett. B **640**, 263 (2006) [arXiv:hep-ph/0602211].

[69] K. Kosack *et al.* [The VERITAS Collaboration], Astrophys. J. **608**, L97 (2004) [arXiv:astro-ph/0403422]; K. Tsuchiya *et al.* [CANGAROO-II Collaboration], Astrophys. J. **606**, L115 (2004) [arXiv:astro-ph/0403592]; F. Aharonian *et al.* [The HESS Collaboration], Astron. Astrophys. **425**, L13 (2004) [arXiv:astro-ph/0408145].

[70] A. Morselli, A. Lionetto, A. Cesarini, F. Fucito and P. Ullio [GLAST Collaboration], Nucl. Phys. Proc. Suppl. **113**, 213 (2002) [arXiv:astro-ph/0211327].

[71] L. Bergstrom, T. Bringmann, M. Eriksson and M. Gustafsson, Phys. Rev. Lett. **95**, 241301 (2005) [arXiv:hep-ph/0507229].

[72] D. Hooper and B. L. Dingus, Phys. Rev. D **70**, 113007 (2004) [arXiv:astro-ph/0210617]; arXiv:astro-ph/0212509.

[73] G. Zaharijas and D. Hooper, Phys. Rev. D **73**, 103501 (2006) [arXiv:astro-ph/0603540].

[74] N. W. Evans, F. Ferrer and S. Sarkar, Phys. Rev. D **69**, 123501 (2004) [arXiv:astro-ph/0311145].

[75] L. Bergstrom and D. Hooper, Phys. Rev. D **73**, 063510 (2006) [arXiv:hep-ph/0512317]; S. Profumo and M. Kamionkowski, JCAP **0603**, 003 (2006) [arXiv:astro-ph/0601249].

[76] E. A. Baltz, M. Battaglia, M. E. Peskin and T. Wizansky, Phys. Rev. D **74**, 103521 (2006) [arXiv:hep-ph/0602187].

[77] J. E. Taylor and A. Babul, Mon. Not. Roy. Astron. Soc. **348**, 811 (2004) [arXiv:astro-ph/0301612].

[78] P. Sreekumar *et al.* [EGRET Collaboration], Astrophys. J. **494**, 523 (1998) [arXiv:astro-ph/9709257].

[79] L. B. Okun, Leptons and Quarks (1982), pp. 228-231.

[80] G. K. Mallot, in *Proc. of the 19th Intl. Symp. on Photon and Lepton Interactions at High Energy LP99* ed. J.A. Jaros and M.E. Peskin, Int. J. Mod. Phys. A **15S1**, 521 (2000) [eConf **C990809**, 521 (2000)] [arXiv:hep-ex/9912040].

[81] D. S. Akerib *et al.* [CDMS Collaboration], Phys. Rev. Lett. **96**, 011302 (2006) [arXiv:astro-ph/0509259].

[82] SuperCDMS (Projected) Phase C [from the Dark Matter Plotter web site, `http://dmtools.berkeley.edu/limitplots/`].

[83] G. J. Alner *et al.* [UK Dark Matter Collaboration], Phys. Lett. B **616**, 17 (2005) [arXiv:hep-ex/0504031].

[84] N. J. C. Spooner *et al.*, Phys. Lett. B **473**, 330 (2000).

I. Low, JHEP **0410**, 067 (2004) [arXiv:hep-ph/0409025].

A. Freitas and D. Wyler, JHEP **0611**, 061 (2006) [arXiv:hep-ph/0609103].

A. Belyaev, C. R. Chen, K. Tobe and C. P. Yuan, Phys. Rev. D **74**, 115020 (2006) [arXiv:hep-ph/0609179].

M. S. Carena, J. Hubisz, M. Perelstein and P. Verdier, Phys. Rev. D **75**, 091701 (2007) [arXiv:hep-ph/0610156].

D. N. Spergel *et al.*, arXiv:astro-ph/0603449.

[85] M. Cirelli, N. Fornengo, T. Montaruli, I. Sokalski, A. Strumia and F. Vissani, Nucl. Phys. B **727**, 99 (2005) [arXiv:hep-ph/0506298].

[86] P. A. Toale [IceCube Collaboration], arXiv:astro-ph/0607003.

[87] N. Arkani-Hamed, S. Dimopoulos and G. R. Dvali, Phys. Lett. B **429**, 263 (1998) [arXiv:hep-ph/9803315]. I. Antoniadis, N. Arkani-Hamed, S. Dimopoulos and G. R. Dvali, Phys. Lett. B **436**, 257 (1998) [arXiv:hep-ph/9804398]; N. Arkani-Hamed, S. Dimopoulos and G. R. Dvali, Phys. Rev. D **59**, 086004 (1999) [arXiv:hep-ph/9807344].

[88] S. Cullen, M. Perelstein and M. E. Peskin, Phys. Rev. D **62**, 055012 (2000) [arXiv:hep-ph/0001166].

[89] P. Burikham, T. Figy and T. Han, Phys. Rev. D **71**, 016005 (2005) [Erratum-ibid. D **71**, 019905 (2005)] [arXiv:hep-ph/0411094];
D. Lust, S. Stieberger and T. R. Taylor, Nucl. Phys. B **808**, 1 (2009) [arXiv:0807.3333 [hep-th]];

L. A. Anchordoqui, H. Goldberg, D. Lust, S. Nawata, S. Stieberger and T. R. Taylor, Phys. Rev. Lett. **101**, 241803 (2008) [arXiv:0808.0497 [hep-ph]].

[90] D. Lust, JHEP **0903**, 149 (2009) [arXiv:0904.4601 [hep-th]].

[91] K. Agashe, R. Contino and R. Sundrum, Phys. Rev. Lett. **95**, 171804 (2005) [arXiv:hep-ph/0502222].

[92] K. Agashe, A. Delgado, M. J. May and R. Sundrum, JHEP **0308**, 050 (2003) [arXiv:hep-ph/0308036].

[93] Y. Grossman and M. Neubert, Phys. Lett. B **474**, 361 (2000) [arXiv:hep-ph/9912408].

[94] K. Agashe, G. Perez and A. Soni, Phys. Rev. D **71**, 016002 (2005) [arXiv:hep-ph/0408134].

[95] C. Csaki, C. Grojean, L. Pilo and J. Terning, Phys. Rev. Lett. **92**, 101802 (2004) [arXiv:hep-ph/0308038].

[96] P. Meade and L. Randall, JHEP **0805**, 003 (2008) [arXiv:0708.3017 [hep-ph]].

[97] B. Hassanain, J. March-Russell and J. G. Rosa, arXiv:0904.4108 [hep-ph].

[98] M. Fierz and W. Pauli, Proc. Roy. Soc. Lonf. A **173**, 211 (1939)

[99] T. Gherghetta and A. Pomarol, Nucl. Phys. B **586**, 141 (2000) [arXiv:hep-ph/0003129];
S. J. Huber and Q. Shafi, Phys. Lett. B **498**, 256 (2001) [arXiv:hep-ph/0010195].

[100] N. Arkani-Hamed H. Georgi and M. D. Schwartz, Ann. Phys. **305**, 96 (2003) [arXiv:hep-th/0210184].

[101] H. Davoudiasl, J. L. Hewett and T. G. Rizzo, Phys. Lett. B **473**, 43 (2000) [arXiv:hep-ph/9911262].

[102] C. Csaki, C. Grojean, J. Hubisz, Y. Shirman and J. Terning, Phys. Rev. D **70**, 015012 (2004) [arXiv:hep-ph/0310355].

[103] G. Cacciapaglia, C. Csaki, C. Grojean and J. Terning, Phys. Rev. D **71**, 035015 (2005) [arXiv:hep-ph/0409126].

[104] A. D. Martin, W. J. Stirling, R. S. Thorne and G. Watt, arXiv:0901.0002 [hep-ph].

[105] K. Agashe, A. Belyaev, T. Krupovnickas, G. Perez and J. Virzi, Phys. Rev. D **77**, 015003 (2008) [arXiv:hep-ph/0612015];
B. Lillie, L. Randall and L. T. Wang, JHEP **0709**, 074 (2007) [arXiv:hep-ph/0701166].

[106] J. Thaler and L. T. Wang, JHEP **0807**, 092 (2008) [arXiv:0806.0023 [hep-ph]];
D. E. Kaplan, K. Rehermann, M. D. Schwartz and B. Tweedie, Phys. Rev. Lett. **101**, 142001 (2008) [arXiv:0806.0848 [hep-ph]];
L. G. Almeida, S. J. Lee, G. Perez, G. Sterman, I. Sung and J. Virzi, Phys. Rev. D **79**, 074017 (2009) [arXiv:0807.0234 [hep-ph]].